Microprocessor Based Protection Of Induction Motors, Using Thermal, Mechanical, And Skin Effect Electrical Models To Predict Motor Temperature Rise

Sp. Coll.
LD
2369.2
.M61
1989

A Thesis

Presented for the

Master of Science in Engineering

Degree

The University of Tennessee, Chattanooga

U.T.C. Library

Nader S. Moharari

May 1989

I am submitting a thesis written by Nader S. Moharari entitled " Microprocessor Based Protection Of Induction Motors, Using Thermal, Mechanical, And Skin Effect Electrical Models To Predict Motor Temperature Rise" I have examined the final copy of this thesis and recommend that it be accepted in partial fulfillment of the requirements for the degree of Master of Science with a concentration in Electrical Engineering.

[redacted]

Dr. Ahmed H. Eltom, Chairperson

We have read this thesis
and recommend its acceptance:

[redacted]

Accepted for the Graduate Division:

[redacted]

Director of Graduate Studies

Dedication

To my wife

ACKNOWLEDGMENT

I would like to express my thanks and appreciation to my advisor Dr. Ahmed H. Eltom for his unlimited help and guidance throughout this work. Also I am indebted to professors Dr. Terrance M. Carney for his fatherly encouragement and support, Dr. Clifford R. Parten, and Dr. Stephanie A. Smullen who served as my thesis committee members.

My gratitude goes above all to my wife Mehry and our families for their patience, encouragement, and support.

ABSTRACT

This study investigates induction motor performance during a variety of system and load conditions. A computer simulation is used to characterize the motor behavior during normal operation, locked-rotor case, high inertia loading, and overloading conditions. Motor temperature at critical points is estimated. A microprocessor protection scheme based on motor temperature is proposed.

Previous studies assume a linear relationship between motor impedance and frequency when calculating motor temperature. In this study an electrical model, based on Maxwell's equations, is used in conjunction with a mechanical model, to represent the motor during dynamic state conditions. The model accounts for the rotor bar skin effect as the motor speed changes.

Motor losses, computed using the electrical model, are fed to a thermal model. Stator, rotor, and core temperatures are calculated. Thermal limit curves are presented. Protection strategies are investigated. A microprocessor based scheme is recommended. The scheme responds to motor temperature and trips the motor only at critical conditions. The scheme is optimal, simple, and easy to implement.

The diagnostic capability of this work is also valuable. For example, the motor acceleration time for a specified load can be calculated by this computer simulation. Thus, if the acceleration time changes it shows that there is a problem in a motor bearing or in some other mechanical part.

TABLE OF CONTENTS

LIST OF TABLES

LIST OF FIGURES

CHAPTER 1

INTRODUCTION

The application of polyphase induction motors in industrial, agricultural, and domestic fields is growing day by day. The study of electrical, mechanical, and thermal characteristics of the induction motors has been evolving since the first decades of this century. In today's highly competitive world, manufacturing design limits are optimized in order to achieve maximum profits while still maintaining specified ratings.

Because of the high cost of repair and downtime, especially for large motors (greater than 1,000 hp), the study of induction motor behavior during abnormal conditions and the design of proper protection schemes have been the most attractive issue for many researchers in recent years. Operating the machine under abnormal conditions may cause overheating, especially in the rotor. In particular, the rotor end-ring in squirrel-cage induction motors is the most vulnerable part during motor overheating.

The squirrel-cage induction motor instead of having windings in the rotor, has rotor conductors cast in slots. Therefore, there is no insulation in the rotor. These type induction motors, due to their longer life time and lower cost than those of the wound rotor machines, are widely used.

The cost of repairing or replacing the damaged motor is not the most important issue. The halt in assembly and production caused by the motor failure is the most significant economic problem. On the other hand, frequent and unnecessary motor trips may be more harmful than losing the machine itself. Avoiding such conditions needs a reliable, optimally protected machine. In order to achieve this, the motor electrical, mechanical, thermal characteristics, and its response to different power system and loading conditions must be analyzed thoroughly.

Today's microprocessor based technology provides new opportunities for the development of protection systems. The skillful use of this modern technology has given us the opportunity to re-examine the basic requirements of motor protection.

The Unresolved Problems

Most of existing conventional protection systems are not reliable. Malfunctioning cases have been reported in large motors while running high inertia loads. The available standard protection systems most often can not distinguish a high inertia starting from the locked rotor condition, therefore the motor can be tripped falsely. This occurs because the high inertia starting time in most cases exceeds the permissible locked-rotor time for a particular motor.

Unbalanced voltages applied at the motor terminals is another case which has not been studied thoroughly. The motor heating due to unbalanced voltage conditions in some cases is very serious, particularly for machines with double-cage or deep-bar rotor design. These machines, because of their rotor bar design, exhibit a high rotor resistance to the flow of negative sequence currents and produce extreme heating during unbalanced conditions. This heating will reduce the motor insulation life and may damage the end-ring joints as well. The effect of negative sequence current and resistance in motor heating can not be sensed by most available protection systems.

Some researchers use approximate methods to consider the effect of rotor negative sequence current and resistance on motor heating. The skin effect and the dependency of the rotor impedance on frequency are ignored in most investigations. In some recent works, linear

approximations were employed for the latter case. However, because of these approximate methods used in some protection schemes, they are not reliable.

Research Objectives

In this study induction motor thermal characteristics during normal, locked-rotor, unbalanced voltages, high inertia loading, and overloading conditions were investigated. Also, as a unique effort the temperature rise in rotor end-ring connector for different percentages of unbalanced voltages is studied properly.

In this investigation an accurate electrical model which accounts for the skin effect phenomena during normal and abnormal operation was used in order to calculate the motor losses and shaft torque. Also, a combination of the electrical, mechanical, and thermal models were used for calculating the motor speed and temperature rise as a function of time.

The basic objective of this research is to estimate the temperature rise of stator conductor, core, and rotor end-ring employing interactive models. The idea is to establish a microprocessor based protection system for induction motors capable of predicting the motor temperature chronologically. The proposed protection scheme only requires measuring the three phase input currents as a function of time. Then a real-time computer program employs the interactive models to calculate the motor temperature rise, and if the temperature exceeds the critical heat set point the system will send a warning message or isolate the motor from the energizing system automatically.

Chapter 2 of this study contains a review of the literature pertaining to induction motor protection systems and their thermal characteristics

during different power system conditions. The skin effect phenomena and the electrical, mechanical, and thermal models for induction motors are discussed in chapter 3. In addition, the calculation process used in the computer program for predicting the motor temperature rise is introduced in this chapter.

In chapter 4, the results of the computer simulation are evaluated. Also, the National Electric Manufacturer Association (NEMA) standard for motor operation under unbalanced condition has been re-examined thoroughly. In this chapter a new thermal limit curve based on the motor temperature for the unbalanced system condition is introduced.

In chapter 5, a microprocessor based relay which responds to motor temperature is proposed. Also in this chapter, the shortcomings of the available motor protection schemes are evaluated.

The overall conclusions of this study are presented in chapter 6.

CHAPTER 2

REVIEW OF LITERATURE

Background

Protection of induction motors has been an attractive subject to many researchers since the introduction of the motor itself. Through the years, a variety of schemes for protection of induction motors have been suggested, and different relays have been manufactured. Most motor protection relays available today exhibit good protective characteristics for high current motor faults and overloads, but do not address the problems of system unbalanced faults and high inertia starting very well. The root of these weaknesses is the lack of application of accurate models for analyzing the induction machines' electrical, mechanical, and thermal characteristics.

Significant research has been done in the area of motor response to unbalanced system voltage (1,2,10). Also, the influence of unbalanced voltage on motor heating has been given special attention, but the available standard recommendations in this subject are not comprehensive (13,15,18). In this study, the influence of unbalanced voltage on induction motor heating is investigated thoroughly.

Widespread use of very large induction motors running high inertia loads in today's modern industries has brought some new doubts about the reliability of existing protection relays. While running high inertia loads, the motor starting time (ST; time required for the rotor to reach running speed) may exceed the permissible locked-rotor time (PLRT). Therefore the locked-rotor protection relay

may operate falsely.

The study of motor heating during normal and abnormal conditions has been the target of many investigators. However, these studies have not been comprehensive, and the results still are not satisfactory. In typical cases the rotor resistance is considered to vary linearly with the motor speed (5,6,11).

Some authors have used electrical models which account for the skin effect, but did not consider thermal models and assumed that the heat generated inside the motor is always adiabatic (1,2). These researchers suggested a motor protection scheme which is based on unbalanced voltage at the motor terminals. They proposed that if the unbalanced voltage exceeds 3 percent the motor should be switched off with a delay time equal to the motor PLRT.

Though 3 percent voltage unbalance is detrimental to motor operation, these conditions are not highly abnormal in the power system and in many cases the motor may be tripped unnecessarily. The motor can withstand an unbalanced condition for a certain period of time before it reaches its thermal limit. By this time the unbalanced condition may be cured or the motor duty cycle may be over.

To protect the motor properly, an electrical model which accurately represents the motor should be used. This model should be correlated with the motor thermal and mechanical models to predict the motor temperature. Then a protection scheme which is based on the motor thermal limits (the maximum tolerable temperature) could be proposed.

In this study electrical and mechanical models, which represent

the motor during dynamic and steady state conditions, are used to calculate the motor speed and losses. The losses are then incorporated in the motor thermal model to predict the motor temperature at any time and in any operating condition. By using the knowledge of motor thermal characteristics, a unique thermal limit curve which is based on the rotor end-ring's temperature and unbalanced voltage percentage is developed. In consequence of these, a microprocessor based motor protection scheme capable of predicting the motor temperature at each moment of motor operation is introduced.

This chapter includes a review of literature pertaining to induction motor heating during different operating conditions. Additional studies are included where necessary to provide an insight to the particular problem of interest.

Symmetrical Component Analyses

The use of electrical models based on symmetrical components has been the usual practice in analyzing the induction motors' characteristics during unbalanced conditions(2,3,10,11). Earlier in this century a powerful tool for analyzing a system of unbalanced voltages was introduced by C. F. Fortescue (17). In his proposed method, he showed that an unbalanced set of n phasors may be resolved into n-1 balanced n phase systems of different phase sequence and one zero phase sequence system. This mathematical tool has become very useful in investigating the response to any unbalanced power system condition. In his method a three phase unbalanced system can be analyzed by using the positive, negative,

and zero sequence networks.

The Single Phase Equivalent Circuit

The single phase equivalent circuit is a powerful tool for simplifying the analysis of unbalanced three phase circuits [2]. The induction motor per phase equivalent circuit has been used in analyzing motor behavior under steady state conditions by many researchers (8,9,16). Since, during unbalanced condition, the current distribution is not the same for the three phases, both the positive and negative sequence single phase equivalent circuits must be used during unbalanced conditions.

Skin Effect and Rotor Bar Design

Early research showed that the dynamic impedance of rotor conductors is frequency dependent (3,16,24). This phenomenon is called the skin effect and has been documented in many areas of electrical engineering (1,2,3,16). High motor efficiency requires very low slip and hence low rotor resistance under rated conditions. On the other hand, to satisfy the conflicting requirements of high efficiency, low slip, and high starting torque (the larger the rotor resistance, the higher the motor torque), designers utilize the skin effect to develop rotors of either double-cage or deep-bar types [18].

Induction Motor Models

Mathematical models are of interest to application engineers because they identify important electrical, thermal, and mechanical interactions in an induction motor [11]. Many existing protection

schemes were based on the results obtained from the classic electrical models, which are not applicable to all types of system and motor conditions. In other studies, in order to compensate for the shortcomings of the classic electrical models in defining the dependency of rotor dynamic impedance, linear approximations, which are inaccurate and do not have a firm scientific root, were used (4,5,6,11).

A rotor bar model which is based on the Maxwell equations and is capable of predicting rotor bar current distribution and effective dynamic impedance has recently been presented [3]. This model was tested in the laboratory and the results established that the model is accurate and reliable (1). This skin effect impedance model, which is used in this study, is based on electrical machine theory. This theory is based on of a set of assumptions applicable to all types of electrical machines.

In the area of thermal characteristics some investigators tried to measure the motor temperature by inserting Resistance Temperature Detectors (RTDs) inside the motor body (7,15), while others made an effort to establish an equivalent thermal circuit for induction motors (11,20,22). In this area, S. E. Zocholl has recently presented a simple and accurate thermal model for the induction motor's stator and rotor.

Thermal models are needed to estimate the temperature at critical points where direct measurement is not possible and where measurement time delays can not be tolerated [11]. In this work Zocholl's thermal models are used as a mathematical tool for predicting the temperature rise of the stator conductor, core, and

rotor end-ring.

The swing equation has been used, in some investigations, as a mathematical tool in order to fit the induction machines' electrical and mechanical aspects together (2,3,11). In this study also the swing equation of the induction motor is employed as the electromechanical model along with the electrical model to predict the motor speed at any moment of motor operation. The advantage of predicting the motor speed is elimination of the need for a speed sensor.

Motor Heating

Motor heating during normal and abnormal conditions has been the focus of many researchers. Particularly, motor heating during unbalanced voltage, locked-rotor, and more recently high inertia loading conditions have been the major issues of interest (10,11,13,14,15,18,23).

There are many valuable works in which the thermal characteristics of the stator, core, and rotor have been investigated thoroughly (6,7,11,20,22). The fact that the rotor temperature rise is more critical than the other parts of the motor has been addressed by some researchers (19,12).

The motor thermal limitations have been classified clearly by R. J. Brighton (12). According to his work, the stator temperature rise is determined by the insulation material class and the knowledge that every 10 to 15 degree centigrade over rated temperature reduces insulation life by 50 percent.

Also he mentioned that the allowable temperature rise for the rotor is limited by the fact that the strength of the material is

reduced at elevated temperatures. The allowable temperature rise of the rotor end-ring is much lower than for the rotor bar of the same material in order to limit the bending stresses in the rotor. This brings up the concept of fatigue life. The rotor cage can be designed for a certain number of starts over the life of the motor [12]. Unfortunately, most U.S. manufacturers do not publish the number of starts for which the motor is designed.

The comparison of motor heating during high inertia starting and the locked-rotor case has recently become an attractive subject for protection engineers. Since there is no motion during the locked-rotor case, the input electrical energy is dissipated as heat in the rotor and stator. During a normal start the input energy divides between heating and accelerating the load. When starting time is significantly less than the permissible locked-rotor time, full speed is reached well before the relay can operate. However, when starting time is prolonged enough to approach or exceed the PLRT the relay assumes a fault is occurring and will operate falsely even though the motor is thermally relaxed [14].

The failure of a large Reactor Coolant Pump (RCP) motor, which was tripped off the line by an instantaneous overcurrent relay during normal starting, was reported by A. N. Eliasen (13).

It is agreed that the acceleration time is essentially a function of the load torque and the load inertia and can be considered entirely variable depending upon what type of machine and load are being driven. The reason for malfunctioning by conventional relays is the ignorance of the effect of load inertia. Also, relays are set based on locked-rotor time and current rather than the actual heating.

Although high inertia starting is very difficult to distinguish from the locked-rotor case, the proposed protection scheme is an attempt to solve this formidable problem.

Another common problem is motor heating during unbalanced system conditions. For safe motor operation, NEMA standards limited voltage unbalance at the motor terminals to a maximum of 1 percent. This may be unrealistically low, as in some rural areas and other countries, voltage unbalance of 3 percent is not uncommon. In this case, in contrast to high inertia starting, conventional relays either can not sense the fault at all (e.g. during high impedance faults) or will operate when the motor has already experienced extreme overheating (2,3,12,23).

The problem arises because of the flow of negative sequence current and the presence of high negative sequence resistance, particularly in the rotor. The negative sequence current causes much more heat per ampere than that of the positive sequence. This happens because the rotor negative sequence resistance is larger than the rotor positive sequence resistance. A ratio of between 3 and 8 for rotor negative to positive resistance has been reported. This feature of the unbalanced systems has been either ignored or approximated in most conventional relays. Since the proposed protection scheme senses all three phase currents, the temperature rise of the motor can be predicted accurately.

Summary

The effects of high inertia starting, unbalanced voltage conditions, and skin effect phenomenon have not been considered in

most protection schemes properly. The dilemma remains due to lack of sufficient study in the areas of dynamic motor operation, balanced and unbalanced voltage systems, and loading conditions. However, there are many studies in which attempts have been made to calculate the motor temperature rise. Some of them employed RTDs for measuring the motor temperature, while others tried to develop thermal models for predicting the motor temperature rise. RTDs, due to the difficulties of inserting them inside the motor and measuring the temperature in a hostile environment (e.g. the influence of magnetic field), are not economical or accurate.

Most proposed thermal models have been too complicated to use in real time. Recently, a useful and simple lumped parameter thermal model has been presented by S. E. Zocholl (11), which is used in this study. In this thesis accurate electrical, mechanical, and thermal models are employed in a proposed microprocessor based protection scheme. This scheme is capable of predicting the motor temperature in a proper interval of time during motor operation in any system and load condition. Also a unique thermal limit curve, which is able to specify the time that the motor reaches its thermal limit for any percentage unbalanced voltage, is developed.

U.T.C. Library

CHAPTER 3

DEVELOPMENT OF THE MODELS EQUATIONS

Protection of induction motors has been one of the most important subjects for many researchers since the invention of the motor itself. Valuable efforts have been made in this area and a variety of relays based on these studies have been manufactured. In spite of these studies, there is no comprehensive protection scheme. The major problems that induction motor protection relays have to deal with are:

1) unbalanced voltage system,
2) overloading,
3) high inertia loading, and
4) the locked rotor condition.

The available motor protection in some situations does not operate properly. In some cases it operates when the motor has already experienced severe overheating (e.g. unbalanced voltage conditions). In other cases it operates unnecessarily when the motor is thermally relaxed (e.g. high inertia starting). The main reason for these malfunctions is the use of models which do not represent the motor characteristics accurately, and the use of thermal limit curves for setting these relays. These curves are intended for use during balanced system conditions but they do not reflect heating due to negative sequence components.

In this chapter, accurate electrical, mechanical, and thermal models are introduced. Then the process of interaction between

these models is explained. Finally, the equations and a computer simulation, on which the proposed protection scheme is based, are developed and explained.

Skin Effect

In wound rotor induction motors, the common practice for developing a high starting torque is to add external resistance through slip rings to the rotor windings. Electric motor designers try to keep the rotor loss low by keeping the rotor resistance low, thus avoiding poor efficiency. The torque developed by the motor is directly proportional to the rotor resistance and inversely proportional to the motor slip. Since the motor slip is equal to one at standstill, a large rotor resistance is needed to develop a high starting torque. This conflicting situation can be solved in wound rotor induction motors easily by employing the above method. For squirrel-cage induction motors, the rotor conductors are not accessible for any external operation.

Because of higher reliability, longer life, and lower cost, squirrel-cage induction motors are widely used for industrial, agricultural, and household purposes. In order to have suitable starting torque, deep-bar, double-cage, and triple-cage induction motors have been designed to use the skin effect phenomena.

At standstill, the rotor frequency equals the stator frequency. As the motor speeds up, the rotor frequency decreases to a very low value (less than 1 Hz in some cases). This is explained by equation 3.1.

$$F_r = S * F_s \tag{3.1}$$

$$S = \frac{\omega_s - \omega_r}{\omega_s} \tag{3.2}$$

$$\omega_s = \frac{120 * F_s}{P} \tag{3.3}$$

where,

F_r = rotor frequency Hz,

F_s = stator frequency Hz,

S = motor slip p.u.,

ω_s = synchronous speed rpm,

ω_r = rotor speed rpm, and

P = the number of poles.

If the core material had infinite permeability, all the leakage-flux lines, produced by the current flowing through the conductor, would close their paths the same way the biggest flux line closes in figure 3.1. However, most of flux lines prefer to close their loop in a shorter path because the core has magnetic resistivity as shown in figure 3.1. The distortion in the biggest flux line's path at the top of the slot is due to the air gap's high magnetic resistivity.

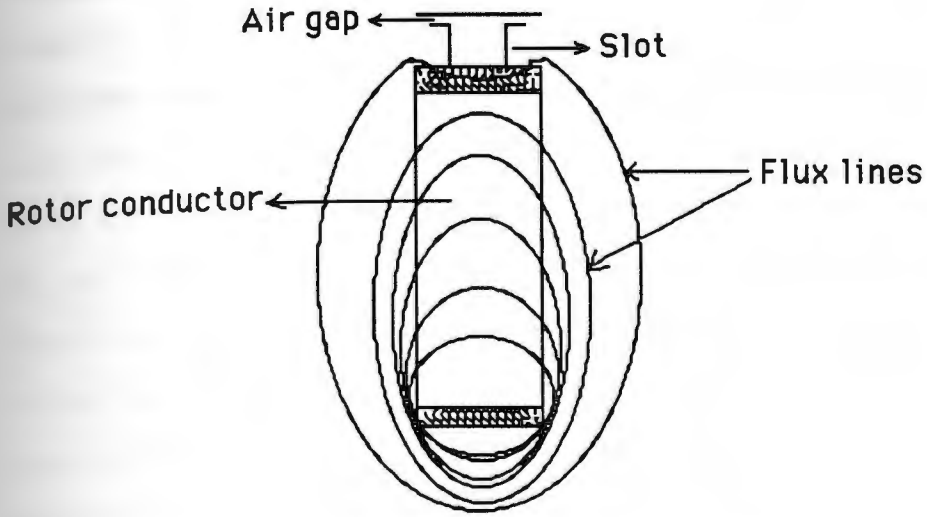

Figure 3.1 The cross section of a deep rotor bar

The leakage inductance is proportional to the number of leakage-flux lines. As shown in figure 3.1 the bottom layers will be surrounded by more leakage-flux lines than those at the top. Consequently the inductance of the bottom layers would be much larger than those of the top layers. Therefore, most the of rotor current will be forced to flow through the layers which are closer to the air gap. In addition, current in the upper layers will lead the current in the lower ones. This phenomenon is called skin effect. The nonuniform current distribution results in an increase in the effective rotor bar resistance and a smaller decrease in its effective leakage inductance [16]. As the motor accelerates, the rotor

frequency decreases, and hence the effect of leakage-flux lines weakens. Consequently, there will be no significant difference between leakage inductances at the top and bottom layers of the rotor bar. Hence the current will be distributed equally over the cross section of the rotor bar, the effective resistance will decrease to its d.c. value, and the effective leakage inductance will increase. Since the distortion in current distribution depends on an inductive effect, the effective resistance is a function of the frequency. It is also a function of the depth of the bar and the permeability and resistivity of the bar material [16].

Figures 3.2 and 3.3 show the rotor effective resistance and reactance of a typical deep-bar rotor as a function of slip. In these figures, the dependency of rotor resistance and reactance on slip is shown clearly. In addition, the figures show the degree of non-linearity of the rotor's impedance with frequency. This non-linearity varies for different bar designs and materials.

Most studies ignore this important feature of rotor impedance. Those who have included it in their work considered an approximate linear relationship between rotor impedance and frequency. This approximate method cannot represent the actual and accurate variation of rotor impedance with frequency.

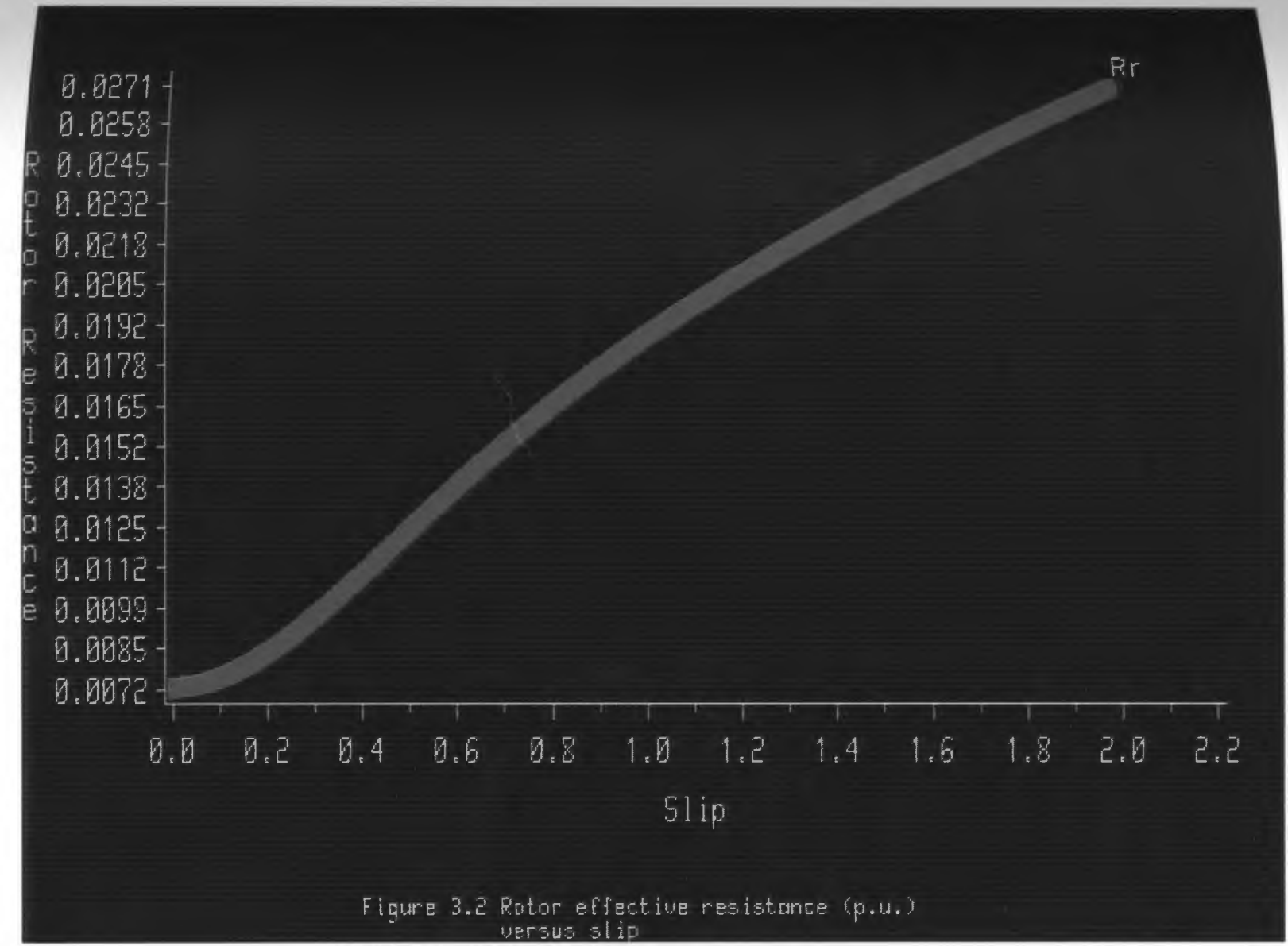

Figure 3.2 Rotor effective resistance (p.u.) versus slip

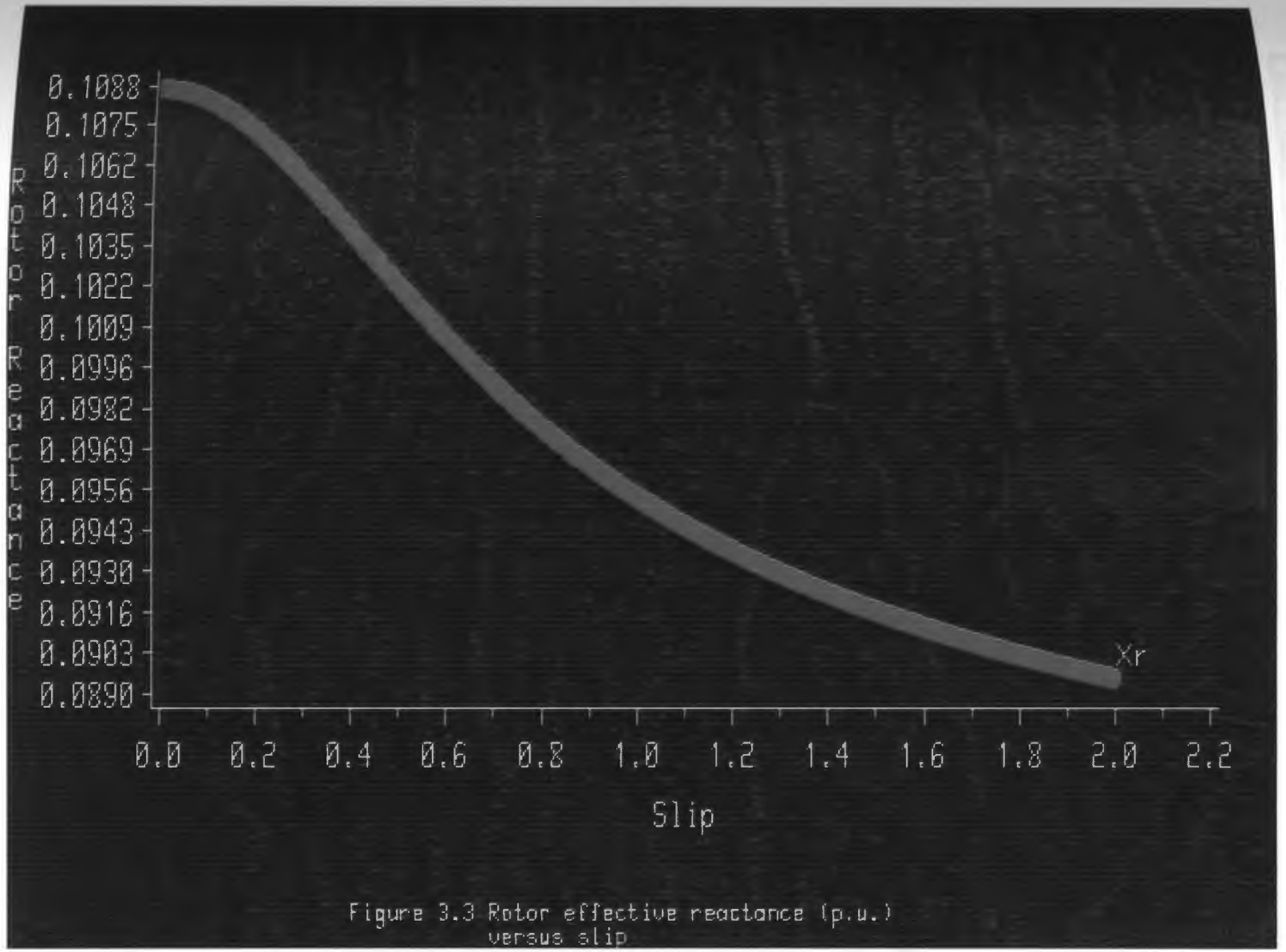

Figure 3.3 Rotor effective reactance (p.u.) versus slip

Electrical Model

It is general practice when computing the inductance of a circuit from Maxwell's equations to separate the inductance into two components: an external inductance and an internal inductance. The external inductance is a function of the geometry of the circuit and the materials involved, and is not a function of the currents flowing in the conductor. The internal inductance, however, is a function of the current distribution in the conductor [3].

Using Maxwell's equations, Ohm's law, and considering the skin effect phenomenon, the rotor bar can be represented by a series of N equivalent circuits shown in figure 3.4.

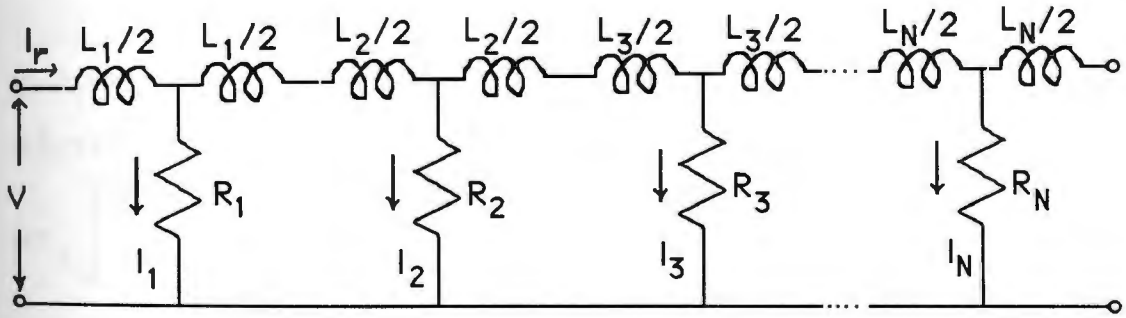

Figure 3.4 Equivalent circuit of the rotor bar.

The rotor current is the sum of the current in each segment:

$$I_r = \sum_{k=1}^{N} I_k \qquad (3.4)$$

This equivalent circuit of the squirrel-cage induction motor rotor bar is capable of predicting the current distribution in the bar. The physical basis and the reasonable assumptions of this model make it a more precise representation of the induction motor than the other proposed models [3].

The parameters of this representation have been calculated in terms of the physical properties of the rotor bar. It is more desirable, however, to express the resistances and inductances of this rotor bar representation in terms of quantities which can be measured by electrical tests.

The rotor bar equivalent circuit of figure 3.4 is valid for both transient and steady state conditions. It was shown (3,24) that the internal impedance of the rotor bar for a steady state condition is:

$$Z=R(1+j)*A*COTH[(1+j)*A] \qquad (3.5)$$

where,

$$A=\sqrt{\frac{\omega_r L}{2R}}$$

$$R=\frac{\ell}{\sigma d w}$$

$$L=\frac{\mu \ell d}{w} \qquad (3.6)$$

ω_r= angular frequency, radians/sec.

ℓ = bar length

d= bar depth

w= bar width

σ= conductivity coefficient

μ = permeability of the core

This impedance can be measured as a function of angular frequency ω_r, and the values of R and L determined. R and L can also be expressed in terms of rotor bar physical parameters, as indicated in equations 3.6. Comparisons of these expressions with the rotor bar segment resistance and inductance show that:

$$R_m = R\frac{d}{H_m}$$

$$L_m = L\frac{H_m}{d} \qquad (3.7)$$

For m=1,2,3,.....,N ,where R_m , L_m , and H_m are the resistance, inductance, and depth of segment H respectively. The parameters of the rotor bar representation of figure 3.4 can then be determined from the electrical properties of the rotor bar.

The accuracy of the rotor bar model with a specific number of bar segments represented can be determined by comparisons of the steady state solutions of that representation with the steady state solution given in equation 3.5.

The required parameters are R and L from equations 3.6, the range of frequencies of interest, and the relative depth of each rotor bar segment. In reference (3) it is noted that convergence is faster if varying depths are used with smaller segments near the top of the bar, where the current will be connected at higher frequencies. For a four-segment approximation, using the top 10 percent for the first

segment, the next 20 percent for the second segment, 30 percent for the third segment, and 40 percent for the last segment is suggested by Ortmeyer (3). A similar division of segments is used throughout this study.

The Skin Effect Impedance Model of the Induction Motor

A motor model capable of calculating the rotor bar current distribution, but neglecting the electrical transients, was developed based on the rotor bar skin effect equivalent circuit. This model is applicable for use in some dynamic motor conditions as well (1,3). The positive and negative sequences of the steady state equivalent circuit of the skin effect impedance model of the induction motor are shown in figure 3.5. A complete detail of this model is discussed by Ortmeyer (3). This model accounts for the non-linear relationship between rotor bar impedance and frequency. The model is accurate and backed by laboratory study (1).

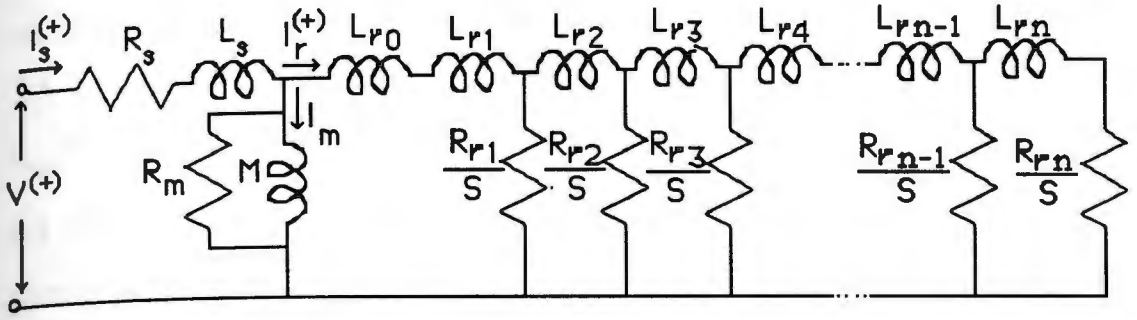

(a)

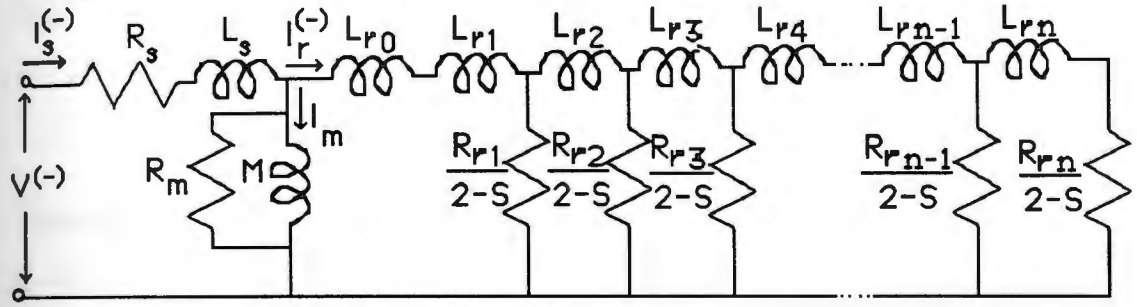

(b)

Figure 3.5 The positive (a) and negative (b) sequences of the skin effect impedance model of the squirrel-cage induction motors

The skin effect models of the induction motor require more specific data than previous induction motor models. From equation 3.5 the internal rotor bar impedance will be:

$$Z_{bar}=R(1+j)*A*COTH[(1+j)*A] \tag{3.8}$$

As the frequency approaches zero (which corresponds to synchronous speed of the rotor.), Z_{bar} can be written as an finite series. As $A=\sqrt{\frac{\omega_r L}{2R}}$, the bar impedance is:

$$Z_{bar}=R[1+\frac{[(1+j)A]^2}{3}-\cdots\cdots]$$

$$=R+j\omega_r\frac{L}{3} \tag{3.9}$$

Therefore, at $\omega_r=0$, the positive sequence rotor resistance R_{rp} is:

$$R=R_{rp} \tag{3.10}$$

The positive sequence inductance L_{rp} consists of external bar leakage inductance L_0 plus internal inductance at $\omega_r=1$

$$L_0+\frac{L}{3}=L_{rp} \tag{3.11}$$

Finally, the values of L_0 and L must be determined. These can be found at $\omega_r=2$ p.u. from either the rotor negative sequence resistance R_m or the rotor negative sequence inductance L_{rn}. At $\omega_r=2$ p.u. the real part of equation 3.8 equals the negative sequence rotor resistance.

$$Re(Z_{bar}) = RA\left[\frac{Sinh(2A)+2Sin(2A)}{Cosh(2A)-Cos(2A)}\right] = R_{rn} \qquad (3.12)$$

In equation 3.12, the quantity inside the brackets is approximately equal to one, so:

$$A \cong \frac{R_{rn}}{R} = \frac{R_{rn}}{R_{rp}} \qquad (3.13)$$

or,

$$L = A^2 * R = A^2 * R_{rp} \qquad (3.14)$$

Then, simply by knowing either R_{rp} and L_{rp}, or A, which is the ratio of the rotor negative and positive sequence resistances, the positive and negative sequence skin effect models can be developed.

Thermal Model

Measurement of the temperature rise of the stator, rotor, and core of squirrel-cage induction motors has been the subject of many investigations. Most of these efforts were concentrated on inserting thermocouples into the stator and rotor slots as well as inside the core. To monitor the rotor temperature of a cage rotor induction machine, the following requirements and operational aspects had to be taken into consideration (7).

1) More than one location on the rotor would need to be monitored for adequate representation of the rotor condition.
2) Information transmission from the rotating body should be through a reliable and relatively maintenance-free system.
3) The circuits would be spinning at the rotor speed and would

need to withstand substantial centrifugal forces.

4) They would have to operate in a relatively hostile environment with possible electrostatic and electromagnetic interference.
5) There is no power supply available on the rotor.

Some other researchers have tried to develop thermal models for induction motors. Most of them are too complicated to use in a computer simulation or do not represent the motor thermal characteristics accurately. In other words, inaccuracy or accuracy is the price of simplicity or complexity in most proposed thermal models.

Most investigators have agreed that monitoring the temperature of the rotor end-rings is the most important step in protecting squirrel-cage induction machines. It is true that the rotor end-rings are cooler than the rotor conductors, because of lower current density in the end-rings. However, the joint points between end-rings and the rotor bars can be damaged easily due to the stress caused by the temperature rise in end-rings, controlling the end-rings' temperature is necessary.

This is very important because in large motor applications the end-ring expansion is the most critical factor during stalling or acceleration. However in small motors, the stator winding temperature is most likely to be the most critical factor [15].

Motor designers point out that different rotor materials and different rotor designs have different limits. A limit temperature of 300 degrees centigrade is frequently used for copper-alloy rotor-

bars. Much smaller values are used for end-rings. U.S.A. standards do not stipulate temperature-limit values for rotors [13]. Some of these limit values are shown in table 3.1 [13].

Table 3.1

Calculated Permissible Adiabatic Total Temperatures in Bars and End-Rings.

Country		End-rings °C	Bar (embedded in core) °C
France		40	–
W. Germany		150-200	300
U.K.		100	300-250
U.S.S.R.		200	–
U.S.A.	(a)	80	240
	(b)	90	340
	(c)	90	290
	(d)	160	290

Thermal models are needed to estimate the temperature at critical points where direct measurement is not possible and where measurement time delay cannot be tolerated [11]. Recently, two separate electrical analogs of the stator and rotor thermal models have been introduced (5,6,11). Since the air gap provides a substantial barrier to heat transfer, the uncoupled thermal models provide good results [11]. In these analog circuits, the heat source is

represented as a constant current generator numerically equal to the motor losses. For instance, stator and core losses are represented by current generators as the heat sources for the stator thermal model of figure 3.6. The ability of both to retain and lose heat is represented by thermal capacitances and resistances. The separate thermal models for stator and rotor are shown in figures 3.6 and 3.7, respectively.

The parameters of this thermal model should be given by the manufacturer based on locked rotor current, and two corresponding values of the permissible locked rotor time when the rotor is initially at ambient temperature and when at operating temperature.

During start, heating is nearly adiabatic since little heat is lost compared to the heat input. While running, the stator conductor heat is dissipated through the stator insulation and finally into the ambient aided by ventilation. Hystersis and eddy current losses heat the iron core directly and rotor conductor heat flows into the rotor iron and out via ventilation and shaft conduction [11]. These processes are emulated by the electrical analog models for the stator and rotor shown in figures 3.6 and 3.7 respectively.

Since these thermal models are mainly related to the motor losses, accurate loss calculation is necessary. To achieve this the motor speed and the rotor resistance must be calculated accurately. These important steps in monitoring the motor temperature have been ignored in most studies (5,6,11).

In this study, these thermal models are used in order to predict the motor temperature rise. They are supported by accurate electrical and mechanical models.

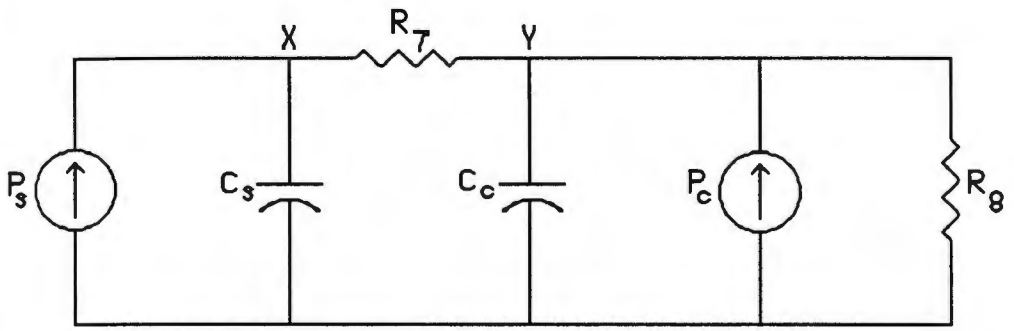

P_s : Stator conductor losses

P_c : Core losses

Y : Core temperature rise

X : Stator conductor temperature rise

C_c: Core thermal capacitor

C_s: Conductor thermal capacitor

R_7: Insulation thermal resistance

R_8: Thermal resistance to ambient

Figure 3.6 Stator thermal model

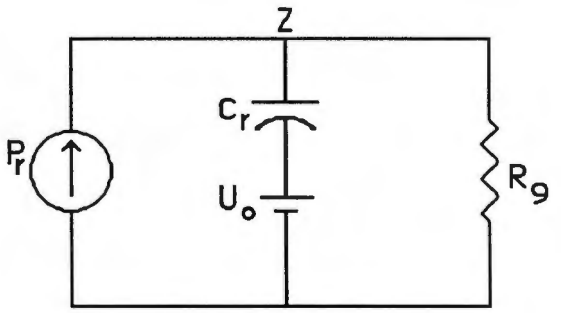

P_r : Rotor conductor losses
Z : Rotor conductor temperature rise
C_r : Rotor conductor thermal capacitance
R_9 : Rotor thermal resistance to ambient
U_o : Ambient temperature

Figure 3.7 Rotor thermal model

Mechanical Model

The total shaft torque and the moment of inertia of the motor and load comprise the mechanical model. The state equation for this system is:

$$\omega^{\bullet} = \frac{T_{em} - T_{lm}}{2H} \qquad (3.15)$$

where,

$\omega^{\bullet}$ is the rate of change of speed with time in per unit,

T_{em} is the motor electromechanical torque in per unit,

T_{lm} is the load torque in per unit, and

H is the constant of inertia in seconds.

Motor Torque

The electromechanical power developed in the motor is represented by losses in the variable resistors in the electrical models of figure 3.5. This power is calculated in terms of the rotor positive and negative sequence losses and the motor slip as shown in equation 3.16.

$$P_{em} = I_r^{(+)2} R_{rp} \frac{1-S}{S} - I_r^{(-)2} R_{rn} \frac{1-S}{2-S} \qquad (3.16)$$

The torque developed is given by equation 3.17.

$$T_{em} = I_r^{(+)2} \frac{R_{rp}}{S} - I_r^{(-)2} \frac{R_{rn}}{2-S} \qquad (3.17)$$

Load Torque

The shaft load T_{lm} would be some function of the motor speed which depends on the type of load driven. In this work, the motor is

assumed to drive a pump. A typical load, which is characterized by an initial value L increasing to a final value F as speed increases, was considered in this work.

$$T_{lm} = L + (F-L)\omega_r^2 \qquad (3.18)$$

where,

L is the initial torque,

F is the final torque,

ω_r is the speed in per unit of synchronous speed.

Application

A combination of the three models which have been introduced is used in this work. In this simulation, the voltage at the distribution bus was assumed to be 1 p.u. By this assumption, and knowing the line and motor initial parameters, the motor losses and torque can be calculated. Then by injecting these losses into the thermal models, the motor temperature can be calculated. Consequently the load torque can be computed given the initial value of slip. Then by the help of the mechanical model and calculated values of T_{em} and T_{lm} the motor speed for the next interval of time can be predicted. From the calculated speed and the rotor resistance, and thus the motor currents as well as the motor losses, can be calculated for the next interval of time. This process continues during the motor operation. The interaction of these models is shown in figure 3.8.

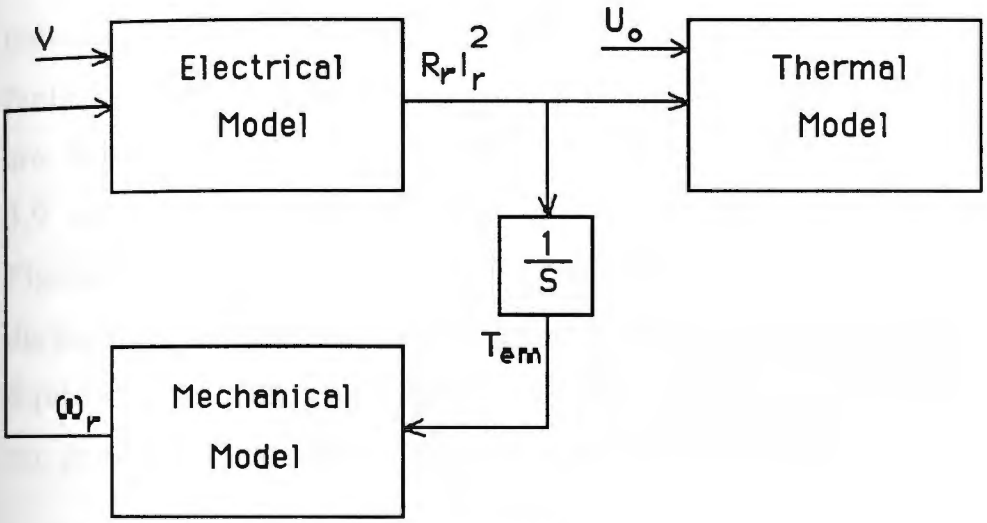

T_{em} is the torque developed by the motor

S is the motor slip

U_o is the ambient temperature

Figure 3.8 Block diagram of interactive models

Motor Temperature Calculation

In the computer simulation the single-phase to ground fault condition has been selected to study the motor behavior under an unbalanced voltage condition. The single-phase to ground fault has been reported to be the most severe fault in motor heating.

The one line diagram of a radial power system feeding an induction motor is shown in figure 3.9. The three phase diagram of a faulted motor is shown in figure 3.10. Since many induction motors are fed from radial distribution lines, the one line diagram of figure 3.9 represents a good basic model for the majority of applications. Figure 3.11 shows the sequence representation of the faulted system during a solid single-phase to ground fault at point F on figure 3.9. Squirrel-cage induction motors are not grounded, therefore there is no path for zero sequence current on the motor side.

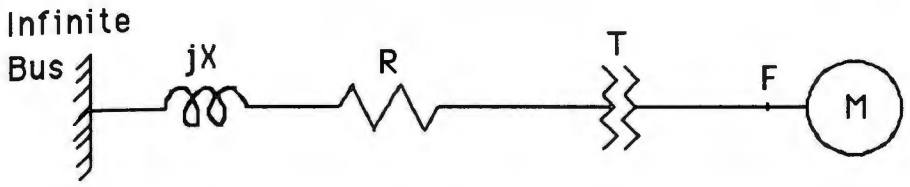

Figure 3.9 One line diagram of a radial power system feeding an induction motor

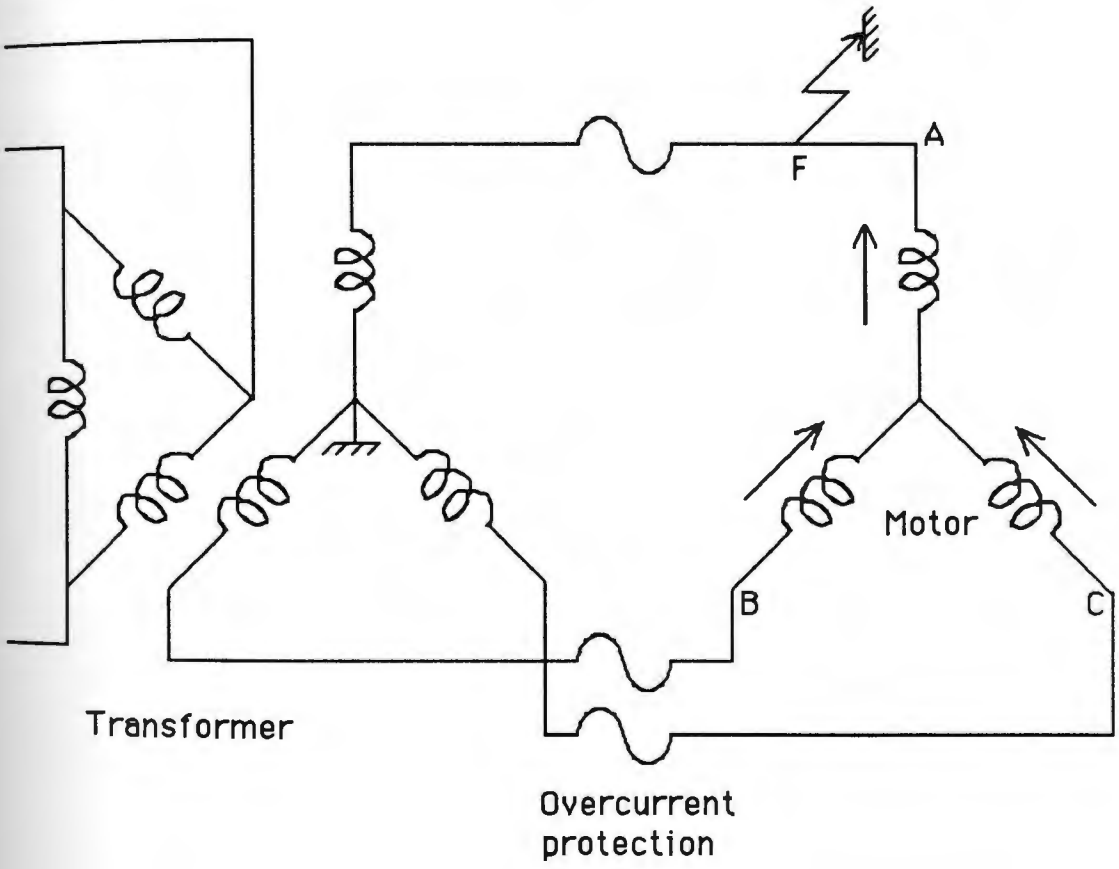

Figure 3.10 Three phase diagram of a faulted motor at point F

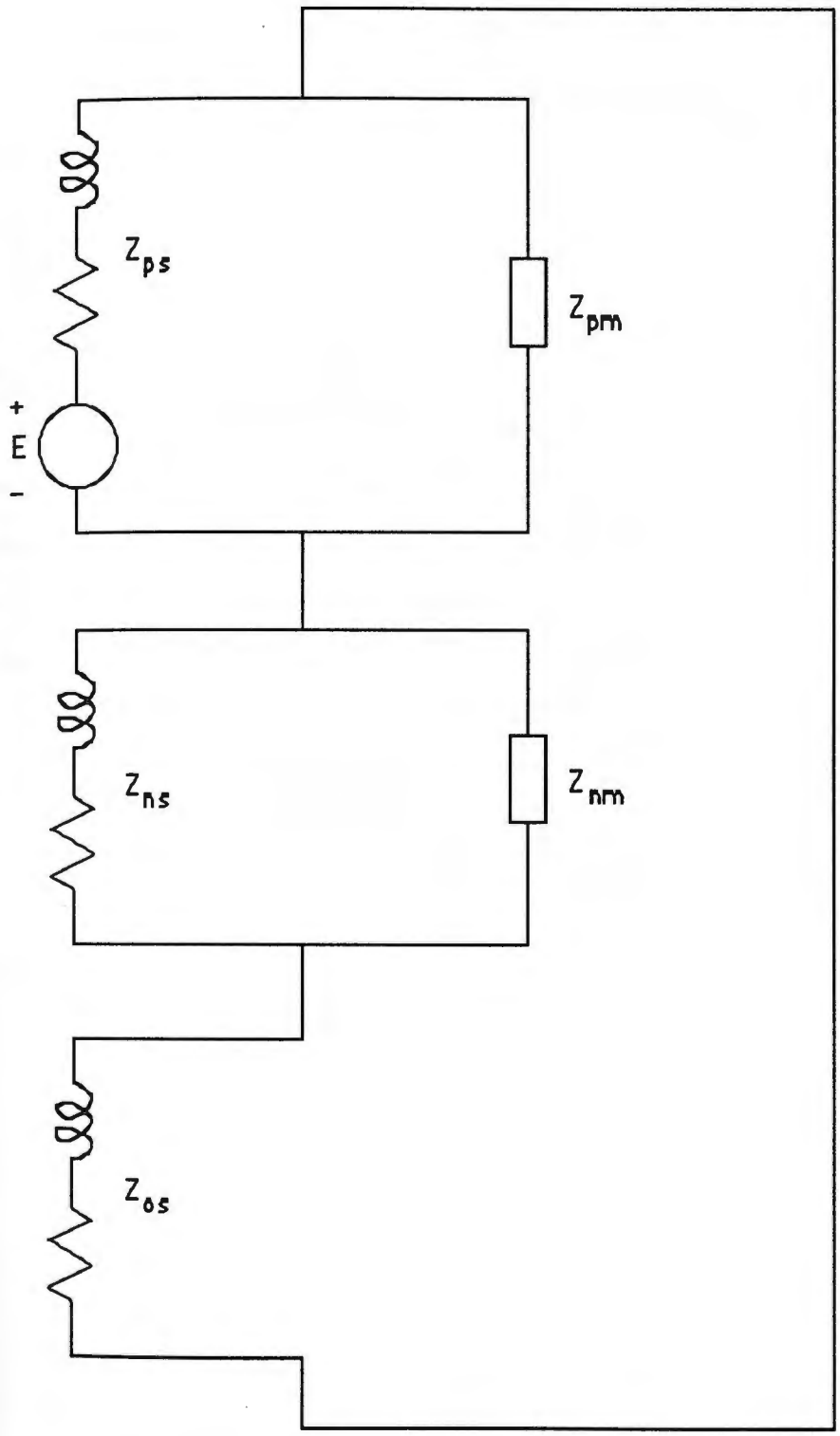

Figure 3.11 Connection of the sequence network for a single-phase to ground fault

In this study the voltage at the distribution bus was assumed to be 1 p.u., which is a reasonable assumption. The initial value of slip can be easily determined. For example, if the motor is about to start the motor speed is equal to zero then:

$$S = 1 - \omega_r \qquad (3.18)$$

where, S is the slip in per unit and ω_r is the motor speed in per unit of motor synchronous speed.

In this step, which can be assumed as the first iteration, by knowing the value of slip and utilizing the electrical model of figure 3.5 the rotor impedance can be calculated. The simplified models after this process and for each interval of time (also each value of slip in that particular interval) are shown in figure 3.12.

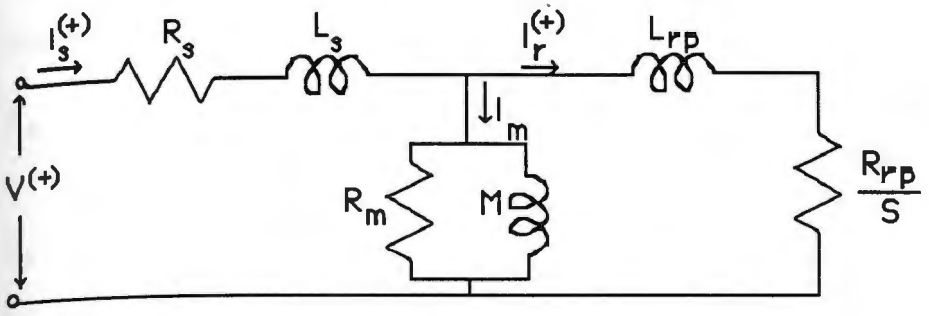

(a)

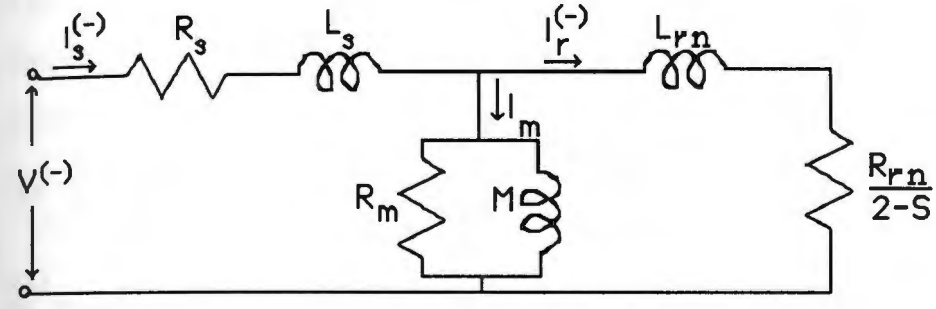

(b)

Figure 3.12 The simplified positive (a) and negative (b) sequence electrical models

$$I_r^{(-)} = I_s^{(-)} \frac{Z_m}{Z_{rn} + Z_m} \tag{3.22}$$

where,

$I_r^{(+)}$ and $I_r^{(-)}$ are the rotor positive and negative sequence currents in each interval of time respectively,

$I_s^{(+)}$ and $I_s^{(-)}$ are the motor positive and negative sequence currents in each interval of time respectively,

Z_m is the core impedance,

Z_{rp} and Z_{rn} are the rotor positive and negative sequence impedance in each interval of time.

After calculating the $I_r^{(+)}$ and $I_r^{(-)}$ the motor losses can be determined:

$$P_s = R_s (I_s^{(+)2} + I_s^{(-)2})$$

or,

$$P_s = R_s (I_A^2 + I_B^2 + I_C^2) \tag{3.23}$$

$$P_r = R_{rp} I_r^{(+)2} + R_{rn} I_r^{(-)2} \tag{3.24}$$

$$P_c = \frac{V^{(+)2}}{R_m} \tag{3.25}$$

where,

P_s is the stator loss,

P_r is the rotor loss,

P_c is the core loss.

Knowing the rotor losses, the torque developed by the motor,

and the load torque, the motor temperature rise then can be determined by the following equations:

$T_{em} = T_p - T_n$

or,

$$T_{em} = I_r^{(+)2} \frac{R_{rp}}{S} - I_r^{(-)2} \frac{R_{rn}}{2-S} \tag{3.26}$$

where,

T_{em} is the electromechanical torque developed by motor,

T_p is the positive sequence torque,

T_n is the negative sequence torque.

Along with the torque calculations, by applying the losses in the thermal models, the temperature rise of the stator conductor and rotor end-rings can be computed. For the thermal models, the state equations are:

$$X^{\bullet} = P_s \frac{1}{C_s} - X \frac{1}{R_7 C_s} + Y \frac{1}{R_7 C_e} \tag{3.27}$$

$$Y^{\bullet} = P_e \frac{1}{C_e} + X \frac{1}{R_7 C_e} - Y \frac{R_7 + R_8}{R_7 R_8 C_e} \tag{3.28}$$

$$Z^{\bullet} = P_r \frac{1}{C_r} - Z \frac{1}{R_9 C_r} \tag{3.29}$$

where, the parameters of the above state equations have been described in figures 3.6 and 3.7.

By calculating the motor losses and using the values of thermal resistances and capacitances for a particular motor the motor temperature rise can be predicted. In this study the Runge-Kutta method is used in order to solve the thermal and mechanical state

defined by NEMA, at the motor terminal in each interval of time. A flow chart and a list of this computer program is presented in Appendix A.

Summary

In this chapter the electrical, thermal, and mechanical models for squirrel-cage induction motors have been introduced. The electrical model presented in this work, which is used to compute the motor torque and losses, has the ability of employing the skin effect phenomenon for accurate calculation of rotor resistance at each moment of motor operation. The inputs for the thermal models introduced are the calculated losses by the electrical model. The outputs are the temperature rise of the stator and rotor conductor. The mechanical model has been used to compute the motor speed at any moment which is necessary for calculating the rotor resistance, torque, and losses by skin effect in the electrical model. Also, the complete calculation process used in the computer simulation has been explained in detail. The results and discussion of the results are the subjects of the next chapter.

CHAPTER 4

RESULTS AND DISCUSSIONS

In this computer simulation, an accurate method for calculating the motor temperature rise has been introduced. This method is applicable for all classes of induction machines. Also, it can be used for analyzing the motor behavior for any motor and system conditions. The following are the special features of this work:

1) use of an advanced skin effect impedance electrical model to properly predict the dependency of the rotor resistance on frequency,
2) employment of mechanical and electrical models to estimate the motor speed under all motor dynamic conditions,
3) use of electrical, mechanical, and thermal models for predicting the stator and rotor temperature at all system and motor conditions,
4) by introducing a new thermal limit curve, the duration of time for rotor end-rings to reach their emergency limit can be predicted. This can be done for any percentage of unbalanced voltage. This prediction is useful because by having this information the motor can be managed to be tripped off at a time which has the least harmful effect on the motor application. Also the motor can be protected properly.

Case Study

The technique developed is used to investigate the thermal, mechanical, and electrical characteristics of an 18000 horse power squirrel-cage induction motor. The electrical, mechanical, and thermal data for this motor are given in Appendix B. In this study the motor behavior during normal operation, locked rotor condition, unbalanced voltage, high inertia loading, and overloading conditions are investigated in detail. In this chapter the results of this study and the discussion of the results are presented.

Normal Operation

The motor thermal characteristic under normal operation has been investigated. A typical load torque with $T_{lm} = 0.25 + 0.67572\,\omega_r^2$ p.u. is assumed. Also the voltage at the distribution bus is assumed to be 1 p.u. As shown in figure 4.1, the accelerating time for this machine is about 16 seconds which is below its permissible locked rotor time (permissible locked-rotor time for this motor is about 17 seconds). The motor current from the standstill to the rated speed is shown in figure 4.2. As it can be seen the motor current at a speed of 0.95 p.u. is four times as much as of the rated current. In this case, the conventional overcurrent relay may not distinguish whether it is a locked-rotor condition or normal acceleration, particularly in high inertia starting. In figure 4.3, the rotor current and loss during normal operation are given. As is shown , the rotor current for a large period of time (from zero speed to almost 0.9 p.u.) is approximately constant. The rotor loss in the same period of time is

decreasing rapidly because of the frequency dependent rotor resistance, which decreases very fast as the motor speeds up. The motor torque-speed characteristic and the load torque-speed characteristic are shown in figure 4.4. Their point of intersection is the motor rated speed. Also the motor torque-time characteristic and the load torque-time characteristic are shown in figure 4.5. Again the torque-time curves cross at rated speed after about 16 seconds. After reaching this point, the motor is spinning at rated speed and the torque developed by the motor and the load torque will be equal. The thermal characteristic of this particular motor during starting is shown in figure 4.6. As is seen, the temperature rise in the rotor conductors reaches almost 59 percent of the critical temperature before it starts to level off, while the stator is completely relaxed. The emergency temperature for the stator and the rotor are 100 and 80 degrees centigrade respectively. When the motor reaches the rated speed the current will decrease, and the stator and the rotor temperature will drop significantly. The temperature rise of the rotor and the stator against time are shown in figure 4.7.

decreasing rapidly because of the frequency dependent rotor resistance, which decreases very fast as the motor speeds up. The motor torque-speed characteristic and the load torque-speed characteristic are shown in figure 4.4. Their point of intersection is the motor rated speed. Also the motor torque-time characteristic and the load torque-time characteristic are shown in figure 4.5. Again the torque-time curves cross at rated speed after about 16 seconds. After reaching this point, the motor is spinning at rated speed and the torque developed by the motor and the load torque will be equal. The thermal characteristic of this particular motor during starting is shown in figure 4.6. As is seen, the temperature rise in the rotor conductors reaches almost 59 percent of the critical temperature before it starts to level off, while the stator is completely relaxed. The emergency temperature for the stator and the rotor are 100 and 80 degrees centigrade respectively. When the motor reaches the rated speed the current will decrease, and the stator and the rotor temperature will drop significantly. The temperature rise of the rotor and the stator against time are shown in figure 4.7.

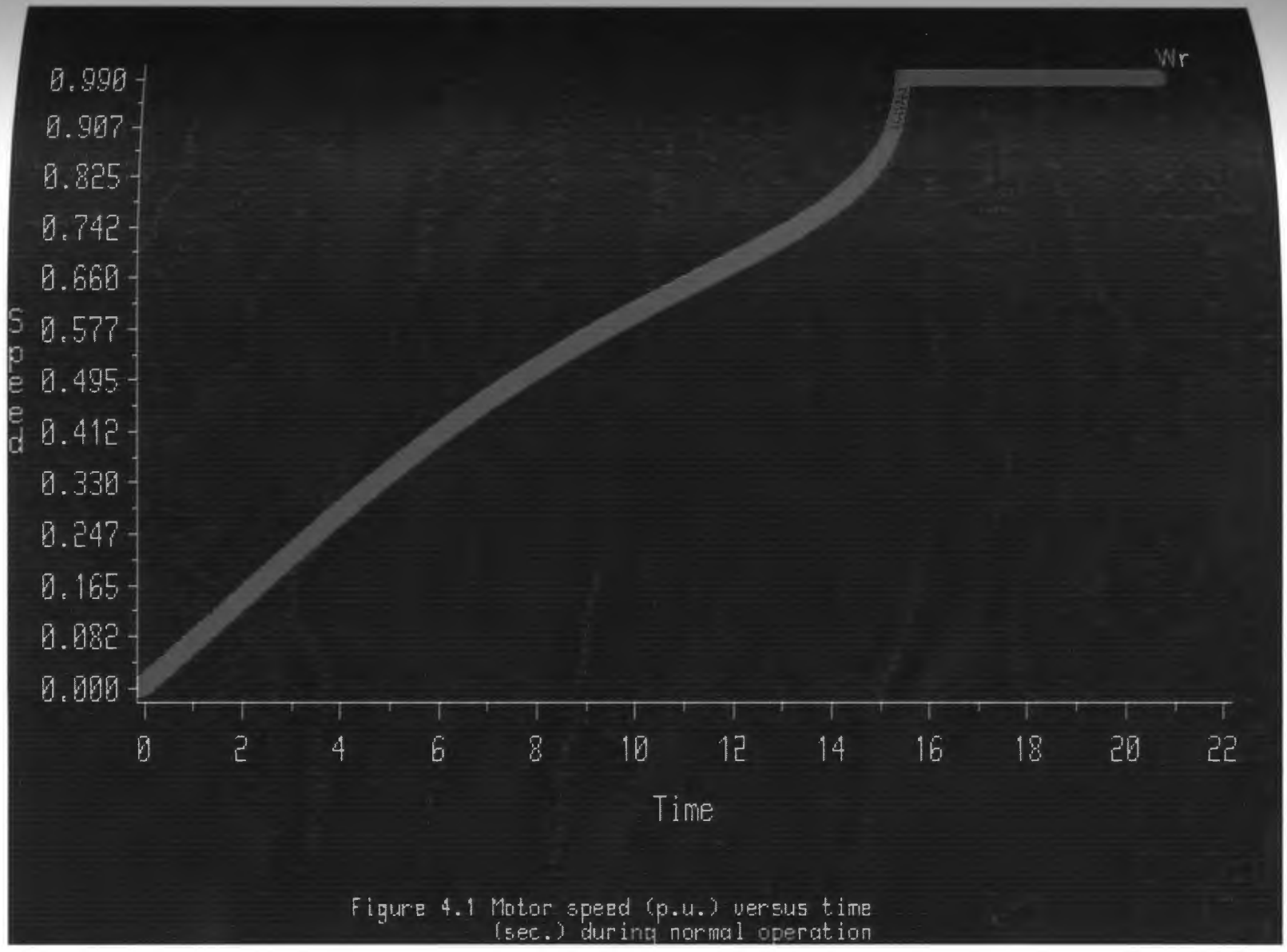

Figure 4.1 Motor speed (p.u.) versus time (sec.) during normal operation

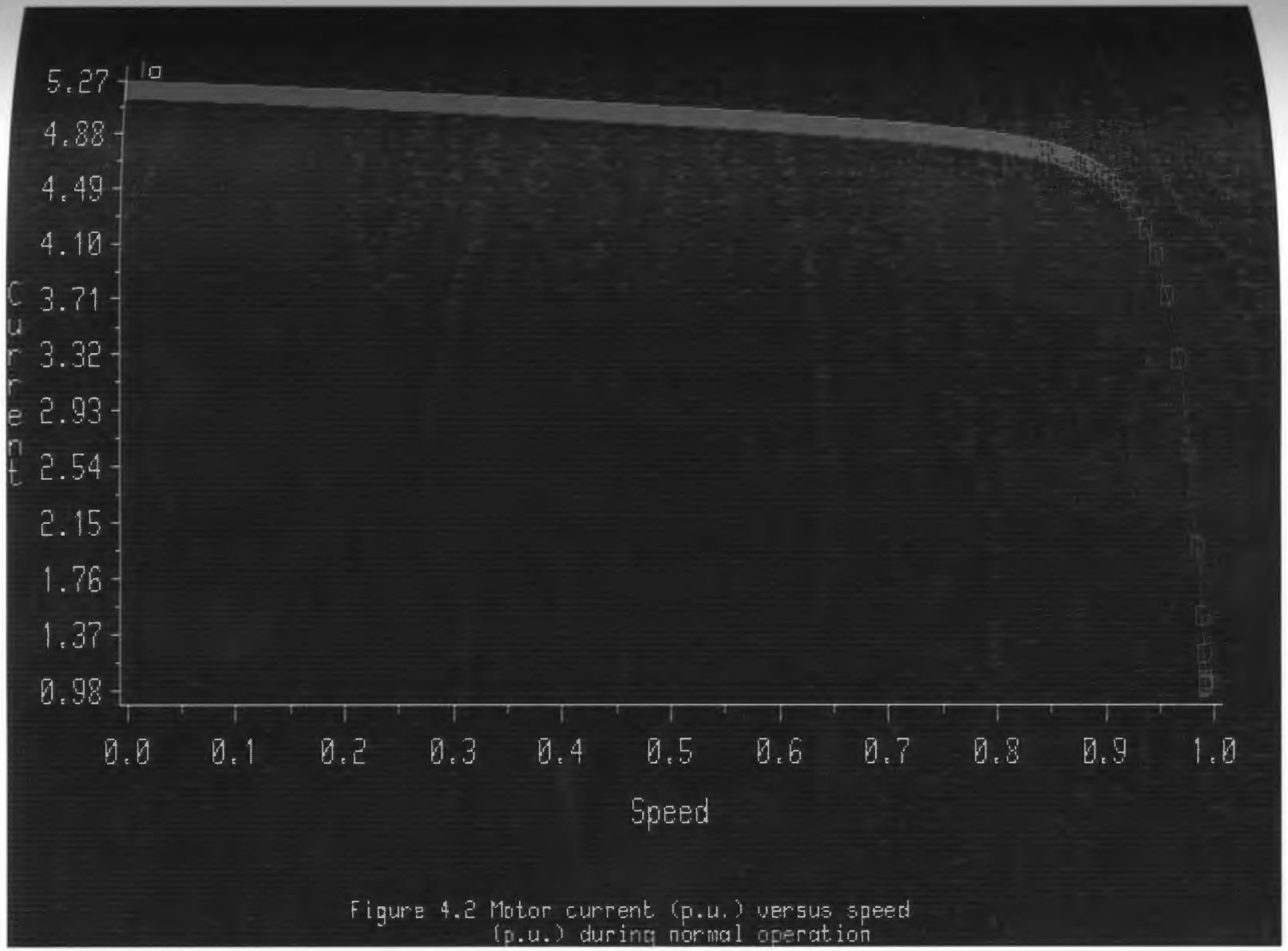

Figure 4.2 Motor current (p.u.) versus speed (p.u.) during normal operation

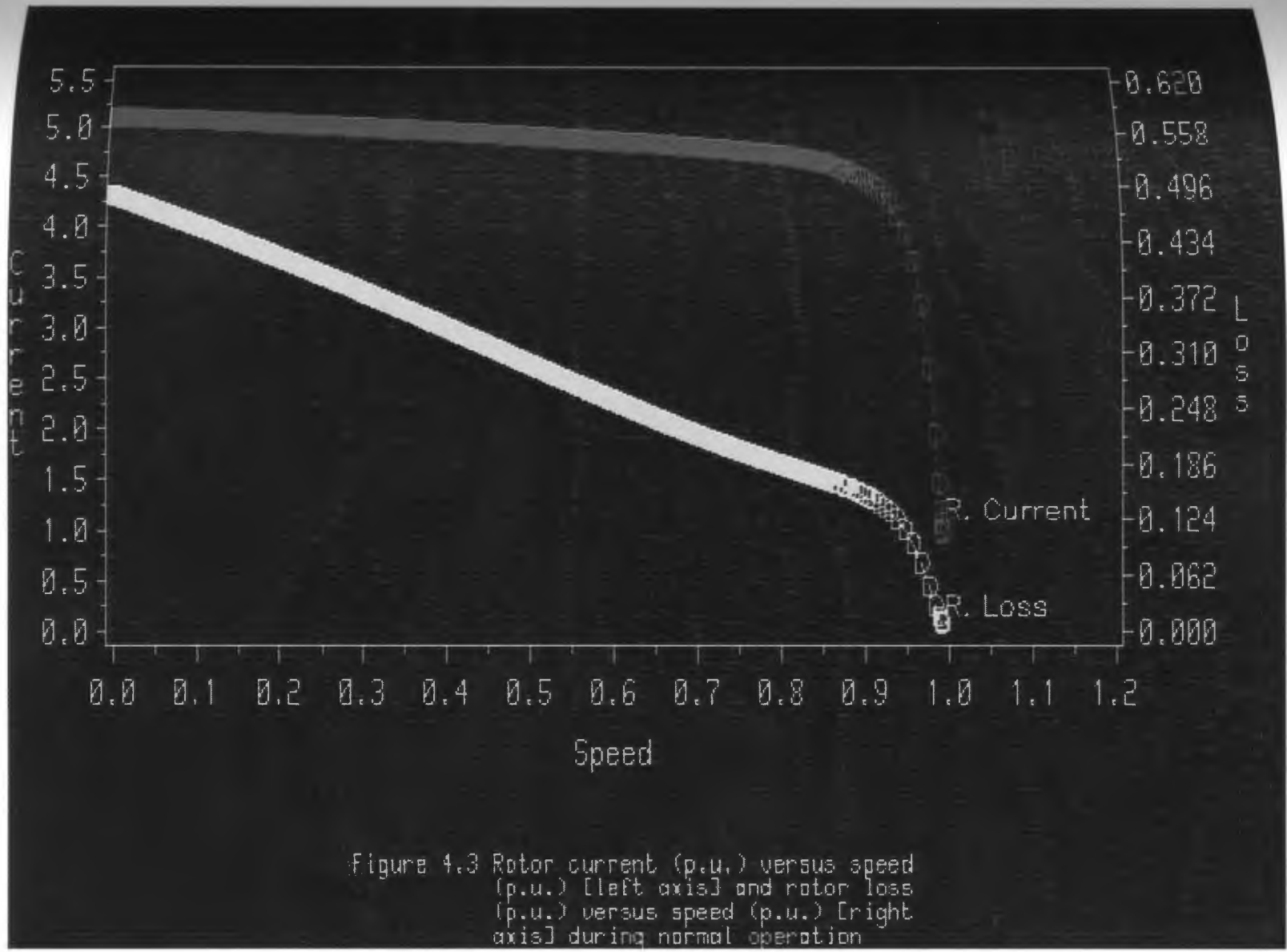

Figure 4.3 Rotor current (p.u.) versus speed (p.u.) [left axis] and rotor loss (p.u.) versus speed (p.u.) [right axis] during normal operation

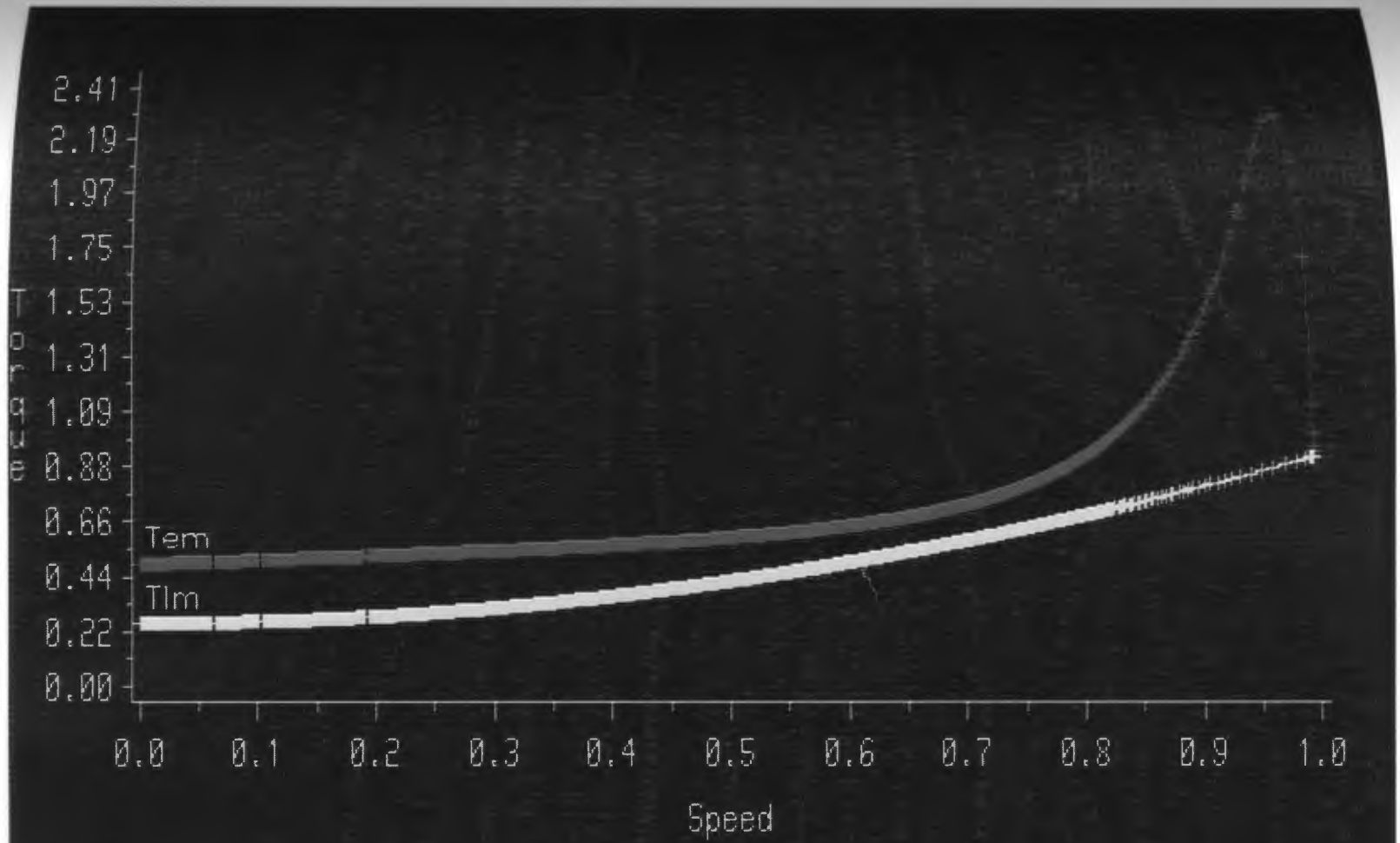

Figure 4.4 Motor electrical torque and mechanical load torque (p.u.) versus speed (p.u.) during normal operatiopn

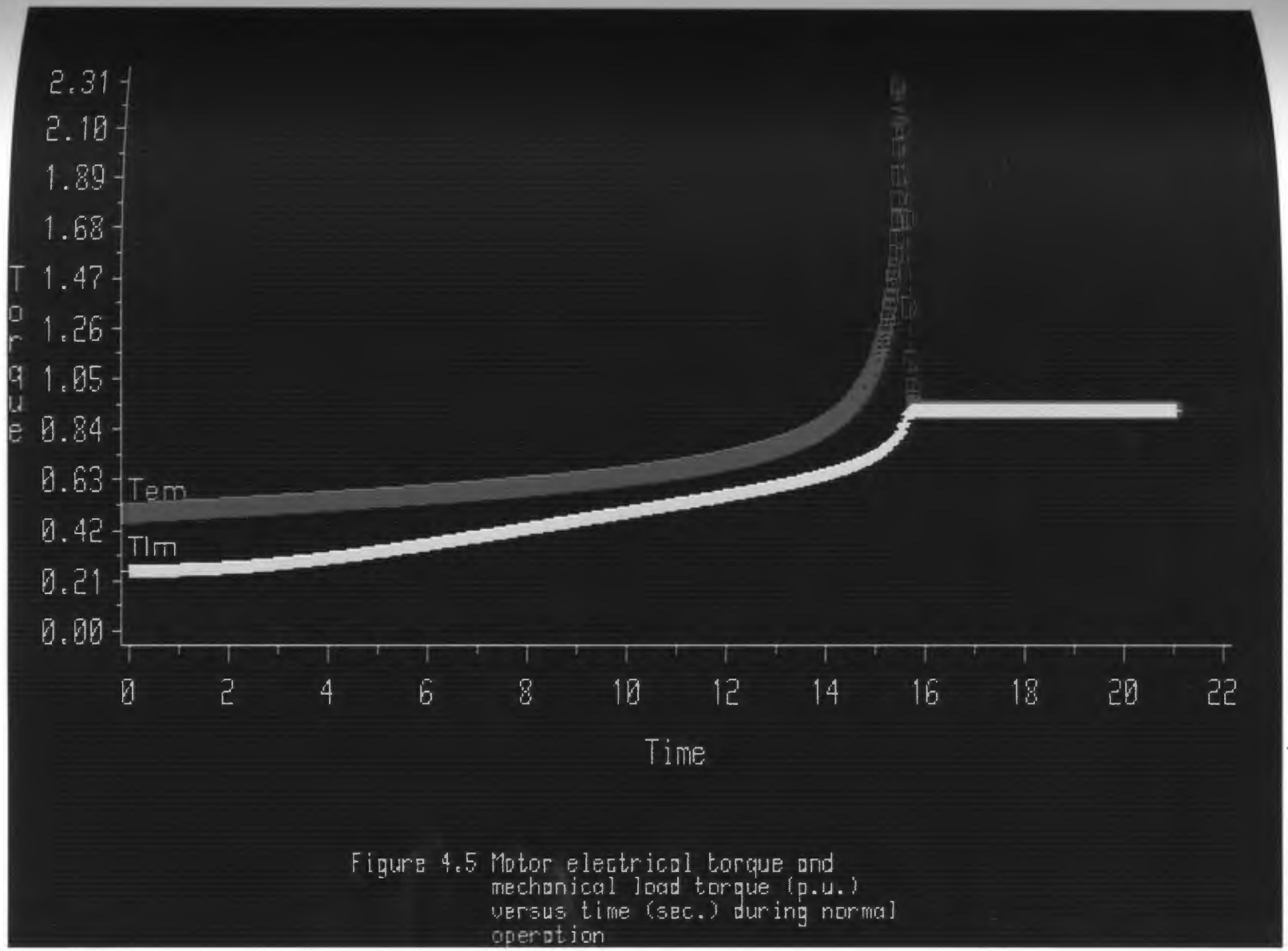

Figure 4.5 Motor electrical torque and mechanical load torque (p.u.) versus time (sec.) during normal operation

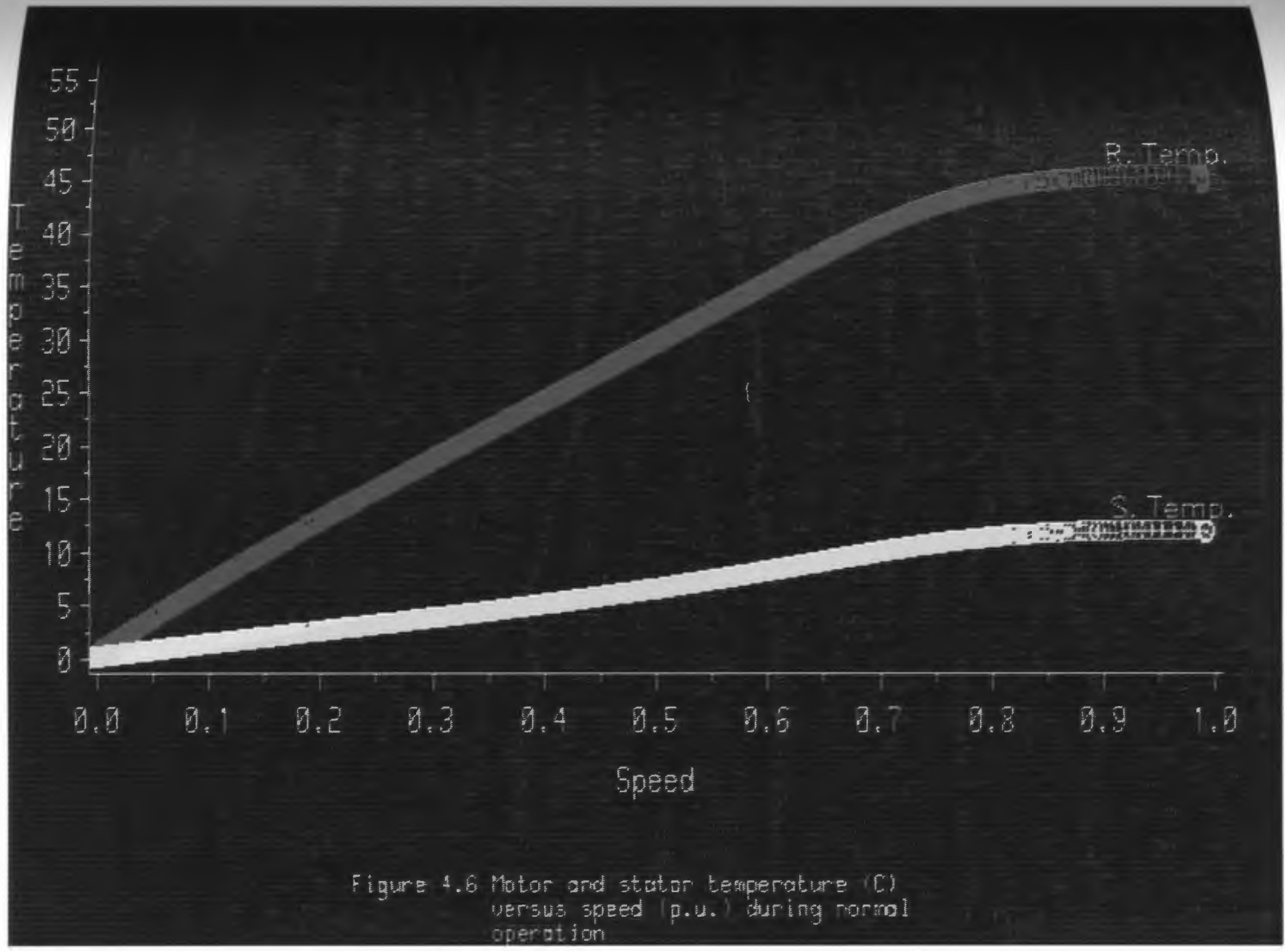

Figure 4.6 Motor and stator temperature (C) versus speed (p.u.) during normal operation

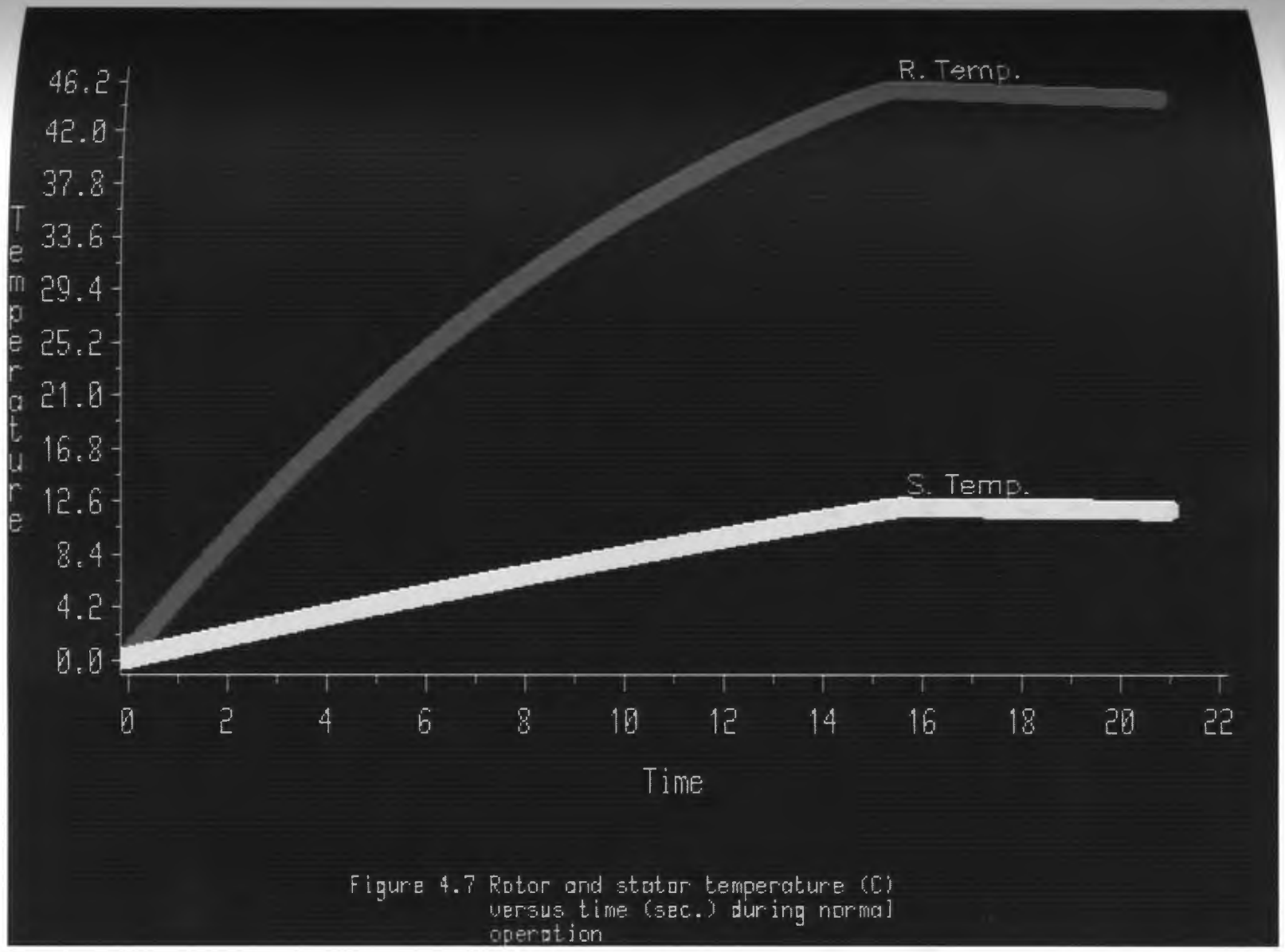

Figure 4.7 Rotor and stator temperature (C) versus time (sec.) during normal operation

Locked-Rotor Condition

When the initial load torque exceeds the starting torque developed by the motor, the motor cannot start. In the locked-rotor case, all input energy is converted to heat.

The thermal characteristic of the motor under the locked-rotor condition is shown in figure 4.8. As is predicted, the constant high locked-rotor current causes severe rotor overheating in almost 17 seconds. The computer program was set to isolate the motor when its temperature reaches the critical point. This cut off is shown in figure 4.8, where the current and torque suddenly dropped to zero level. Also the rotor and stator temperature started to drop after the motor was tripped from the system.

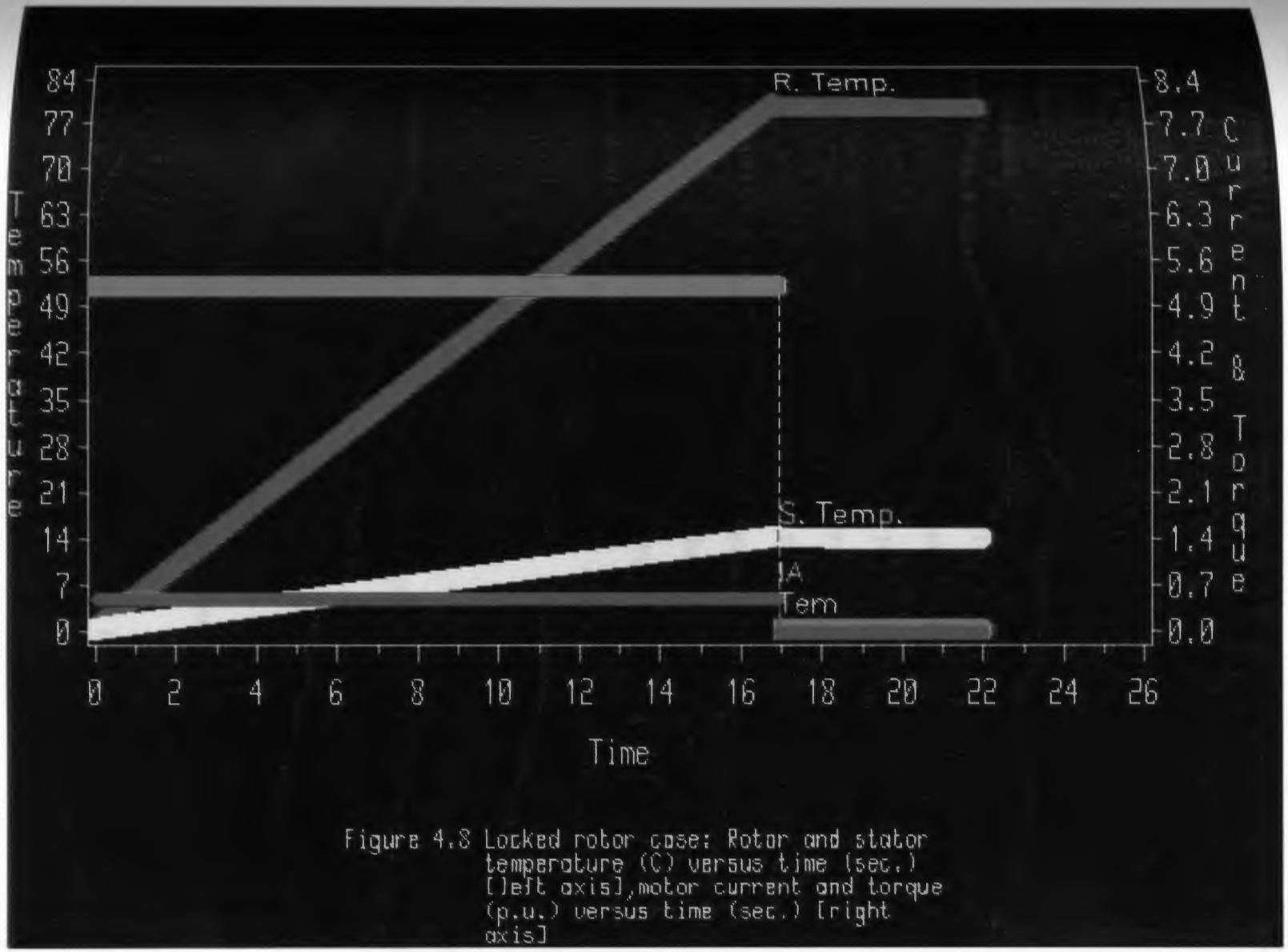

Figure 4.8 Locked rotor case: Rotor and stator temperature (C) versus time (sec.) [left axis], motor current and torque (p.u.) versus time (sec.) [right axis]

Unbalanced System Conditions

In order to study the effect of applying unbalanced voltage to the terminals of the motor, a single-phase to ground fault at the terminal of the motor was simulated. The single-phase to ground fault has been reported to be the most detrimental fault in motor heating (1,2,3).

Operation of polyphase induction motors with unbalanced voltages is undesirable. It causes ill effects such as excessive overheating and poor efficiency. Under unbalanced conditions, the motor current can be separated into positive and negative sequence components using the symmetrical component method as is discussed in chapter 3. The positive sequence component produces a magnetic flux wave in the motor air gap which travels in the direction of the motor rotation, and the negative sequence component produces a magnetic flux wave which travels in the reverse direction. The flux traveling in the reverse direction causes the development of a retarding torque. This retarding torque must be countered by increased torque in the direction of rotation, and hence by increased current levels in the motor. In extreme cases, the retarding torque can be of sufficient magnitude to cause the motor to stall [2].

Additionally, the interaction of the positively and negatively travelling flux wave causes vibrations that may cause resonance, be injurious to bearings, to insulation, and interconnecting mechanical equipment.

The damaging heat level to which the motor is subjected is due to the fact that the reverse rotating field induces rotor currents at

twice stator frequency minus slip. Because of the skin-effect ,the effective rotor resistance to these currents is between 3 to 8 times as much as of the positive sequence rotor resistance. The negative sequence currents therefore produce more rotor heat per ampere than positive sequence current.

At steady state operating points, problems due to unbalanced voltage are avoided by ensuring that the permissible level of voltage unbalance will not cause destructive overheating and by designing the motor mechanical system so that no mechanical resonances occur near 120 Hz. At the dynamic state level, the interaction of an induction motor with an unbalanced power supply has not been closely studied. Protection of the motor from these problems is largely limited to overcurrent and overload protection to prevent motor overheating.

Motor Heating During System Unbalanced Faults

System unbalanced faults are very common and can occur anywhere from the motor terminals up to the transmission system. These faults are caused by insulation failure between phase conductors or between phase conductors and earth, or both.

Motor performance during this fault has not been studied thoroughly. No attempt has been made to estimate the motor temperature during this fault. Motor protection is largely limited to overload and overcurrent protection. These relays only sense phase currents. These currents do not reflect the actual rotor heating during unbalanced system conditions. Therefore, the motor protection relays may operate after or long before the motor has

experienced serious rotor overheating.

In this study, the motor performance and heating during a single phase to ground fault is studied. Since most faults occur at the motor terminals, in this study the fault is assumed to occur at motor terminals. Also, the system is considered to have a positive and negative sequence impedance of 0.0001+j0.05055 p.u. and a zero sequence impedance of j0.051 p.u. on the motor rating taken as a base.

Depending on the fault impedance, motor load, and motor class the motor may stall or continue carrying its full load during the unbalanced condition (1,2).

In this study, the motor under investigation is supposed to operate as a pump while carrying a load of $T_{lm} = 0.25 + 0.67572\,\omega_r^2$ p.u. A single-phase to ground fault was simulated to study the performance of the motor under unbalanced conditions, and to estimate the rotor end-rings' temperature.

It is assumed that the motor has been running at rated speed. A single-phase to ground fault occurred on phase A at the motor terminal. The fault impedance is assumed to be j0.05 p.u. on the motor rating taken as a base. The positive and negative sequence torques developed by the motor during the fault are shown in figure 4.9. The load torque and the net torque developed by the motor are shown in figure 4.10. The motor would not be able to handle the load and the motor stalled. Also the load torque characteristic and the torque developed by the motor against time are shown in figure 4.11. The initial point (t=0) corresponds to the time when the fault

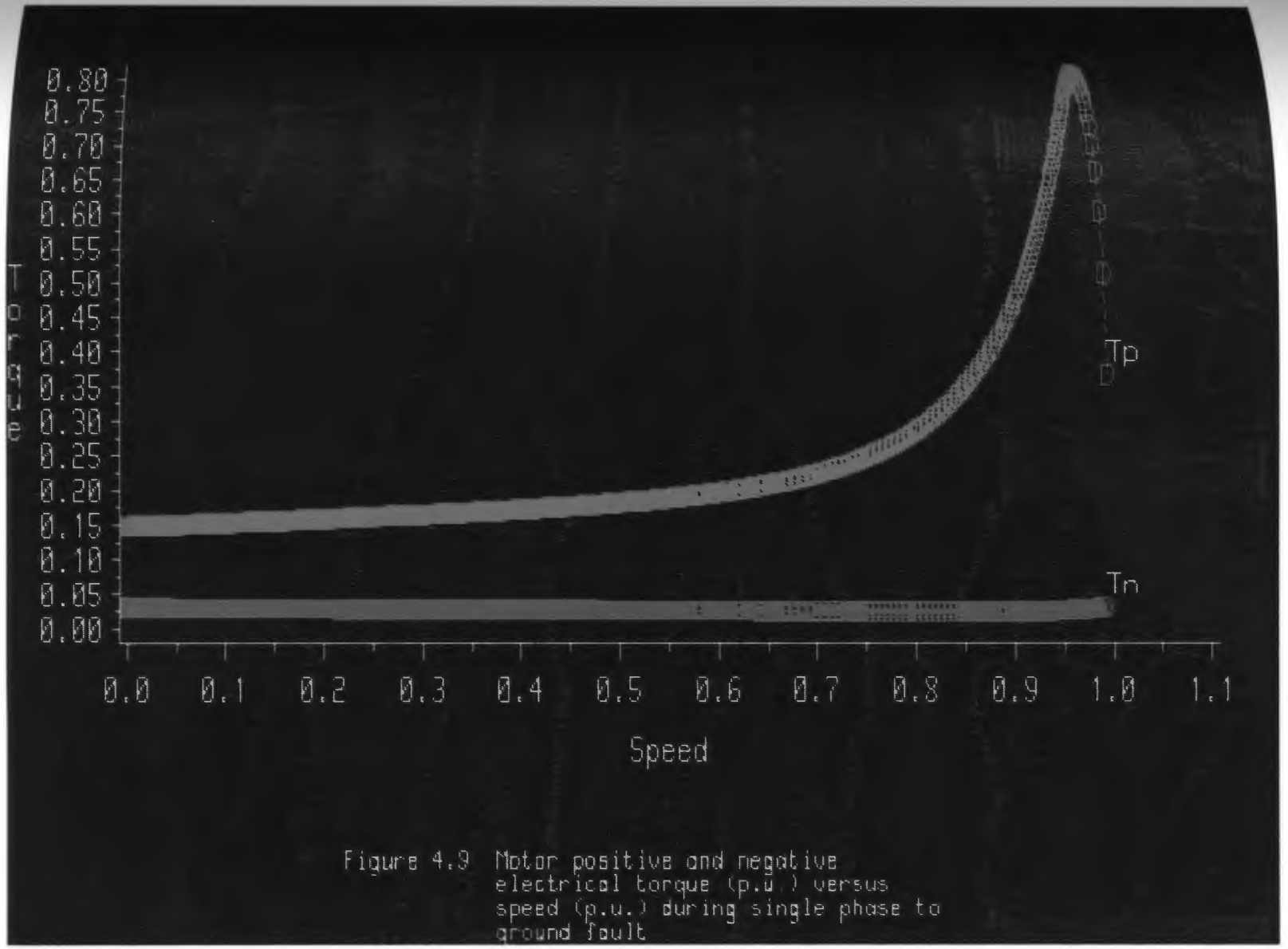

Figure 4.9 Motor positive and negative electrical torque (p.u.) versus speed (p.u.) during single phase to ground fault

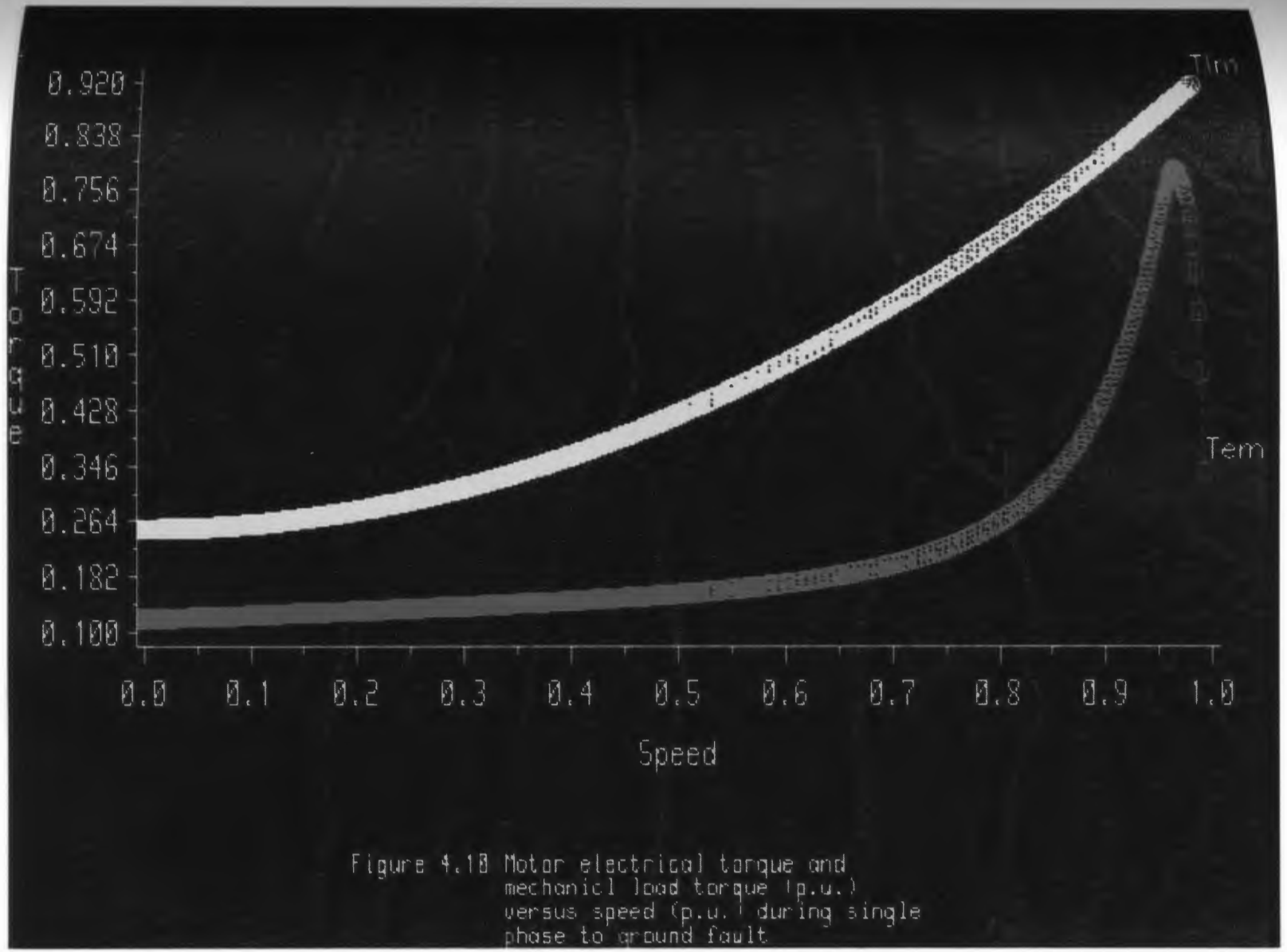

Figure 4.18 Motor electrical torque and mechanical load torque (p.u.) versus speed (p.u.) during single phase to ground fault

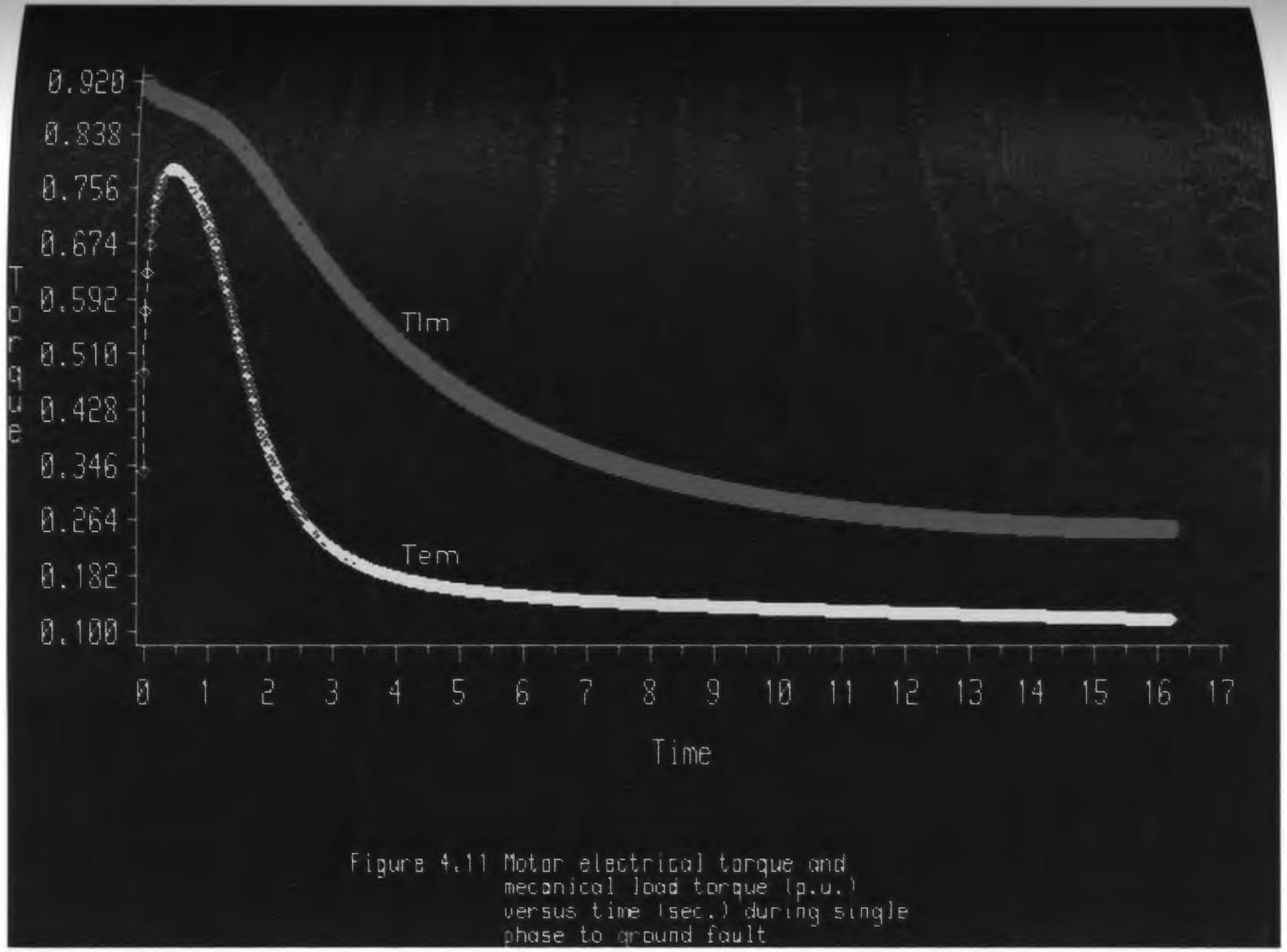

Figure 4.11 Motor electrical torque and mecanical load torque (p.u.) versus time (sec.) during single phase to ground fault

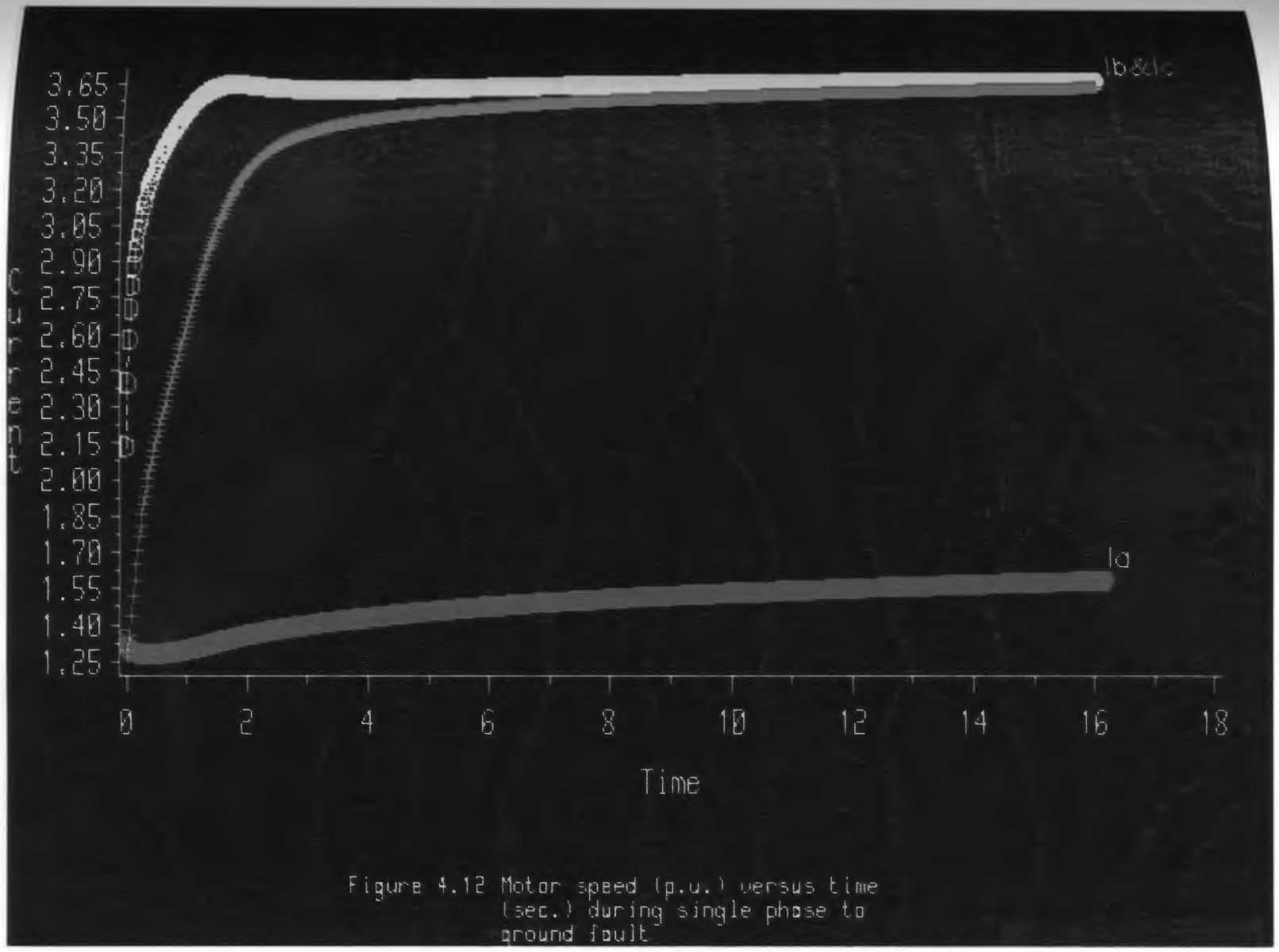

Figure 4.12 Motor speed (p.u.) versus time (sec.) during single phase to ground fault

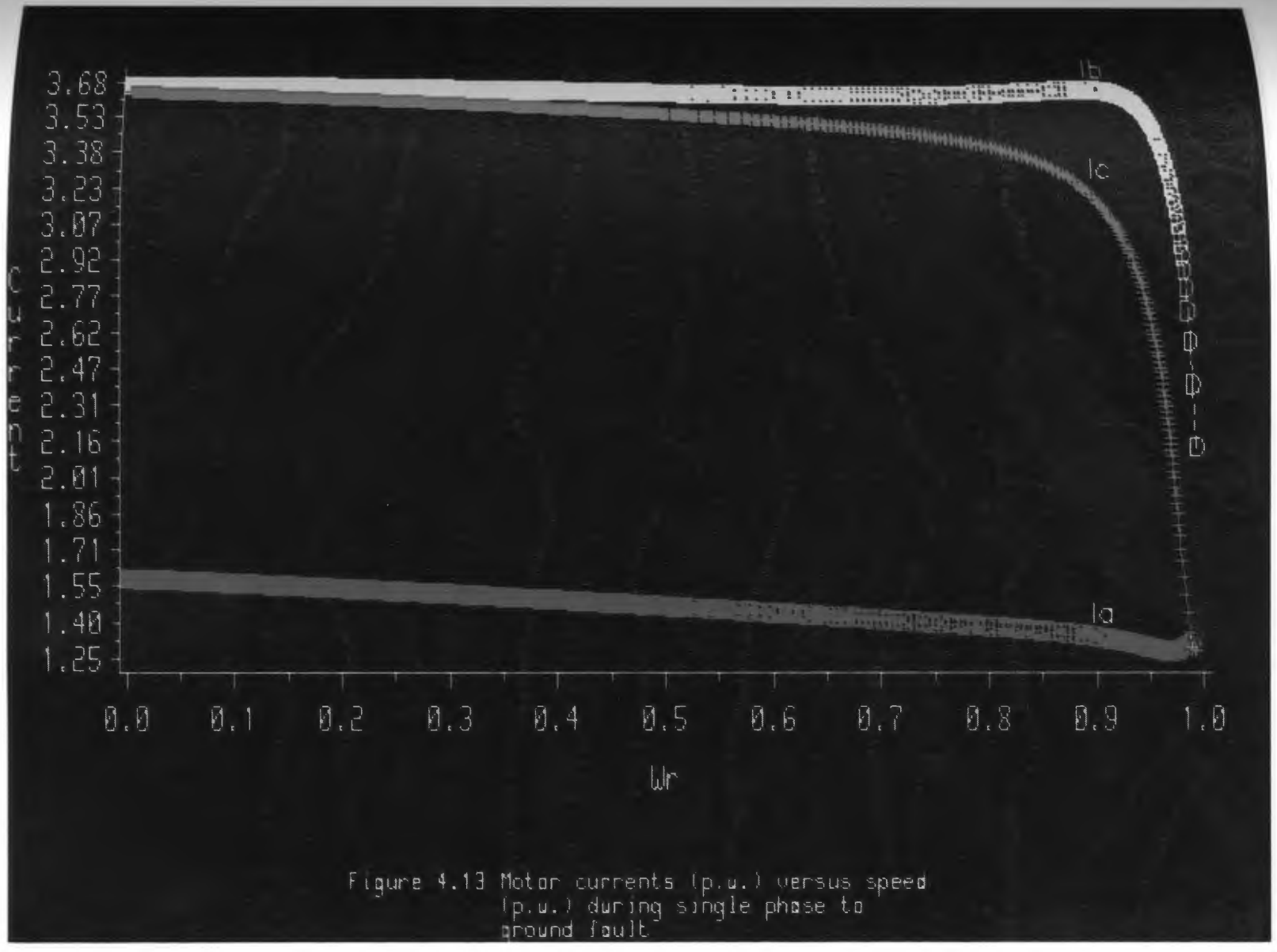

Figure 4.13 Motor currents (p.u.) versus speed (p.u.) during single phase to ground fault

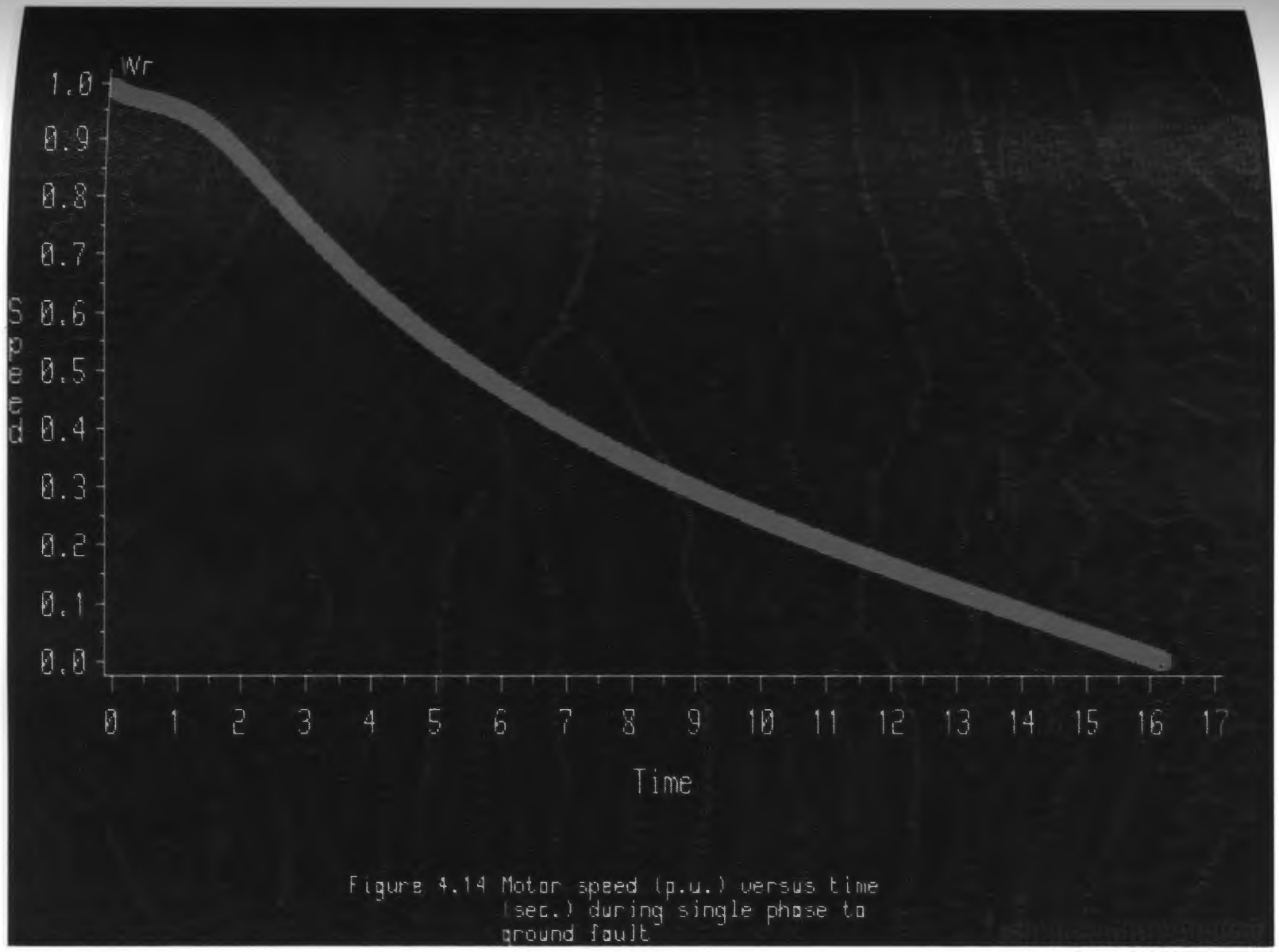

Figure 4.14 Motor speed (p.u.) versus time (sec.) during single phase to ground fault

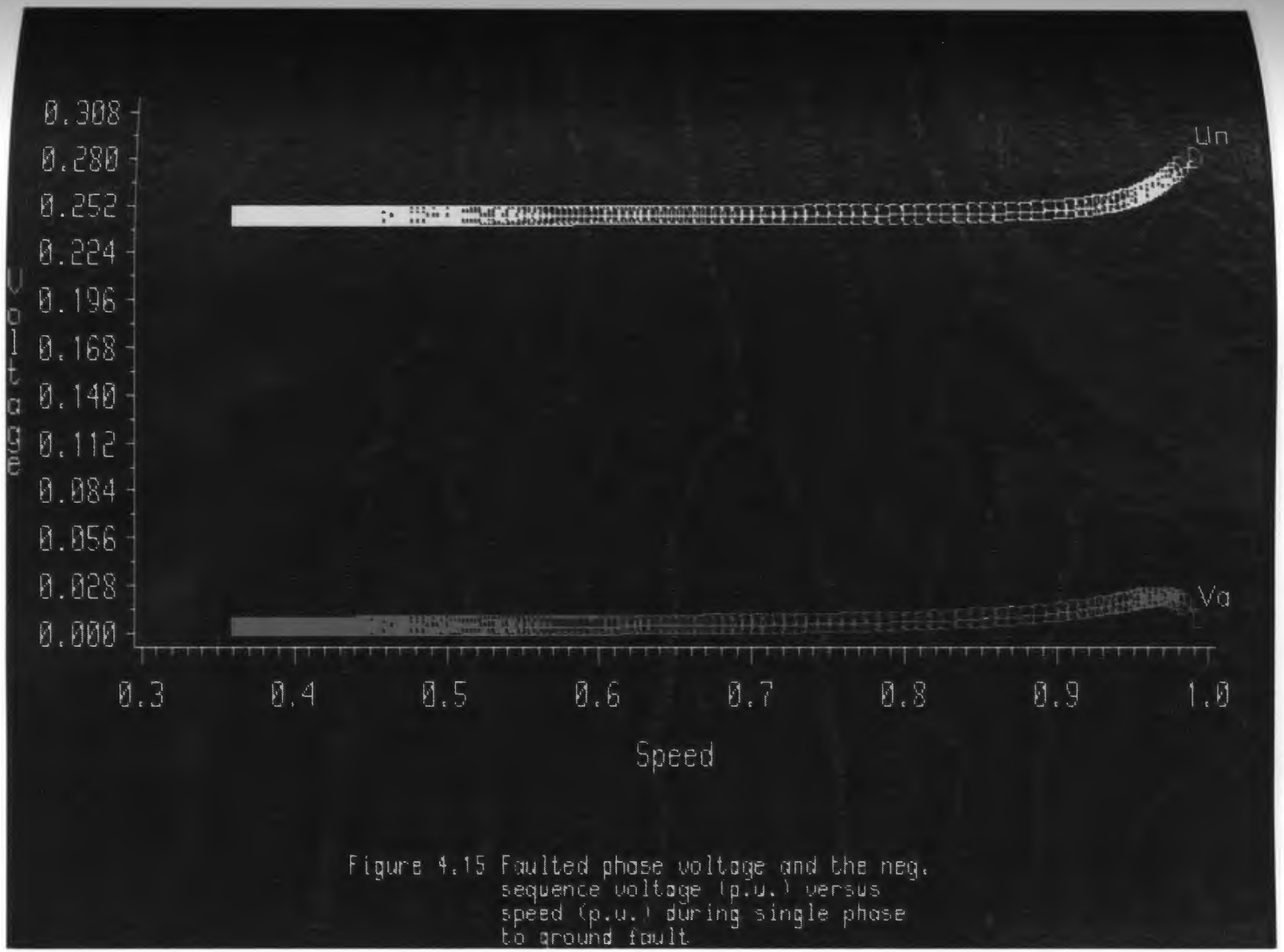

Figure 4.15 Faulted phase voltage and the neg. sequence voltage (p.u.) versus speed (p.u.) during single phase to ground fault

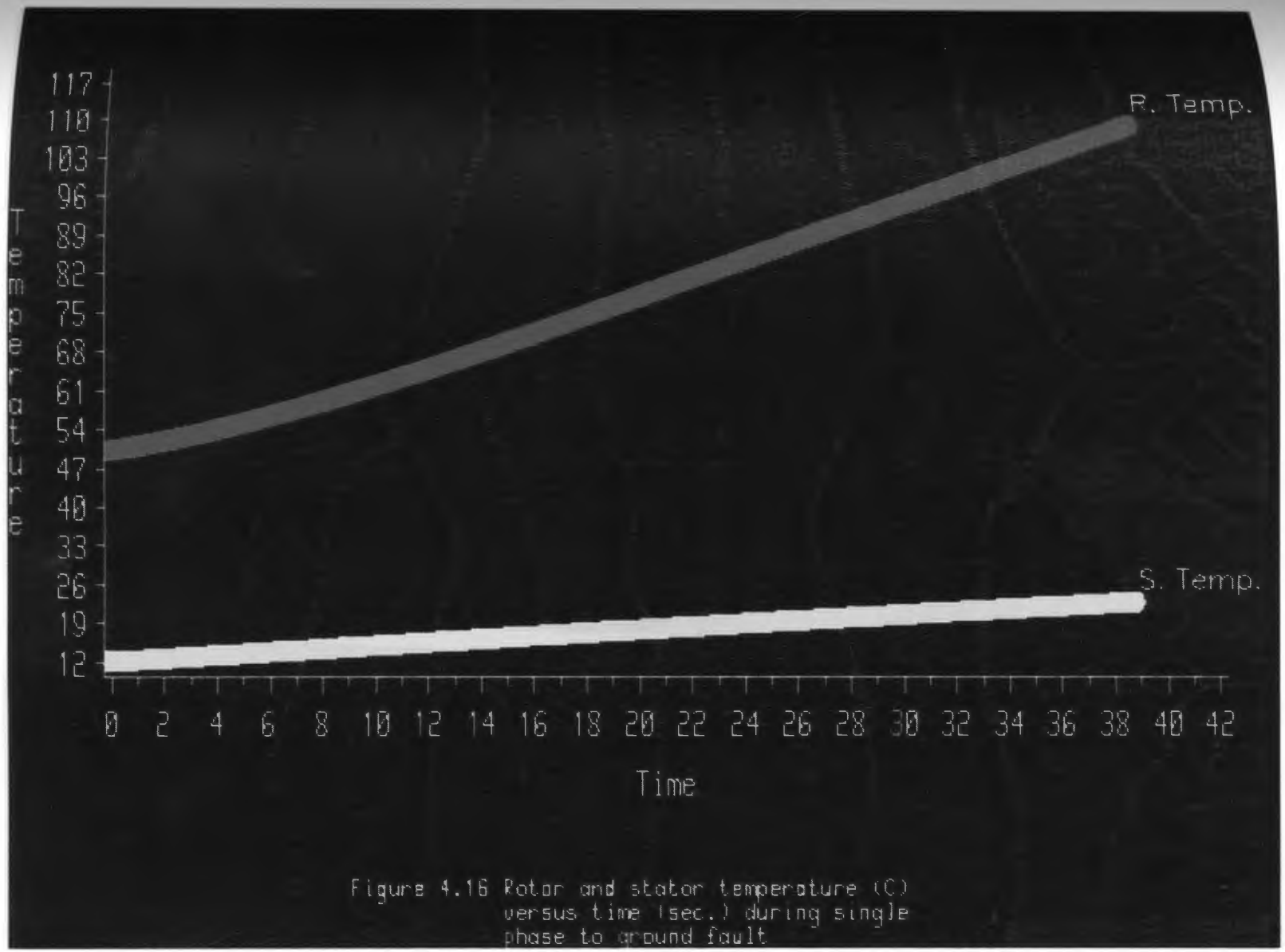

Figure 4.16 Rotor and stator temperature (C) versus time (sec.) during single phase to ground fault

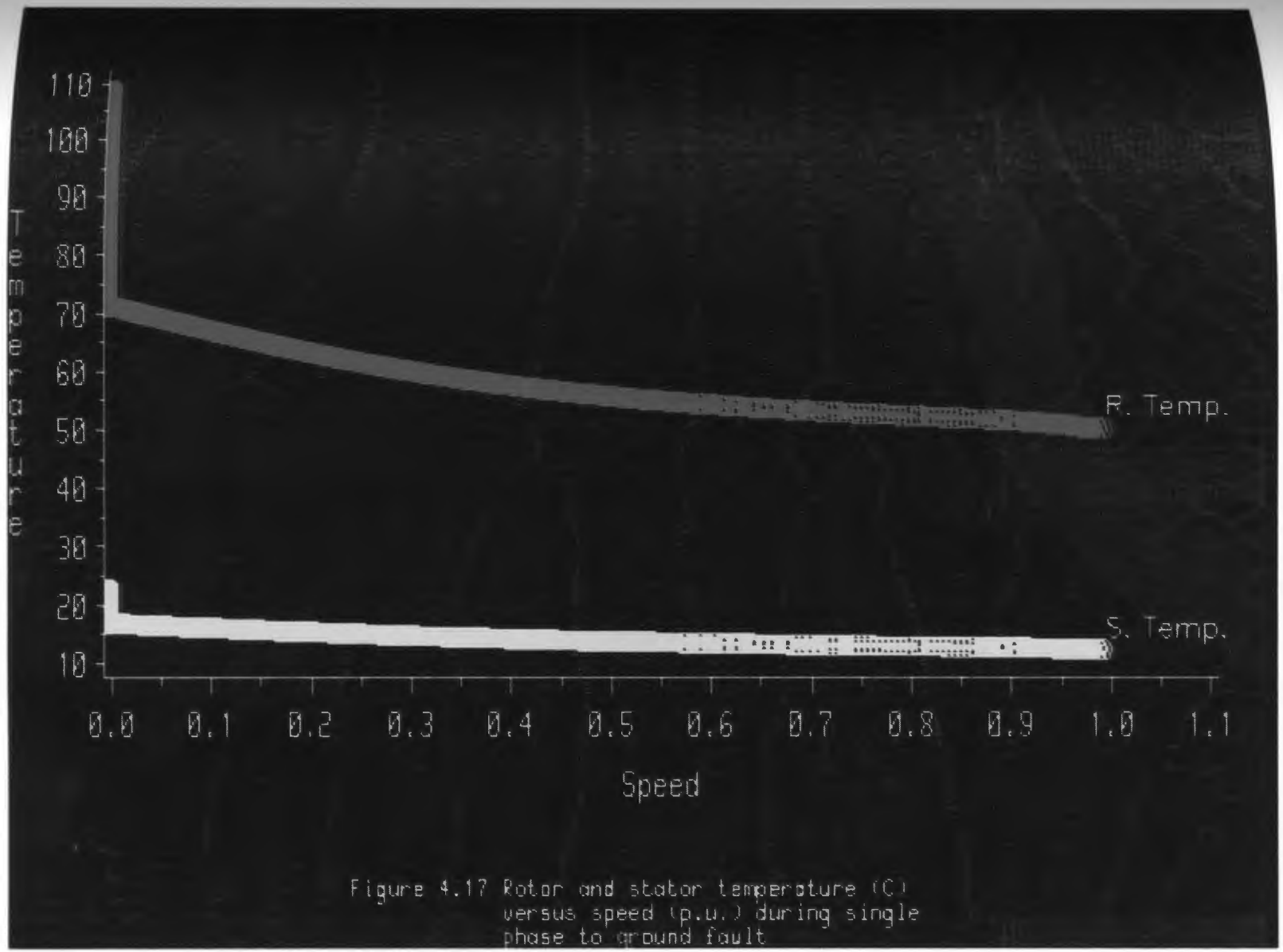

Figure 4.17 Rotor and stator temperature (C) versus speed (p.u.) during single phase to ground fault

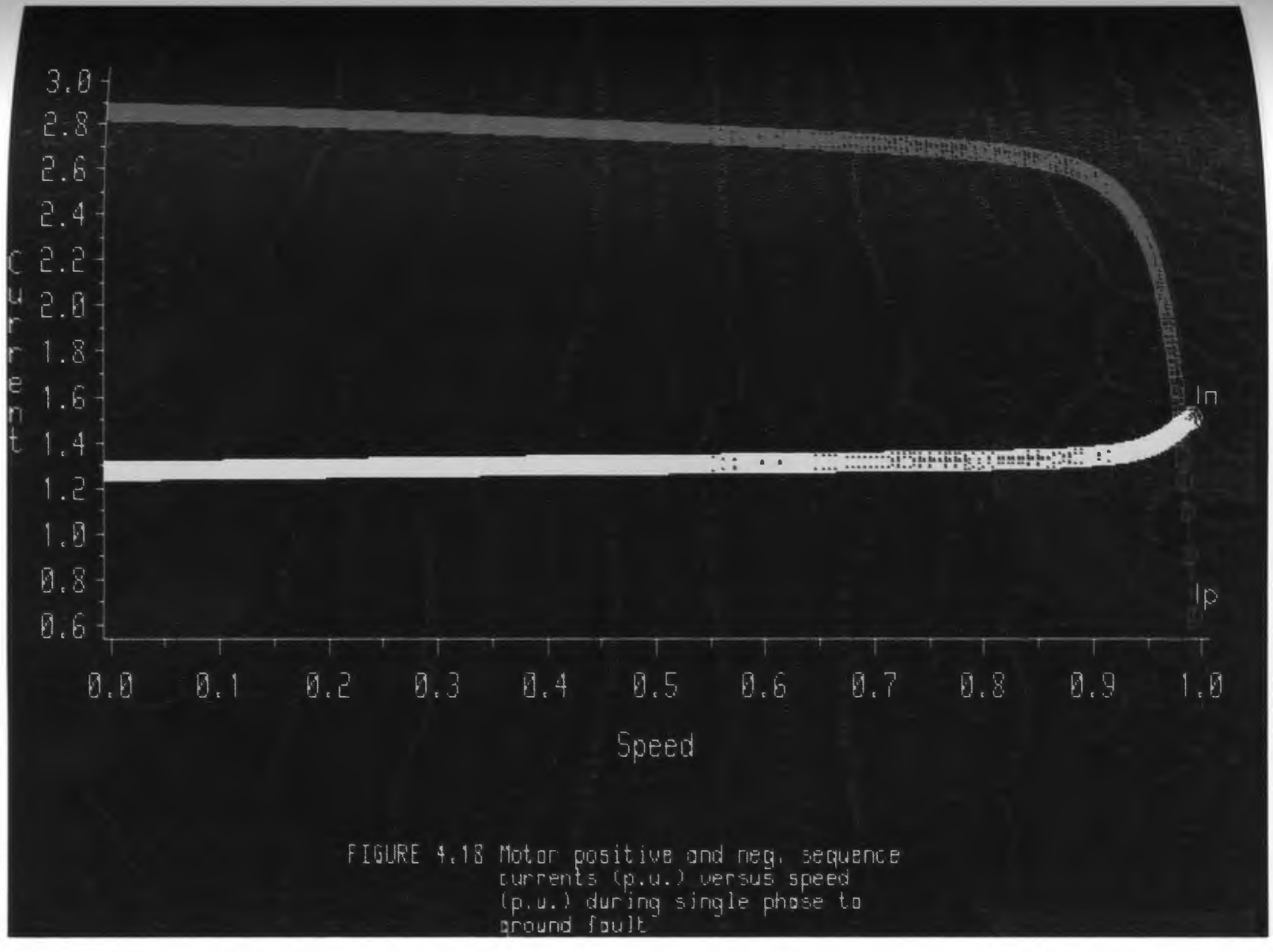

FIGURE 4.18 Motor positive and neg. sequence currents (p.u.) versus speed (p.u.) during single phase to ground fault

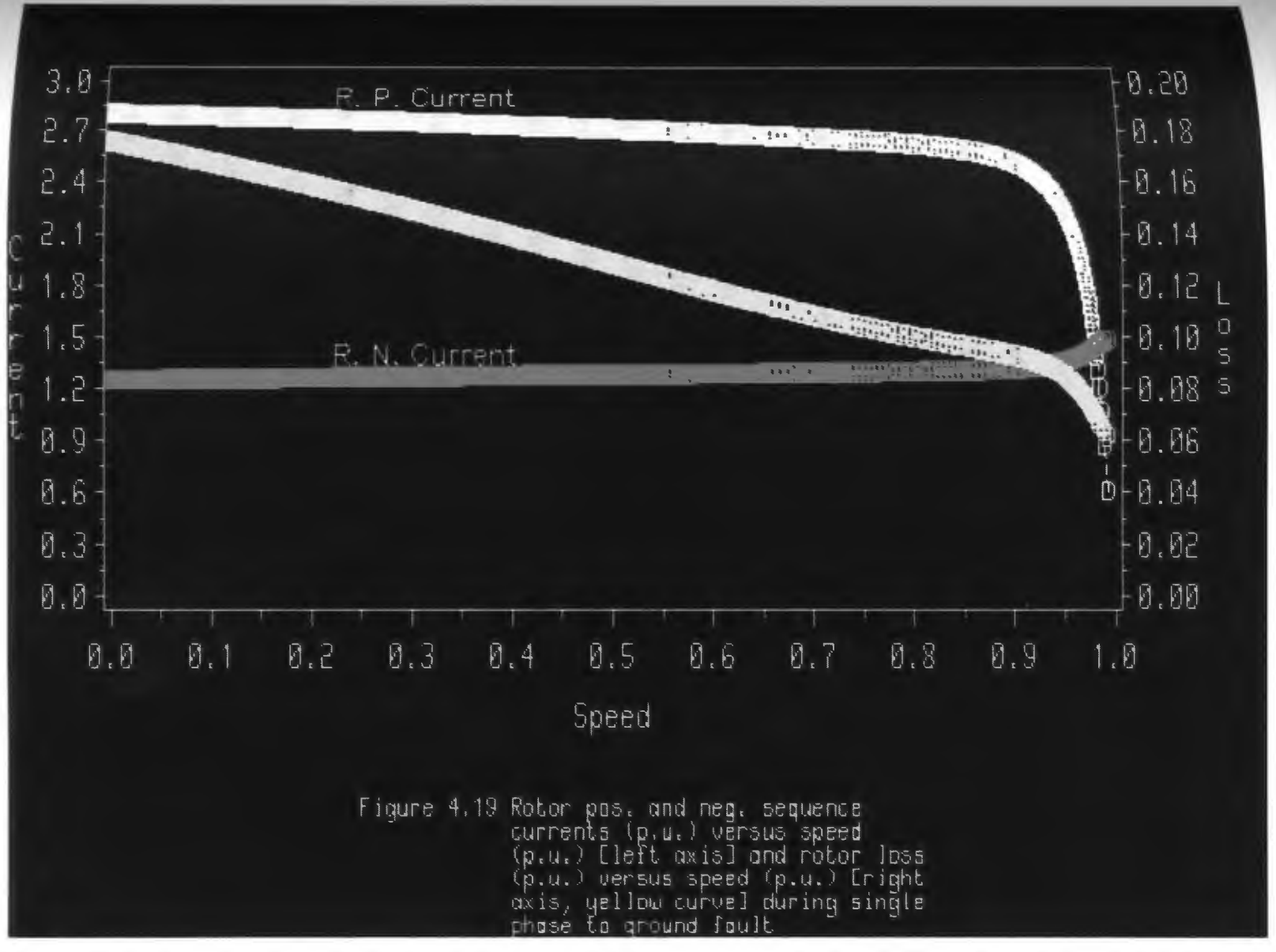

Figure 4.19 Rotor pos. and neg. sequence currents (p.u.) versus speed (p.u.) [left axis] and rotor loss (p.u.) versus speed (p.u.) [right axis, yellow curve] during single phase to ground fault

High Inertia Loading

High inertia loading is a very difficult task for conventional protection schemes to detect. The starting time for a motor carrying a high inertia load is often longer than the permissible locked-rotor time. For this reason the existing protective relays operate mistakenly while the motor is thermally relaxed. In this work, the constant of inertia H (defined in table C.1) has been changed from 1.74 seconds to 2.27 seconds in order to investigate the motor thermal performance during high inertia loading. As is shown in figure 4.20, the motor reaches rated speed in about 20 seconds. This is longer than the permissible locked-rotor time for this particular motor. The thermal characteristics of the motor, while operating under high inertia load, are shown in figures 4.21 and 4.22. The maximum temperature rise in the rotor in this case is about 70 percent of the critical point. After reaching rated speed this temperature starts dropping. One of the objectives of the proposed protection scheme is to avoid tripping the motor unnecessarily. The motor current behavior during high inertia start up is the same as that during the normal condition, as is shown in figure 4.23. The time-speed characteristic is shown in figure 4.24. The motor load and torque against motor speed are shown in figure 4.25. In this case, as has been discussed, the current characteristic under high inertia and normal loading with $T_{lm} = 0.25 + 0.67572\,\omega_r^2$ p.u. is the same. The only difference that causes more heat in the high inertia case is the long start up time. In the high inertia case, for a particular interval of time the increase of speed is less than that during the same interval

of time for the normal case. Therefore the motor is experiencing the same heat for a longer period of time. Thus, the heat peak during high inertia starting is higher than that during normal operation. However, the motor is still far below its thermal limit.

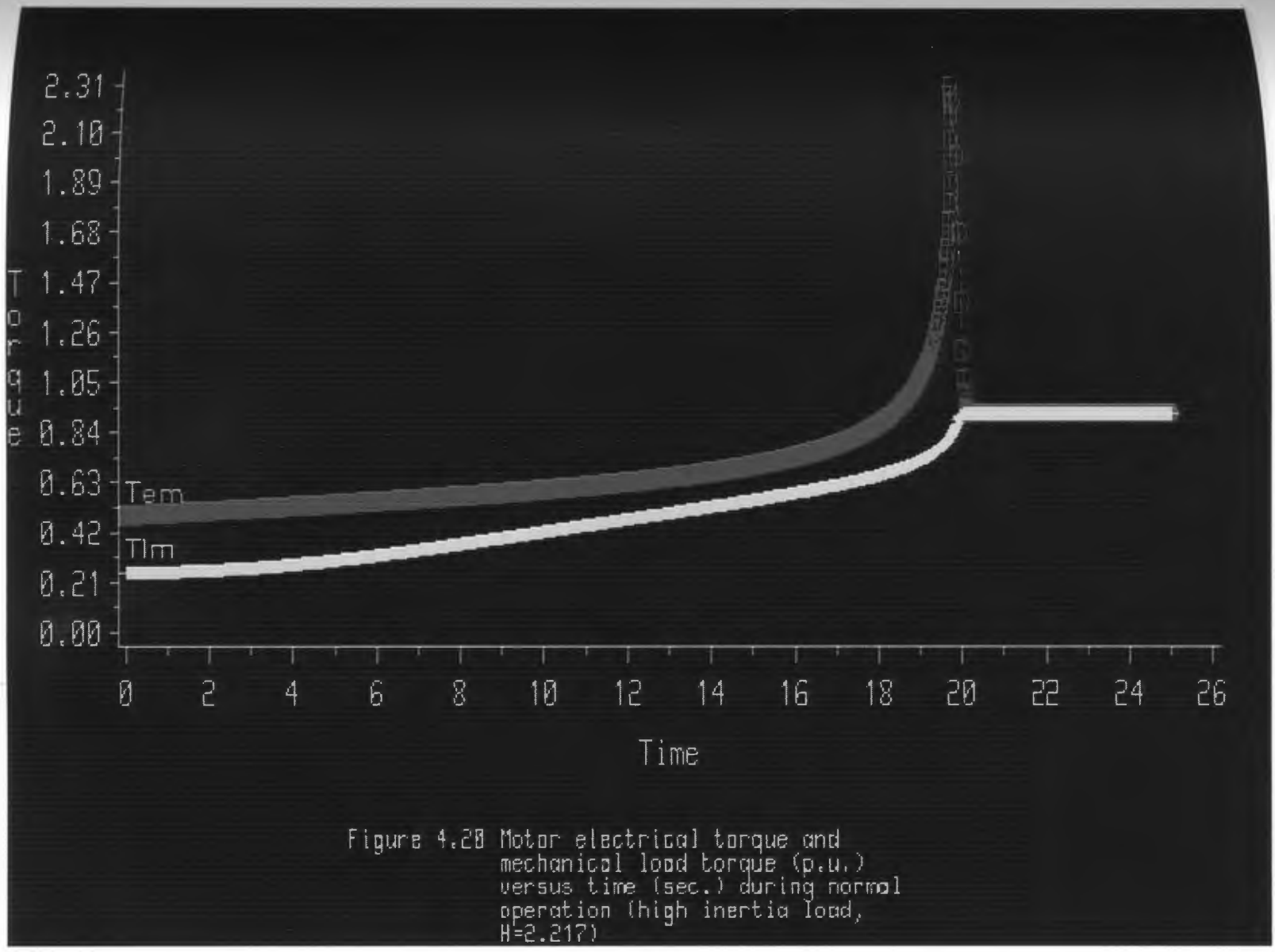

Figure 4.28 Motor electrical torque and mechanical load torque (p.u.) versus time (sec.) during normal operation (high inertia load, H=2.217)

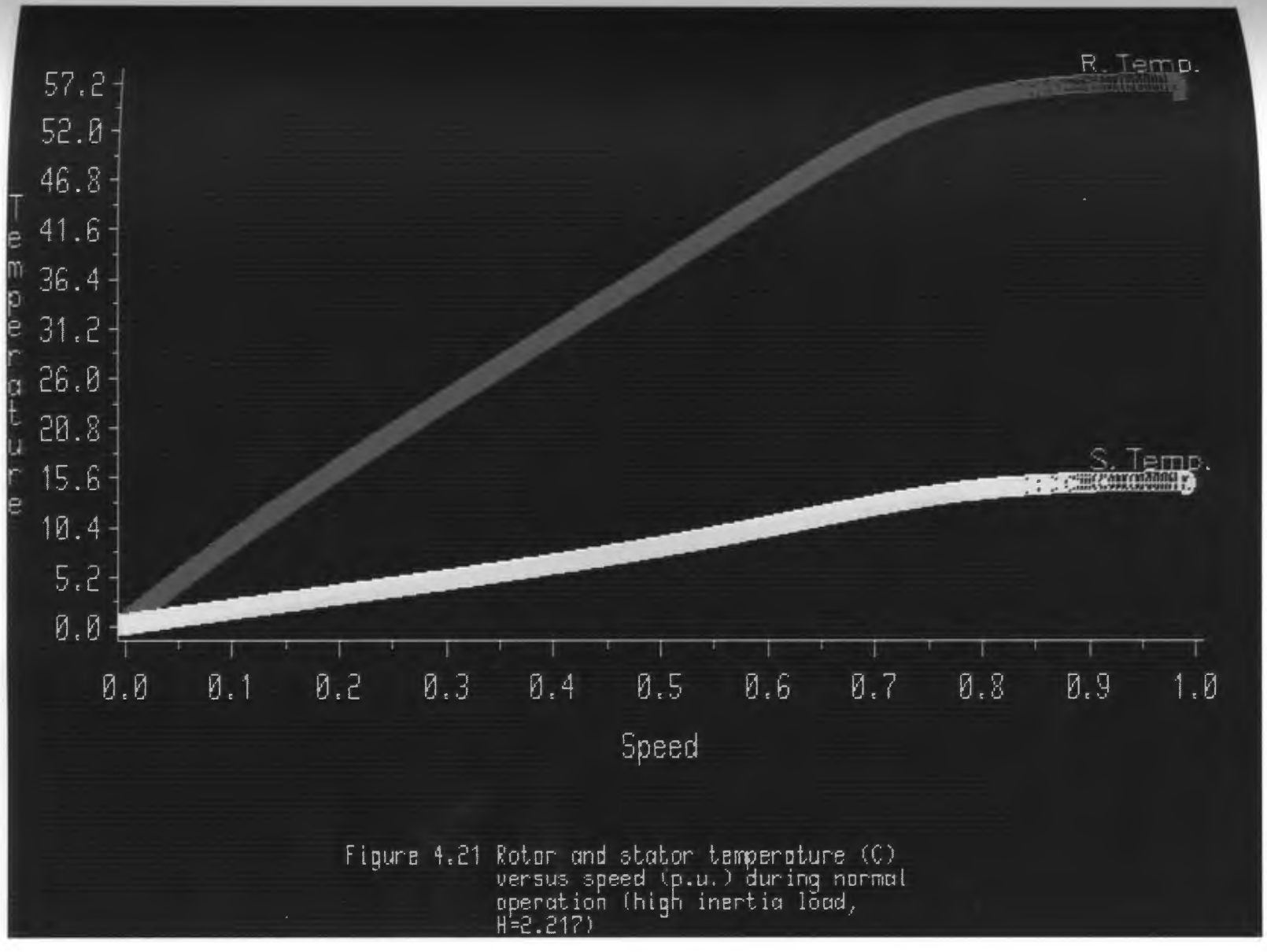

Figure 4.21 Rotor and stator temperature (C) versus speed (p.u.) during normal operation (high inertia load, H=2.217)

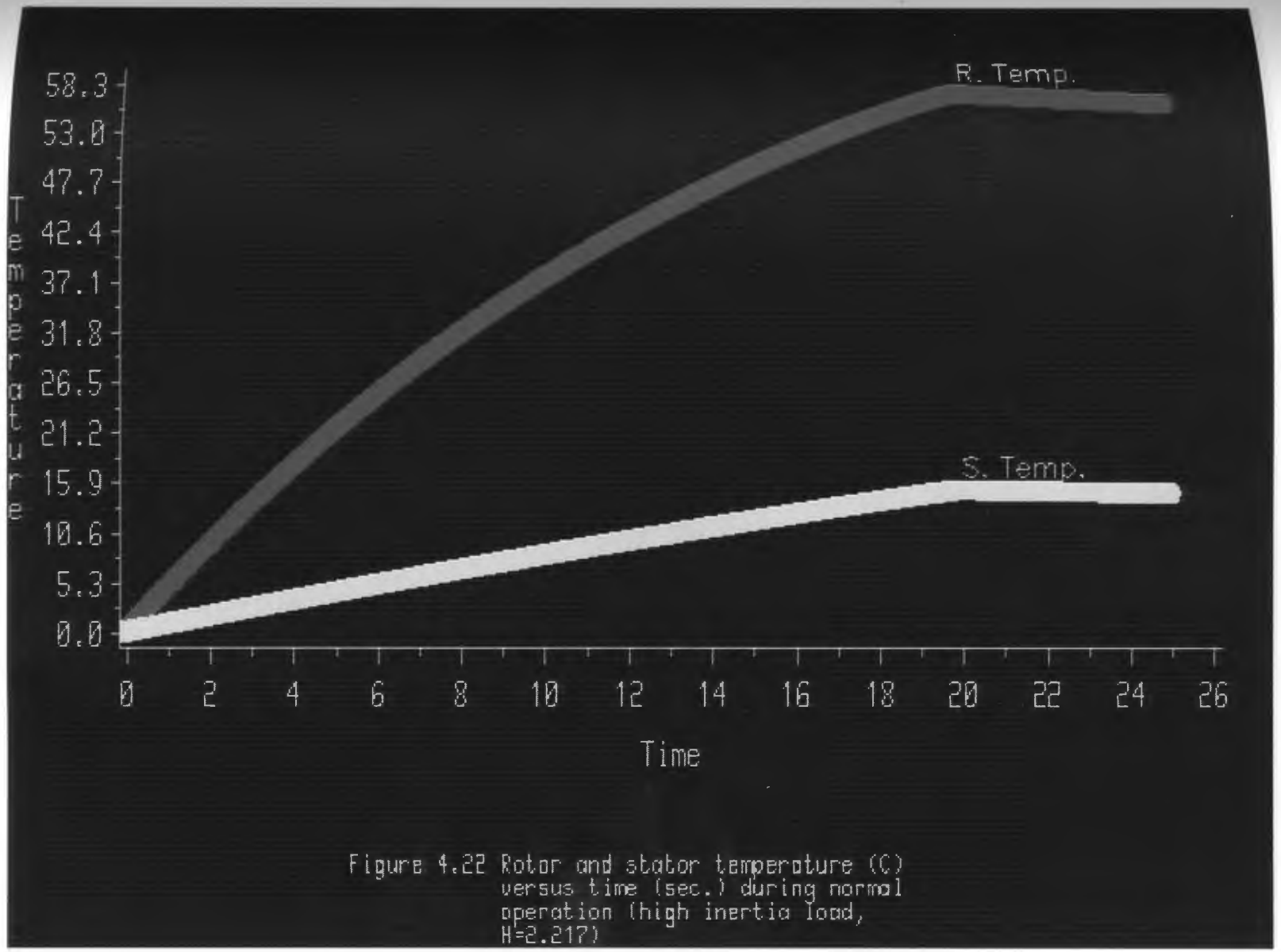

Figure 4.22 Rotor and stator temperature (C) versus time (sec.) during normal operation (high inertia load, H=2.217)

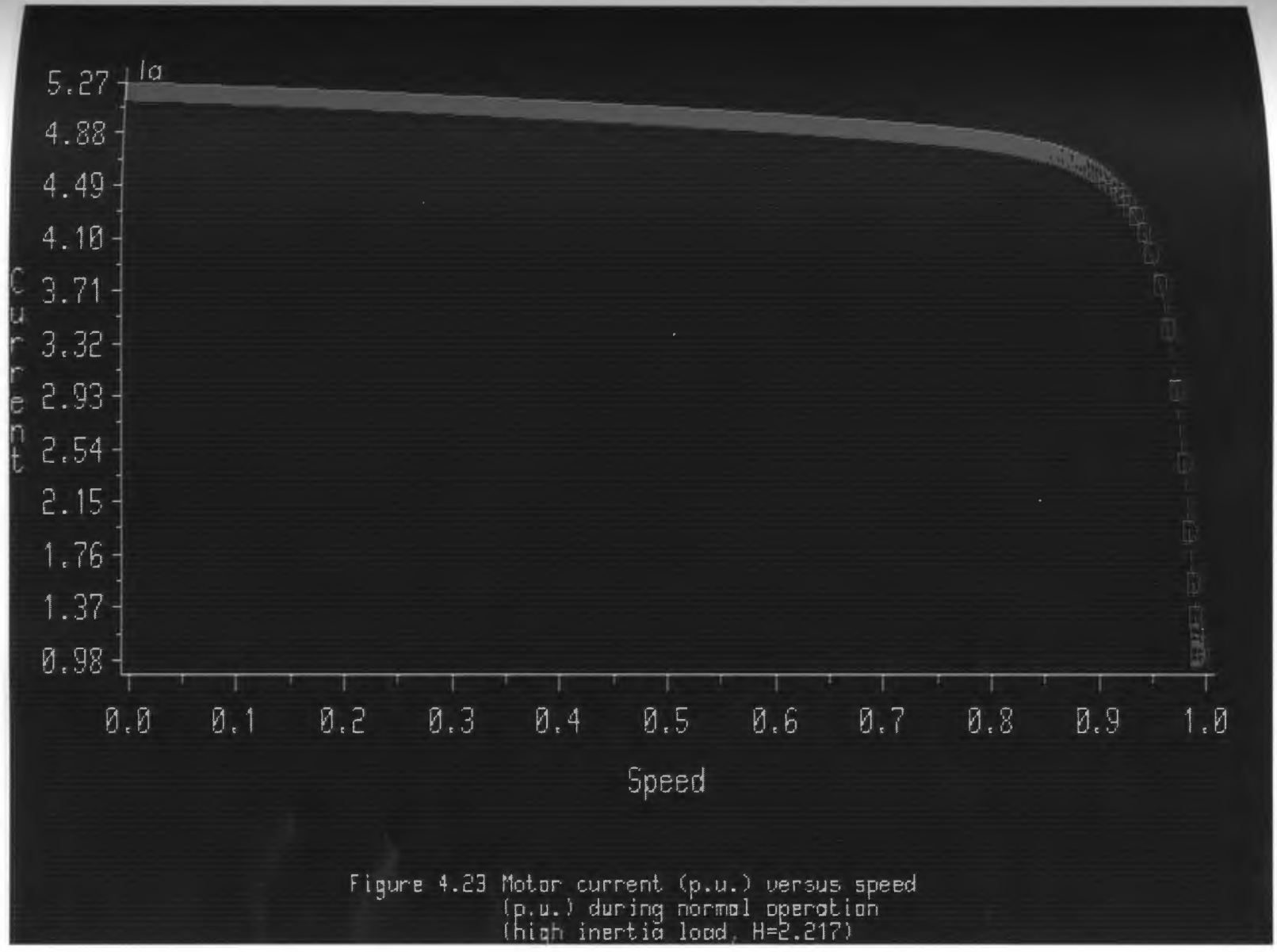

Figure 4.23 Motor current (p.u.) versus speed (p.u.) during normal operation (high inertia load, H=2.217)

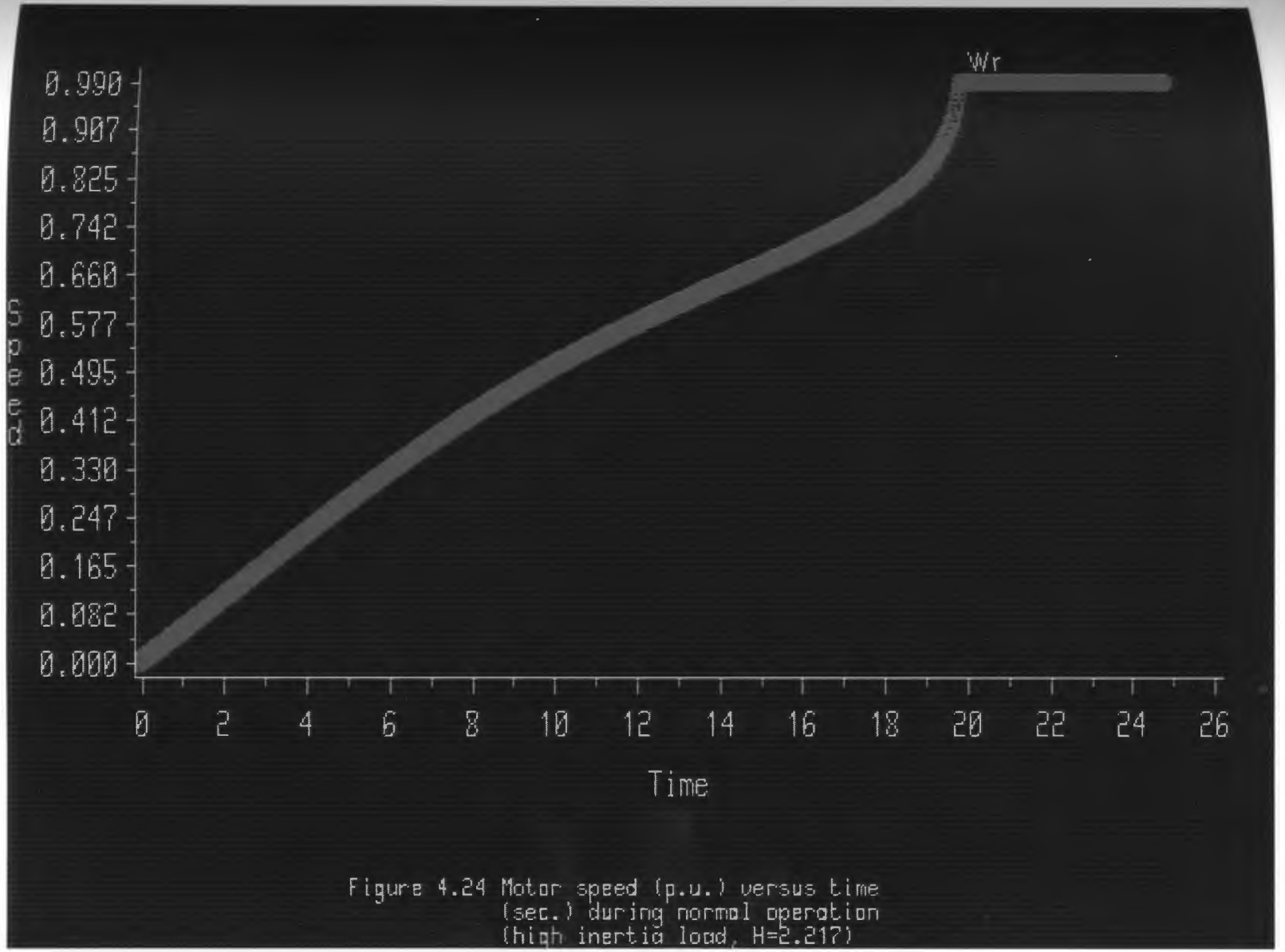

Figure 4.24 Motor speed (p.u.) versus time (sec.) during normal operation (high inertia load, H=2.217)

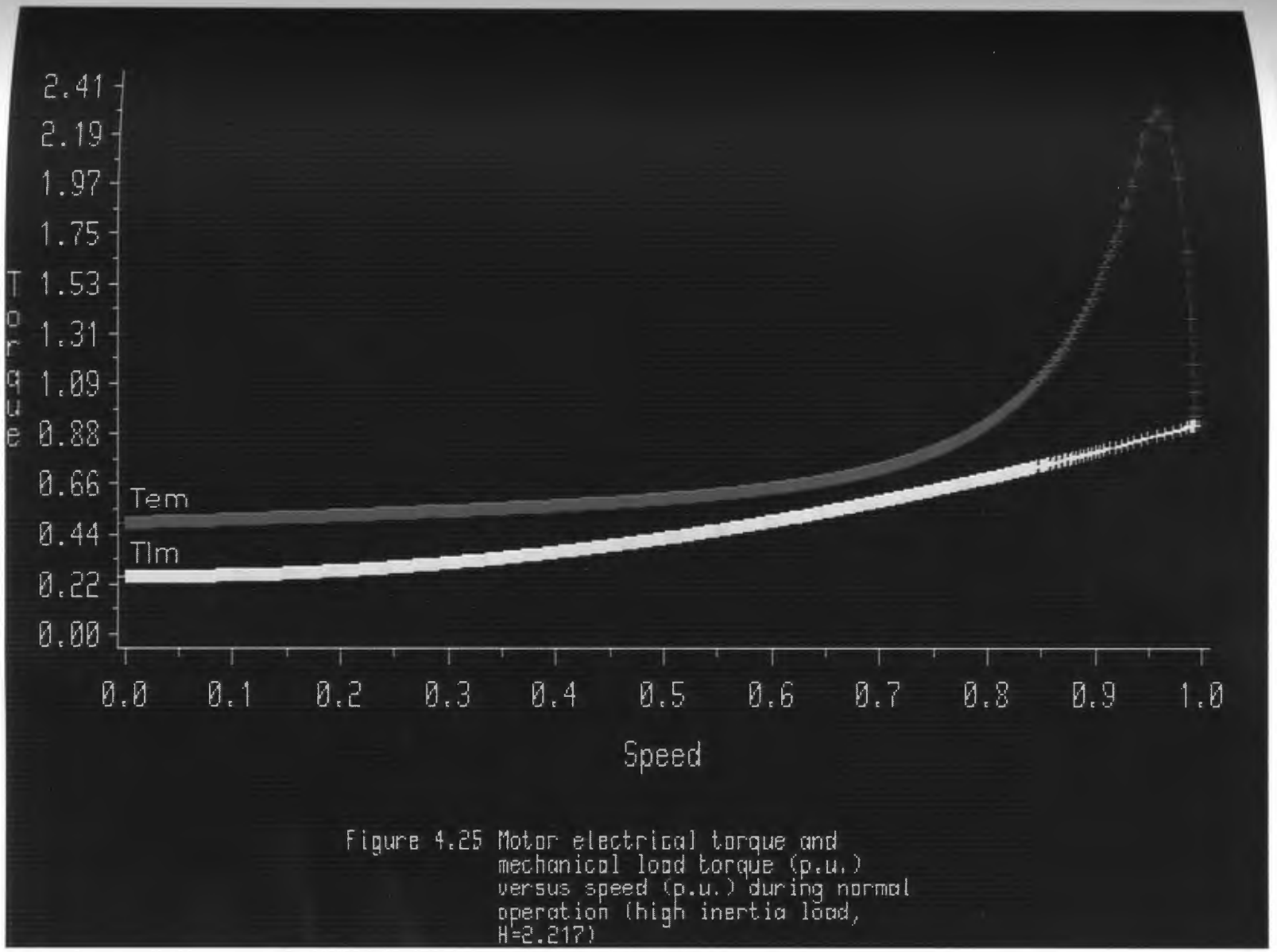

Figure 4.25 Motor electrical torque and mechanical load torque (p.u.) versus speed (p.u.) during normal operation (high inertia load, H=2.217)

Overloading Condition

In this work, induction motor performance during a variety of normal and abnormal system and load conditions has been re-examined. One of these cases is the overloading condition. To investigate this condition the motor load is increased by 25 percent. The motor electrical, mechanical, and thermal characteristics are then studied. In this study it is assumed that the motor is driving a pump. Therefore the load is a function of motor speed. As a result of overloading, the acceleration time is longer than that in normal operation. Also, the motor rated slip increases, but not significantly.

The motor time-speed characteristic is shown in figure 4.26. As it is seen after about 27 seconds, the motor reaches rated speed. The current during start up in the overload condition is shown in figure 4.27. The starting current is the same as that of normal operation, but the running or the final current is almost 25 percent more than the rating current. In such a case the conventional overload relay will operate and isolate the motor from the power system, while the rotor is heated up to almost 70 degrees centigrade which is less than its thermal limit. The thermal characteristics of the motor are shown in figures 4.28 and 4.29. The rotor current and loss are shown in figure 4.30. As is expected, the rotor current is more than that of normal operation. The rotor loss at stand still for the overload case is larger than that of normal operation, while the running rotor loss is almost equal to the rated rotor loss.

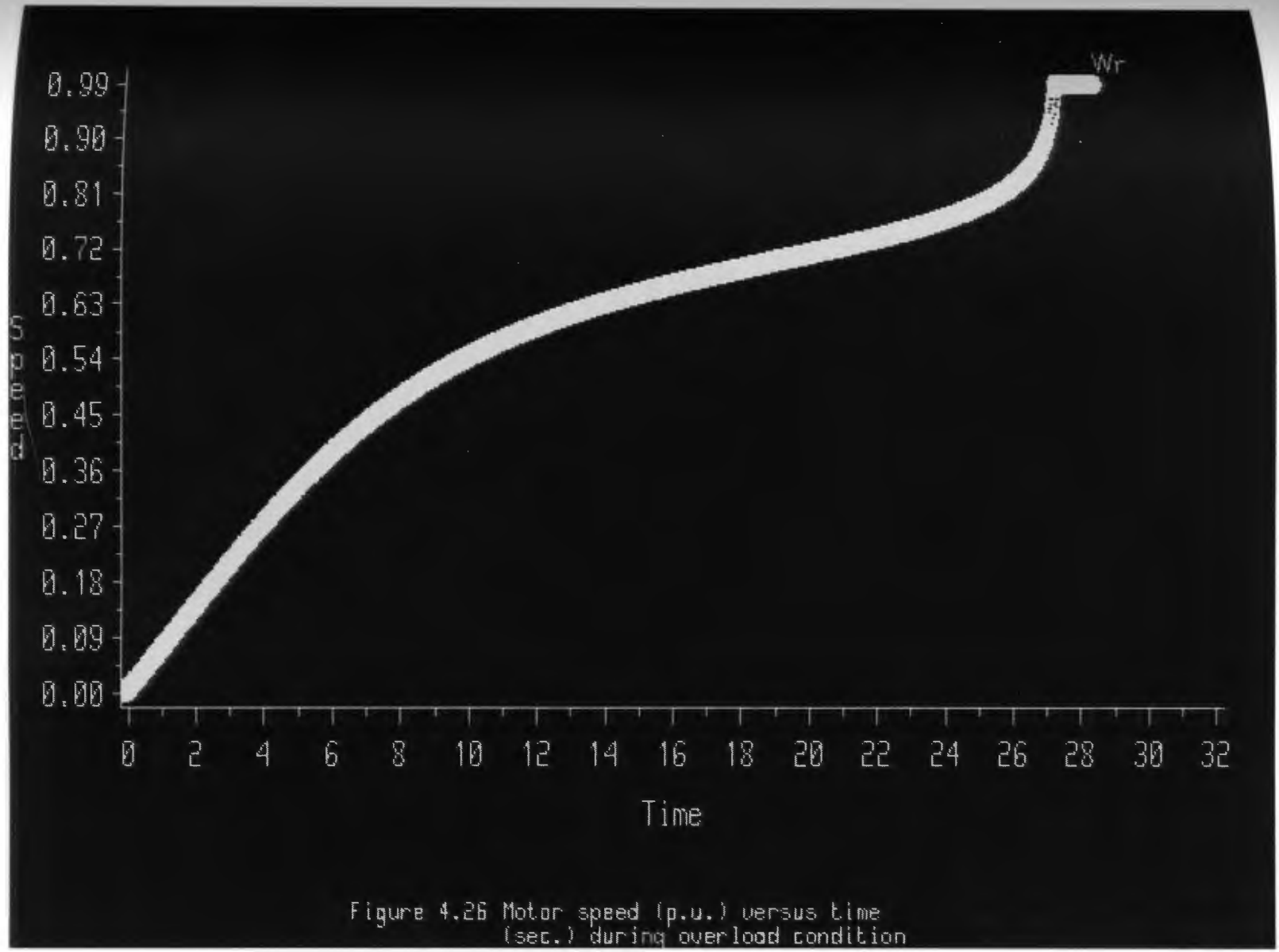

Figure 4.26 Motor speed (p.u.) versus time (sec.) during overload condition

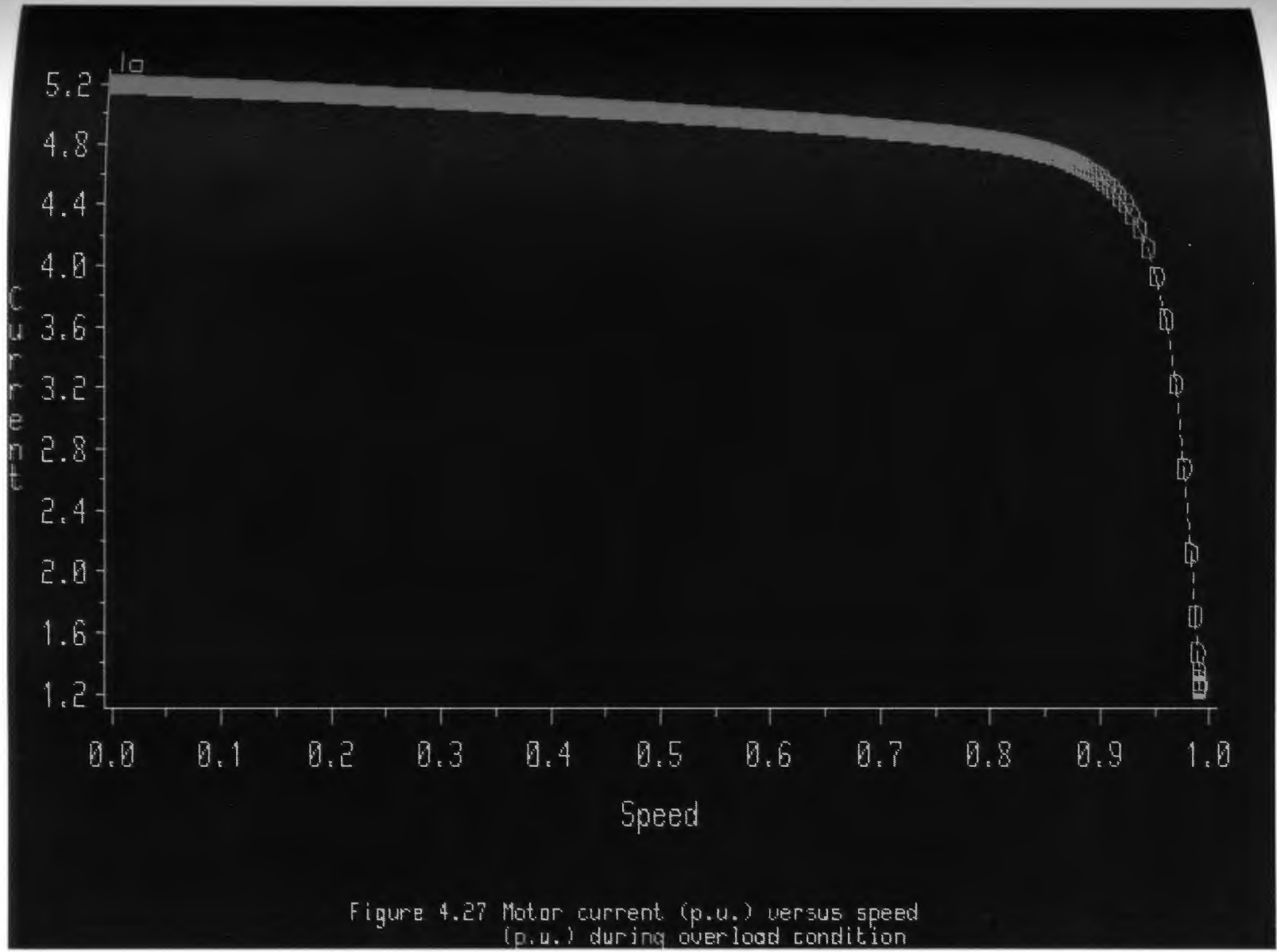

Figure 4.27 Motor current (p.u.) versus speed (p.u.) during overload condition

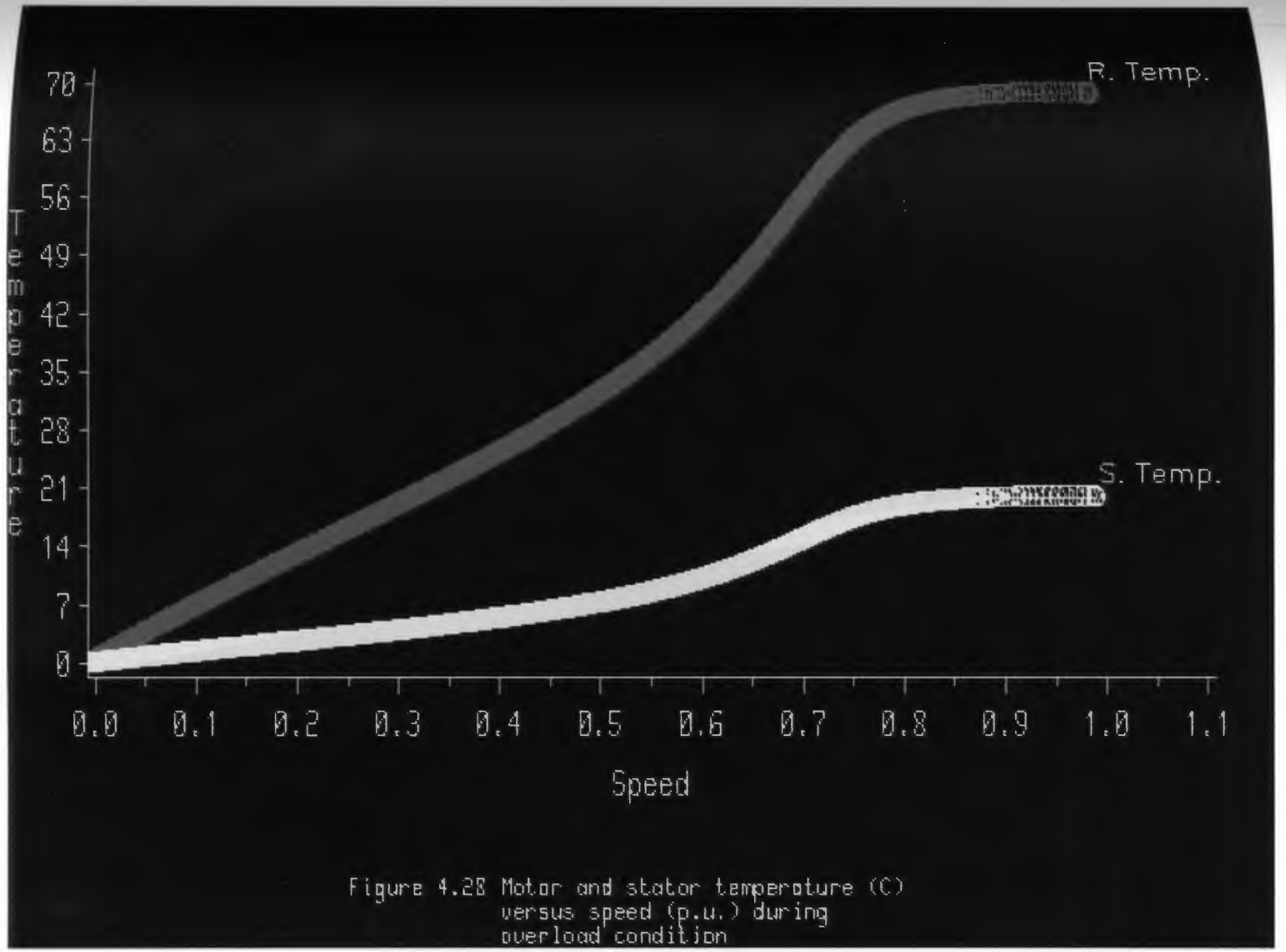

Figure 4.28 Motor and stator temperature (C) versus speed (p.u.) during overload condition

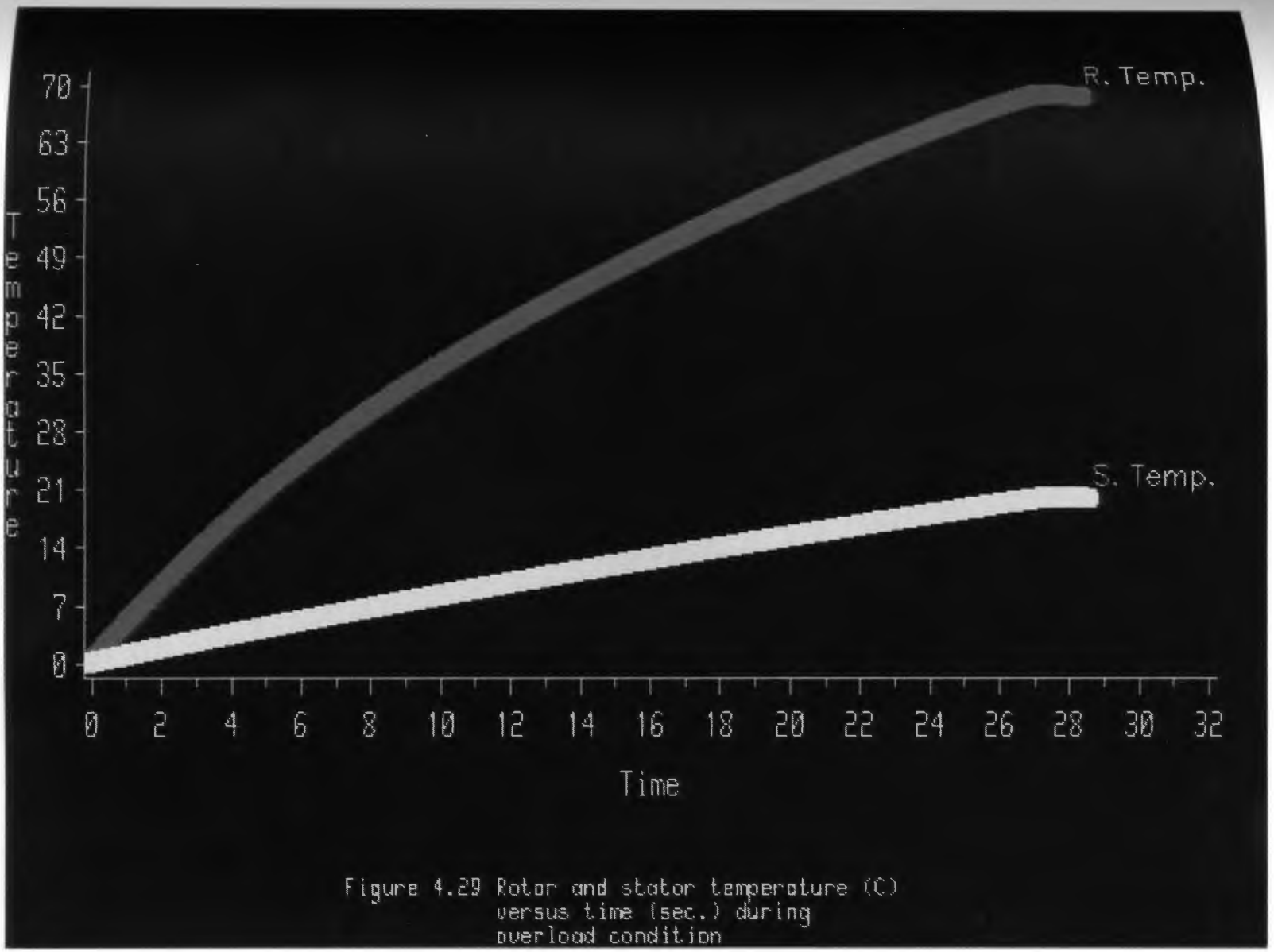

Figure 4.29 Rotor and stator temperature (C) versus time (sec.) during overload condition

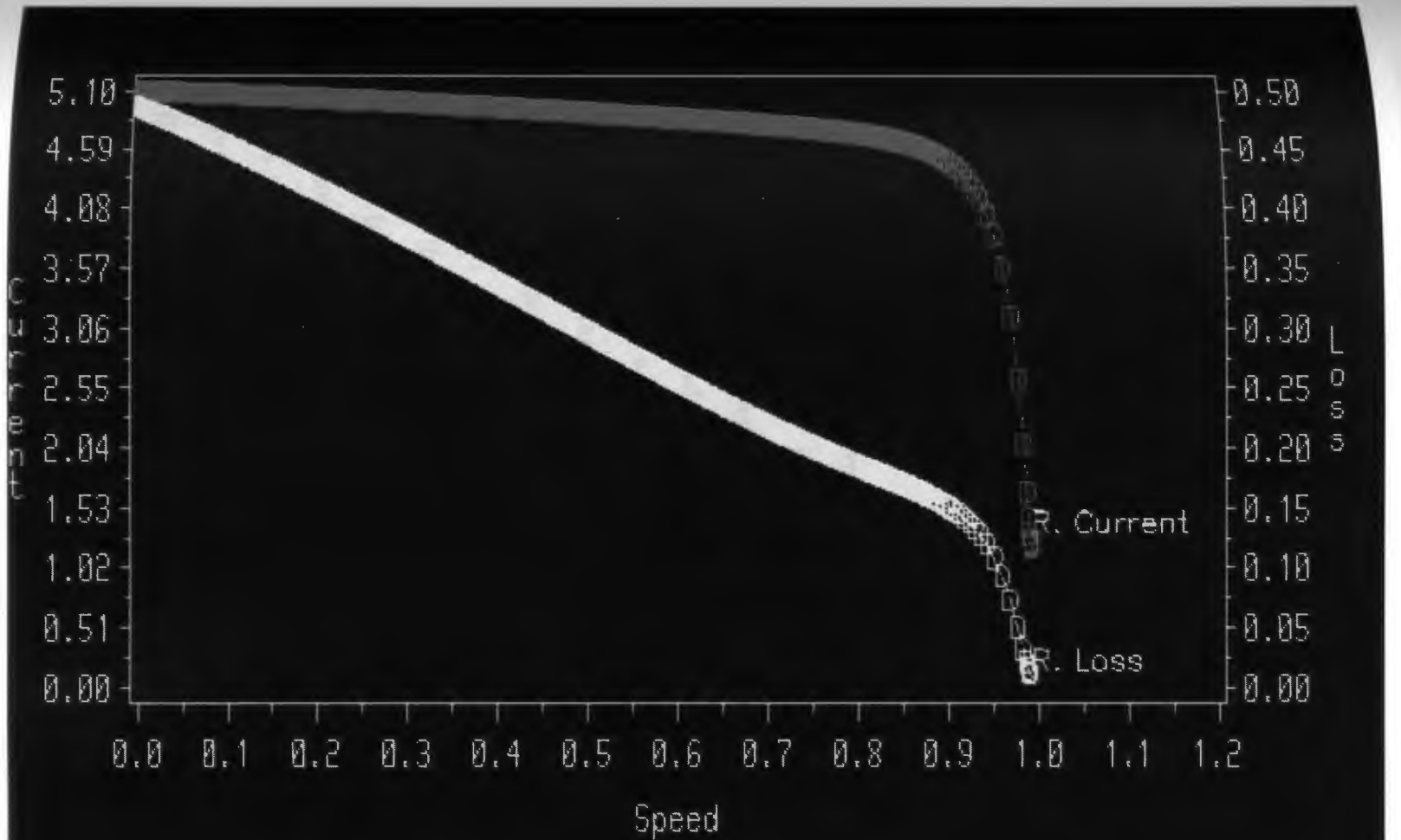

Figure 4.38 Rotor current (p.u.) versus speed (p.u.) [left axis] and rotor loss (p.u.) versus speed (p.u.) [right axis] during overload condition

Thermal Limit Curves

The available induction motors' protection schemes are generally limited to overload and overcurrent relays (especially motors below 1000 hp). Setting of both the overload and overcurrent units is decided by the thermal limit curves of the protected motor. Any part of these curves is limited by one of the following:

1) the allowable temperature rise for the rotor bars,
2) the allowable temperature rise for the rotor end-ring connector, and
3) the stator insulation material class.

Each point on the thermal limit curve represents the maximum time that the motor could tolerate the corresponding current during balanced system conditions. The curve itself is mainly intended for setting the overload and overcurrent to protect the motor during abnormal conditions with balanced system operation.

During unbalanced system conditions negative sequence voltages are applied to the motor terminals. To satisfy this requirement a.c. current having a frequency of almost 120 Hz circulates in the rotor. Therefore, the increase of rotor resistance is even more pronounced and a ratio of up to eight times between positive and negative sequence resistance has been reported. This accounts for a much greater rate of heating per unit of current in the negative sequence circuit than that produced per unit of current in the positive sequence circuit. Of course this heating increases because of an increase in magnitude of the negative sequence currents and the rotor negative sequence resistance.

In the proposed protection scheme, the use of thermal limit curves is not necessary. Just to show the versatility and the ability of the interactive models, the thermal limit curve for the rotor was drawn. These thermal limit curves for normal operation and faulted condition are shown in figure 4.31. As is expected during unbalanced condition and for a specified current, the motor reaches its thermal limit faster than during normal operation. Conventional relays are set by the information given by the thermal limit curve during normal operation. Even if these relays are set properly, they must differentiate small changes in current to detect fault conditions (e.g. in high inertia starting). Therefore there is always a risk of false operation.

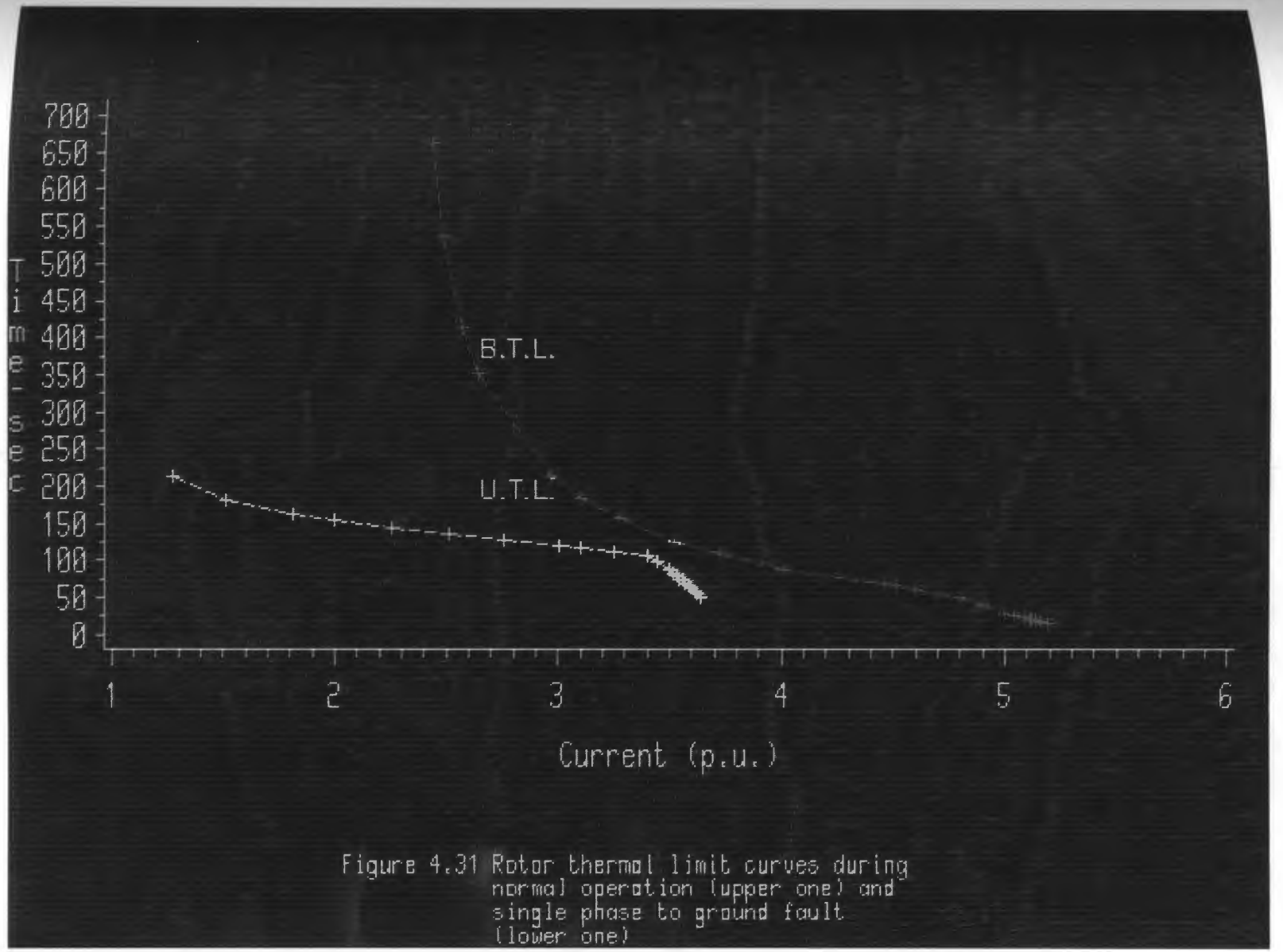

Figure 4.31 Rotor thermal limit curves during normal operation (upper one) and single phase to ground fault (lower one)

Percent Unbalanced Voltage (PUV)

The percent unbalanced voltage is defined by NEMA as the maximum phase voltage deviation from the average of all three phase voltage times 100.

$$PUV = \frac{(\text{Max. Voltage Deviation from Avg. Voltage}) * 100}{\text{Avg. Voltage}} \qquad (4.1)$$

Figure 4.15 shows the variation of faulted phase voltage and motor negative sequence voltage against motor speed during a solid single-phase to ground fault at the motor terminal with a PUV of 99.57 percent. According to NEMA motor standards, a maximum unbalanced voltage up to 1 percent at the motor terminal is permitted. This recommendation is not suitable for all motors of different classes, sizes, and loads. In addition, the type and condition of the fault must be considered. Faults in power systems are not always bolted faults. Power transformers are often grounded through impedances in order to limit the fault current to a predetermined level. The ground resistance is not always zero. This depends on the condition of the soil, whether it is rocky, dry, wet, etc. The ground resistance may be high enough that the system overcurrent protection may just see a normal current during the fault and may not operate.

In this study, the thermal characteristics of the motor under investigation has been investigated thoroughly. It is assumed that the rotor temperature prior to the fault was 56 degrees centigrade. By employing different fault impedances, different percent

unbalanced voltages are simulated. The result of this unique investigation is shown in figure 4.32. An unbalanced voltage in the range of 100 percent to almost 70 percent applied to the motor terminal causes the motor to be stalled and to reach the critical temperature very fast. In the range below 70 percent (PUV) the motor does not stall and the machine continues to run with a speed between 0.977 to 0.992 p.u. depending on the PUV. This case may be very dangerous for the motor. Under 5.9 percent PUV the motor is completely relaxed and never reaches the critical heat point. Note that at 5.9 percent PUV the motor has a derating factor of 10.8 percent.

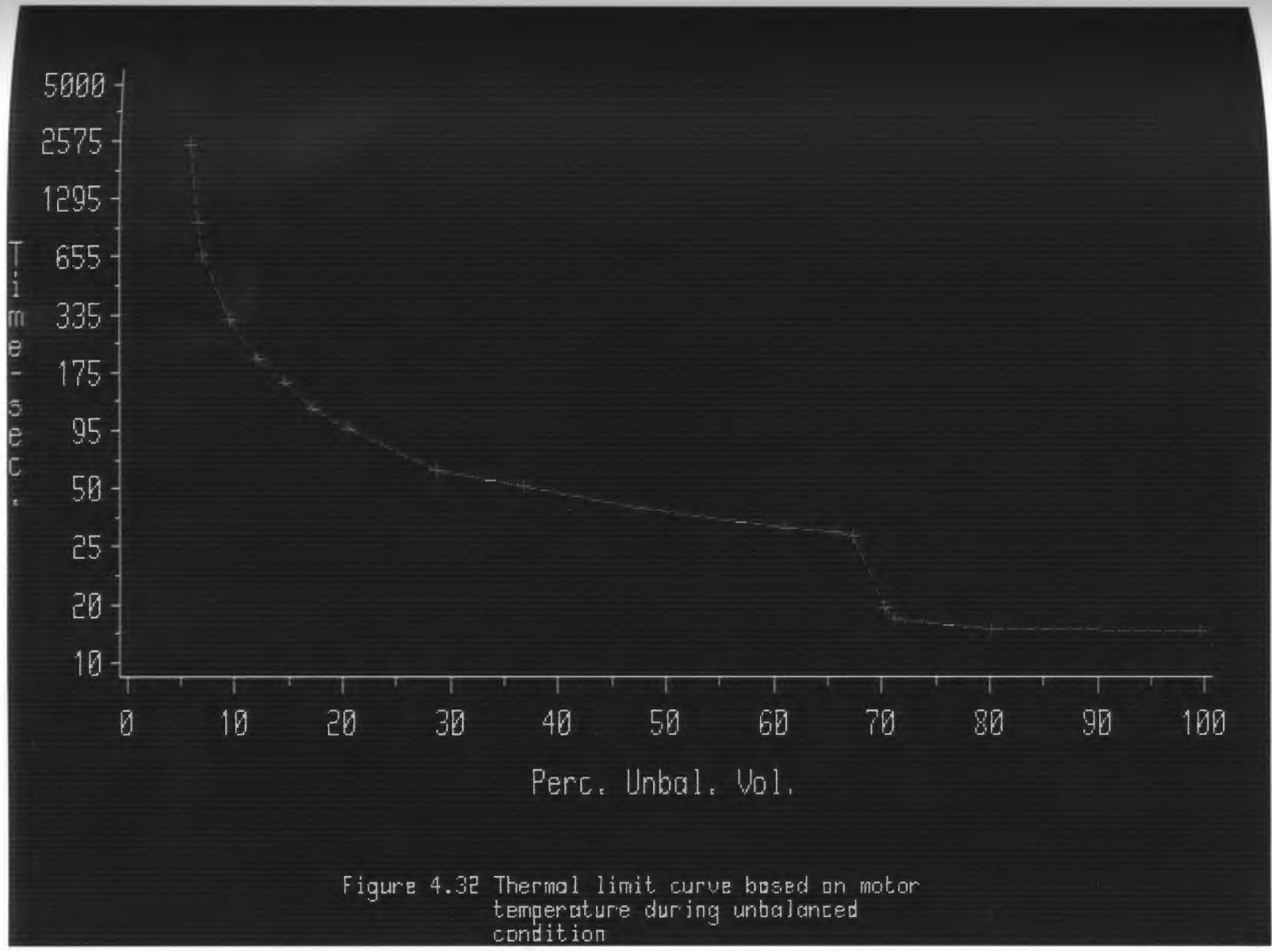

Figure 4.32 Thermal limit curve based on motor temperature during unbalanced condition

Summary

In this chapter the complete results of this research have been presented. The motor under investigation has been examined for normal, locked-rotor, unbalanced voltage, high inertia loading, and overloading conditions. The electrical, mechanical, and thermal characteristics of the induction motor have been analyzed thoroughly. The stator conductor's and rotor end-rings' temperature rise have been computed accurately. A unique thermal limit curve capable of presenting the temperature rise for different PUVs has been introduced. By employing this valuable thermal limit technique the motor can be optimally protected, thus avoiding unnecessary trips when the temperature is below the critical point.

Throughout this chapter a calculation method for induction motors' temperature has been introduced. It has been shown that this method is applicable for any system and load condition. The motor temperature varies over a wide range. Thus, proposing a protective relay which responds to temperature is the next objective of this work.

The computer simulation used in this study can be employed to design a microprocessor based protective relay. This will be covered in detail in the next chapter.

CHAPTER 5

MICROPROCESSOR BASED RELAY

Today using microprocessor based technology in protective relays is becoming a more common practice. This is because of the potential of this technique for analyzing the protected system. However, it is a fact that a microprocessor based scheme by itself can not make any significant improvement if the theory and system modeling behind the hardware technology have not been investigated thoroughly. For instance, as has been discussed earlier in this work, the overcurrent relay cannot protect the motor properly even if the relay is designed by employing microprocessor technology. However some researchers (26), in order to cure the inability of overcurrent relay to distinguish a high inertia starting from the locked-rotor case, have suggested using an under impedance relay in series with the overcurrent relay. Still, as S. E. Zocholl (6) mentioned, the relay has to differentiate very small changes in motor impedance in a short period of time. Some other designers (4,25), in order to consider the effect of negative sequence current and rotor negative sequence resistance, employed an approximated constant value which neglected the dependency of rotor resistance on frequency. Even Zocholl did not consider the dynamic features and the non-linear relationship between rotor resistance and frequency.

The foundation of all available microprocessor based relays, from the hardware technology point of view, is the same. The differences among them are inputs, program, and outputs. In other

words, the modeling and analysis method behind the technology are different. Therefore as far as the hardware technology is concerned, this work offers nothing very different.

The significance of this work lies in employing an accurate electrical model which represents the induction motor well. By using this model along with the mechanical model, the motor speed can be calculated in real time. Then, by knowing the motor speed, the rotor impedance can be calculated using the electrical model. At this step, having the calculated rotor impedance, the motor losses and temperature rise can be computed using the electrical and the thermal models respectively. The complete and accurate analysis of the induction motor without any approximation method or ignoring any electrical, mechanical, and thermal characteristics, is the unique feature of this work. However, like any other research this study could not be accomplished without the help of other researchers' work and ideas.

Since in this work the motor temperature is calculated accurately, an optimum protection scheme can be proposed. In this protection scheme it is more convenient to measure the currents at the motor terminals instead of calculating them. This continuous current measurement minimizes the need for extra data about the power system to which the motor is connected. Having the measured currents and using the symmetrical components as a mathematical tool, the motor negative and positive sequence currents can be calculated. Measuring three phase voltages at the motor terminals is necessary only when the load driven by the motor could not be modeled. In this case in order to calculate the motor slip, the

following steps must be taken. By measuring voltage and current for a particular phase, the motor impedance for that phase can be calculated using equation 5.1.

$$Z=R+jX=V/I \tag{5.1}$$

where,

Z is the motor impedance,

R and X are the motor resistance and inductance respectively,

V and I are the measured voltage and current for one phase.

This impedance measurement must equal the motor impedance calculated by the electrical model.

$$Z=R+jX=Z_m$$

$$\mathcal{R}e(Z)=\mathcal{R}e(V/I)=\mathcal{R}e(Z_m) \tag{5.2}$$

where,

Z_m is the calculated impedance by the electrical model,

$\mathcal{R}e$ is the symbol for the real part of each side of equation.

The only unknown is the motor slip which can be computed by solving the equation 5.2.

The calculation process after having the measured currents and voltages is shown in equations 5.3 and 5.4.

$$\begin{bmatrix} I_A^{(0)} \\ I_A^{(+)} \\ I_A^{(-)} \end{bmatrix} = \frac{1}{3}\begin{bmatrix} 1 & 1 & 1 \\ 1 & a & a^2 \\ 1 & a^2 & a \end{bmatrix}\begin{bmatrix} I_A \\ I_B \\ I_C \end{bmatrix} \tag{5.3}$$

$$\begin{bmatrix} V_A^{(0)} \\ V_A^{(+)} \\ V_A^{(-)} \end{bmatrix} = \frac{1}{3} \begin{bmatrix} 1 & 1 & 1 \\ 1 & a & a^2 \\ 1 & a^2 & a \end{bmatrix} \begin{bmatrix} V_A \\ V_B \\ V_C \end{bmatrix} \qquad (5.4)$$

where,

I_A, I_B and I_C are the three phase measured currents flowing inside the motor,

$I_A^{(+)}$ and $I_A^{(-)}$ are the positive and negative sequence currents of phase A respectively,

V_A, V_B, and V_C are the three phase measured voltages at the motor terminals,

$V_A^{(0)}$, $V_A^{(-)}$, and $V_A^{(+)}$ are the zero, negative, and positive sequence voltages of phase A at motor terminals respectively, and

$a = -0.5 + j0.866 = 1 \angle 120^\circ$

$a^2 = -0.5 - j0.866 = 1 \angle 240^\circ$

$a^3 = 1 = 1 \angle 360^\circ$

Since the squirrel-cage induction motors are not grounded, there is no zero sequence current flowing through the motor.

The block diagram of the microprocessor based protection system is shown in figure 5.1. Since, in the proposed protection system, measuring all three phase currents is necessary, any phase

shift between measured analog signals must be avoided. Therefore, all filters must have the same gain and phase shift. Three phase currents and voltages feed into low pass filters (LPF) through current transformers (CT) and voltage transformers (VT) respectively. The sample and hold amplifiers (S/H) will take the samples from analog input signals. The signals are then passed by a multiplexer (MUX). The multiplexer sends the sampled analog signals from the (S/H) to the analog/digital converter (A/D) one by one
in a logical order. After this step, the digital signals will be stored in memory in the programmer microprocessor chip. The computation process begins and the calculated temperature will be compared to the set thermal limits. If the temperature approaches or exceeds the set point, the relay will send an alarm or trip signal through the output buffers. When the program is put in the microprocessor the motor parameters can be stored in predetermined memories for further usage. The currents flowing inside the motor are variable data that must be measured continuously and sampled at proper intervals of time (in this work, 0.2 seconds). Then by knowing the input currents and using the formulas in chapter 4, the motor temperature can be calculated. In this study, a microprocessor based protection scheme which responds to temperature has been proposed. This protective relay is based on accurate motor modeling and analysis. Designing the hardware is beyond the scope of this study. The author hopes to accomplish it in a succeeding project.

CHAPTER 6

CONCLUSION

In this study, the behavior of squirrel-cage induction motors under a variety of normal and abnormal system and load conditions has been investigated. A computer simulation was used to examine the response of the motor to different conditions such as locked-rotor, high inertia loading, overloading, and normal operations. The shortcomings of the existing motor protection schemes have been discussed. Finally a new microprocessor based protection relay has been proposed.

Most of the studies in this area ignore at least one basic feature of induction motors. Some of these studies considered only the positive sequence network's parameters. Others included the effect of negative sequence network's parameters by employing an approximate constant value. The rotor's frequency dependent resistance, which has a significant influence on motor heating, has been neglected in most studies.

From another point of view, most existing motor protective relays respond to current, voltage, or impedance. Since the variation of these parameters (current, impedance...) in some cases is the same (e.g. the locked-rotor case and high inertia starting) relay malfunctioning occurs. There are some relays which operate based on information taken from resistance thermal detectors (RTDs), but designers generally agree that RTDs are not economical, reliable, and fast enough.

In this study, the effect of the negative sequence network's parameters and the skin effect phenomena in motor heating was investigated thoroughly. This has been done by employing an accurate impedance electrical model. Also, a motor mechanical model was used to predict the motor speed with the help of the electrical model. Finally, a thermal model was used to predict the motor temperature rise based on motor losses calculated by the electrical and mechanical models.

The advantage of the proposed scheme is the accuracy of the models which were used. The proposed scheme predicts the motor temperature directly. Conventional relays, regardless of shortcomings of the theory behind them, must be adjusted to distinguish a very narrow range of variation of current, voltage, or impedance.

The other important and specific feature of this work is the introduction of a thermal limit curve based on motor temperature for the unbalanced system condition. This thermal limit curve is able to indicate how long it takes for the rotor end-rings to reach the emergency limit for any percentage of unbalanced voltage at the motor terminals. This is valuable for comparison with more traditional thermal limit curves which do not include as detailed modeling. The diagnostic capability of this work is also valuable. For example, the motor acceleration time for a specified load can be calculated by this computer simulation. Thus, if the acceleration time changes it shows that there is a problem in a motor bearing or in some other mechanical part.

Finally, a microprocessor based protection relay has been introduced. This relay is suitable for all types of induction motors

and is capable of protecting the motor properly during a variety of system and load conditions. The relay responds to motor temperature. Whenever the motor temperature approaches or exceeds its emergency limit, the relay will send either a warning signal to the operator or a signal directly to the motor breaker to isolate the motor from the energizing system.

Using accurate models, the performance of the induction motor during a variety of system and load conditions has been re-examined. By means of a computer simulation, a temperature calculation method for induction motors has been introduced. Also a microprocessor based protection scheme, which responds to temperature, has been proposed. The author is planning to design the hardware of the proposed relay in a succeeding project.

BIBLIOGRAPHY

BIBLIOGRAPHY

1. Eltom, A. H., Induction Motor Behavior During Single Phase to Ground Fault, M.S. Thesis, Clarkson, New York: Clarkson College of Technology, March 1982.

2. Eltom, A. H., Induction Motor Behavior During Single and Double Phase to Ground Fault, Ph.D. Dissertation, Clarkson, New York: Clarkson College of Technology, 1984.

3. Ortmeyer, T. H., Analysis of Induction Machine Dynamics During Power System Unbalanced, Ph.D. Dissertation, Iowa State University, Ames, Iowa 1980.

4. Meissel, S. M. and Brandolino, J., Design and Application of a Microprocessor Based Motor Protection Relay With Historical Analysis for Large Motors, Georgia Power Company, Atlanta, Georgia 1987.

5. Zocholl, S. E., Abnormal Starting of High Inertia Drive Induction Motors: A Case for Rotor Thermal Protection, BBC Brown Boveri, Inc., Allentown, PA.

6. Zocholl, S. E., Narendra, S. and Ravi, I., Techniques for Evaluating Advanced Motor Protection Relays Using Computer Controlled Test Equipment, BBC Brown Boveri, Inc., Allentown, PA, 1987.

7. Tilak Silyambalapitiya, D. J., McLaren, P. G. and Acarnley, P. P., A Rotor Condition Monitor for Squirrel-Cage Induction Machines, IEEE Trans. on Indust. Appl., Vol. IA-23, No.2, March/Aprill 1987.

8. Clarke, Edith, Circuit Analysis of A-C Power Systems, Volume 1, Symmetrical and Related Componenets, New York: John Wiley and Sons, Inc., London, 1961.

9. Clarke, Edith, Circuit Analysis of A-C Power System, Volume 2, New York: John Wiley and Sons, Inc., London, 1950.

APPENDICES

APPENDIX A

Program Flow Chart and Program Listing

The Flow Chart of Computer Program

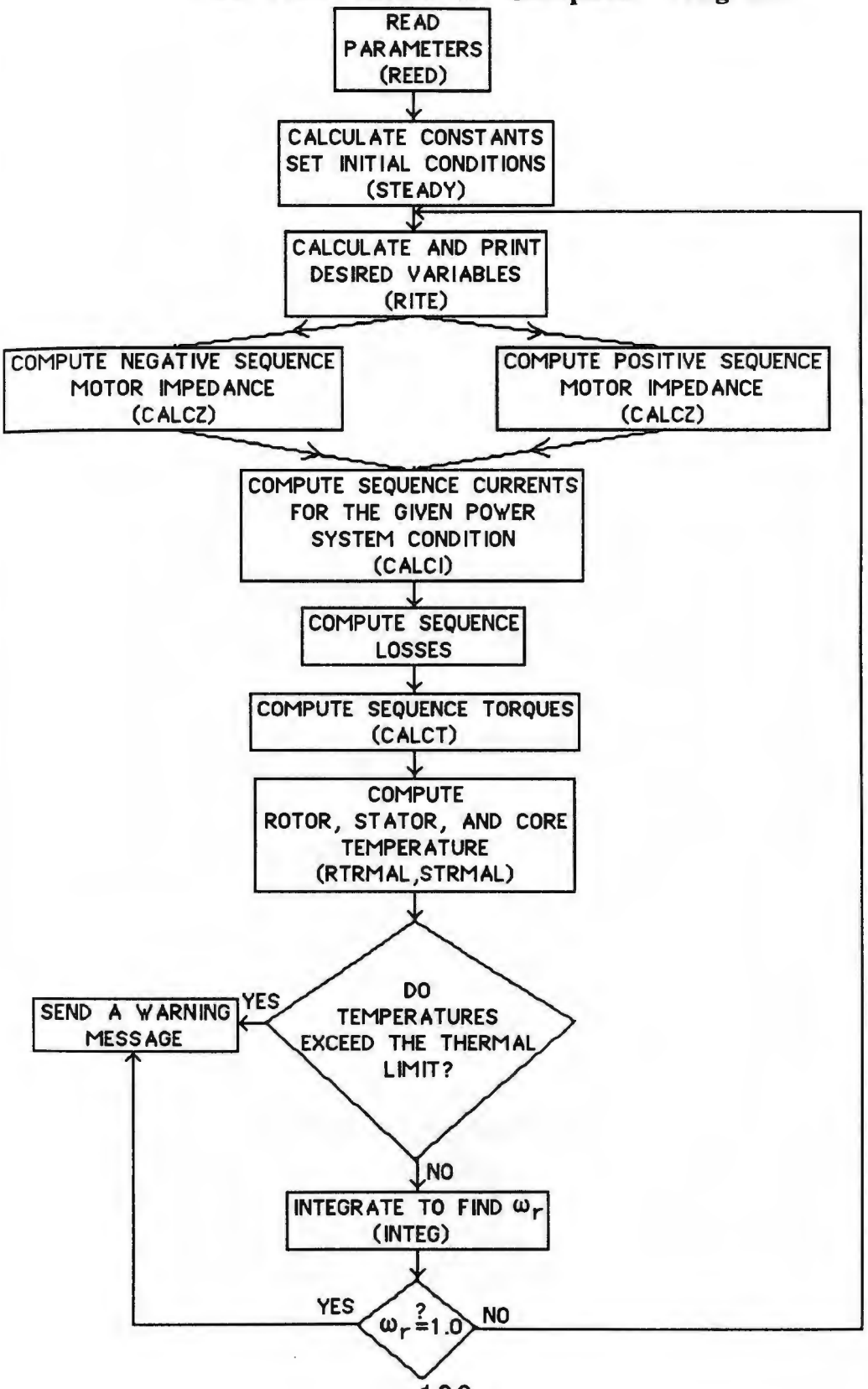

Program Listing

```
/FILE 7 N(FOP1) NEW(REPL)
/FILE 8 N(FOP2) NEW(REPL)
/FILE 9 N(FOP3) NEW(REPL)
/FILE 10 N(FOP4) NEW(REPL)
/FILE 11 N(FOP5) NEW(REPL)
/FILE 12 N(FOP6) NEW(REPL)
/FILE 13 N(FOP7) NEW(REPL)
/FILE 14 N(FOP8) NEW(REPL)
/FILE 15 N(FOP9) NEW(REPL)
/LOAD FORTGI

C ***********************************************************************
C *    EVALUATION OF INDUCTION MOTOR THERMAL                            *
C *    CHARACTERISTICS UNDER VARIOUS UNBALANCED                         *
C *    CONDITIONS. THERMAL, MECHANICAL, AND SKIN EFFECT                 *
C *    ELECTRICAL MODELS ARE USED.                                      *
C ***********************************************************************

C ***********************************************************************
C *                          MAIN PROGRAM                               *
C ***********************************************************************

      COMMON/BL1/XY(6),XDOT(6),T,DELT,LINES,L,N,TFINAL,
     2NDIFF
      CALL REED
      CALL STEADY
      WRITE(6,60)
C     DISTURBANCE STARTS*****DISTURBANCE STARTS*****
      CALL MSTART
      WRITE(6,10)
  100 FORMAT(2X,'TIME',3X,'POSITIVE SEQUENCE',7X,'NEGATIVE
     2SEQUENCE',7X,/10X,'VPM',5X,
     3'IPS',6X,'TP',5X,'VNM',5X,'INS',6X,'TN',6X,
     4'WR',5X,'SLIP'.4X,'TEM',5X,'TLM',5X,
     5'VAPK',5X,'IAPK',4X,'IBPK',4X,'ICPK',3X,'TEMP
     6RISE'
```

```
      READ(5,100) RL,XL,UP,UN,PHIPN,F,XCAP
      WRITE(6,101)RL,XL,UP,UN,PHIPN,F,XCAP
      READ(5,102) RT,XT,NPHASE
      WRITE(6,103) RT,XT,NPHASE
      READ(5,99)RS,XS,XM,RM
      WRITE(6,104)RS,XS,XM,RM
      READ(5,105)NCIRC,XG
      WRITE(6,110)XG
      DO 1 J=1,NCIRC
      READ(5,98)RR(J),XR(J)
1     WRITE(6,106) J,RR(J),XR(J)
      XR(NCIRC)=XR(NCIRC)+XG
      ZMAG=CMPLX(0.0,XM)
      ZSTAT=CMPLX(RS,XS)
      RKR=0.0
      RK4(1)=0.0
      RK4(2)=0.0
      READ(5,97)H,TLO,TL2,WR
      WRITE(6,107)H,TLO,TL2,WR
      READ(5,108)DELT,N,TFINAL
      WRITE(6,109)DELT,N,TFINAL
      READ(5,111)R90,R91,C3,R7,R80,R81,C1,C2
      WRITE(6,114)R90,R91,C3,R7,R80,R81,C1,C2
100   FORMAT(7F9.4)
101   FORMAT('SYSTEM DATA RL='.F9.4,2X,'XL=',F9.4,2X,
     2'BUS VOLTAGE POS. SEQ.'.F9.4,2X,'NEG. SEQ.',F9.4,2X,
     3'PHIPN=',F9.4,2X,'F=',F9.4,2X,/,'XCAP=',F9.4)
103   FORMAT('TRANSFORMER DATA RT=',F9.4,2X,'XT=',F9.4,2X
     2'2 OR 3 PHASE BANK',I3)
102   FORMAT(2F9.4,I3)
99    FORMAT(3F10.8,F10.5)
104   FORMAT('STATOR DATA RS=',F10.8,2X,'XS='.F10.8,2X,
     2'MAG. IND. XM=',F10.8,2X,'MUTU. RES. RM=',F10.5)
105   FORMAT(I3,F10.8)
98    FORMAT(2F10.8)
106   FORMAT(20X,I3,10X,F10.8,5X,F10.8)
97    FORMAT(4F9.4)
```

```
107  FORMAT('MECHANICAL DATAH=',F9.5,2X,'TLO=',F9.5,2X,
    2'TL2=',F9.5,2x,'WR=',F9.5)
108  FORMAT(F9.4,I3,F9.4)
109  FORMAT(' DELT=',F9.4,2X,'N=',I3,2X,'TFINAL=',F9.4)
110  FORMAT(' ROTOR IMPEDANCES CKT NO.',5X,'RESISTANCE',5X
    2,'REACTANCE','GAP REACTANCE XG=',F10.8)
111  FORMAT(8F7.3)
114  FORMAT(' R90=',F7.3,2X,'R91=',F7.3,2X,'C3=',F7.3,/,'R7=',F7.3,2X,
    2'R80=',F7.3,2X,'R81=',F7.3,2X,'C1=',F7.3,2X,'C2=',F7.3)
     RETURN
     END

C ***********************************************************************
C *    "STEADY" FINDS PRE-DISTURBANCE INITIAL VALUES OF  *
C *    VARIABLES.                                        *
C ***********************************************************************

     SUBROUTINE STEADY
     COMPLEX (I,V,Z)
     COMMON/BL1/XY(6),XDOT(6),T,DELT,LINES,L,N,TFINAL,
    2NDIFF
     COMMON /BL2/IP,IN,VPM,VNM,TP,TN,TEM,TLM,WR,SLIP,ZPM,
    2ZNM,INR,IPR,ZPR,ZNR,VOM
     COMMON/BL3/RL,XL,UP,UN,PHIPN,F,RT,XT,NPHASE,RS,
    2XS,XM,H,TLO,TL2,XCAP,RM
     COMMON/BL4/VPB,VNB,Z11,Z12,Z22,IO,ACF
     COMMON/BL6/ZCAP,ZL,ZNL
     SQ2=SQRT(2.0)
     SQ3=SQRT(3.0)
     SQ32=SQ3/2.0
     PAI=3.141593
     WZ=2.0*PAI*F
     ACF=.5/H
     T=0.0
     LINES=1
     L=1
     ZA=COMPLX(-.5,SQ32)
```


U.T.C. Library

```
      ZASQ=CMPLX(-.5,-SQ32)
      NDIFF=1
      DO 300 J=1,6
      XY(J)=0.0
300   XDOT(J)=0.0
      XY(1)=WR
      VPB=CMPLX(UP,0.0)
      PHIPNR=PHIPN*PAI/180.0
      A=UN*C0S(PHIPNR)
      B=UN*SIN(PHIPNR)
      VNB=CMPLX(A,B)
      ZL=CMPLX(RL,XL)
      XNL=XL
      ZNL=CMPLX(RL,XNL)
      X=-XCAP
      ZCAP=CMPLX(0.0,X)
      Z11=CMPLX(RT,XT)
      Z12=-Z11/3.0
      Z22=Z11*2.0/3.0+CMPLX(RL,XL)
      RETURN
      END

C ***************************************************************************
C *    "MSTART" SETS INITIAL VALUES FOR STARTING THE    *
C *    MOTOR.                                           *
C ***************************************************************************

      ENTRY MSTART
      CALL PLANT(T,XY,XDOT)
      RETURN
      END

C ***************************************************************************
C *    "RITE" PRINTS OUT COLUMNS OF INTEGRATION RESULTS. *
C ***************************************************************************

      ENTRY RITE
```

```
  COMMON/BL7/FDOPR,RKR,COEF(1,2),R90,R91,C3,RLOSS
  COMMON/BL8/FDOT(2),RK4(2),COEFF(2,4),R7,R80,R81,C1,C2,
2SLOSS,CLOSS
  RIM=REAL(IP)
  AIMI=AIMAG(IP)
  CPRAMS=SQRT(RIM*RIM+AIMI*AIMI)
  RIM=REAL(IN)
  AIMI=AIMAG(IN)
  CNRMS=SQRT(RIM*RIM+AIMI*AIMI)
  VPM=IP*ZPM
  RV=REAL(VPM)
  AIV=AIMAG(VPM)
  UPM=SQRT(RV*RV+AIV*AIV)
  VNM=IN*ZNM
  RV=REAL(VNM)
  AIV=AIMAG(VNM)
  UNM=SQRT(RV*RV+AIV*AIV)
  IA=IP+IN
  VAM=VPM+VNM+VOM
  R=REAL(IA)
  AI=AIMAG(IA)
  CA=SQRT(R*R+AI*AI)
  R=REAL(VAM)
  AI=AIMAG(VAM)
  UA=SQRT(R*R+AI*AI)
  IB=IP*ZASQ+IN*ZA
  IC=IP*ZA+IN*ZASQ
  AI=AIMAG(IB)
  R=REAL(IB)
  CB=SQRT(R*R+AI*AI)
  R=REAL(IC)
  AI=AIMAG(IC)
  CC=SQRT(R*R+AI*AI)
  IR=IPR+INR
  CROT=CABS(IR)
  VBM=VPM*ZASQ+VNM*ZA+VOM
  VCM=VPM*ZA+VNM*ZASQ+VOM
```

```
      UB=CABS(VBM)
      UC=CABS(VCM)
      AV=(UA+UB+UC)/3.0
      DM=AV-UA
      PVU=DM*100./AV
      RRP=(REAL(ZPR))*SLIP
      XPR=AIMAG(ZPR)
      RRN=(REAL(ZNR))*(2.-SLIP)
      XRN=AIMAG(ZNR)
      RLOSS=TP*SLIP+TN*(2.-SLIP)
      CLOSS=UPM/RM
      SLOSS=RS*(CPRM**2+CNRMS**2)
      CALL RTRMAL(SLIP)
      T=T-DELT
      CALL STRMAL(SLIP)
      T=T-DELT
      SQ1=80./SQRT(3.)
      SQ2=100./SQRT(3.)
      RKR=RKR*SQ1
      RK4(1)=RK4(1)*SQ2
      RK4(2)*SQ2
      RKR=RKR+50.
      RK4(1)=RK4(1)+12.
C     IF(RKR.GE.80.0)CALL HELP
      WRITE(6,302)SLOSS,RLOSS
  302 FORMAT(2X,'SLOSS=',F8.5,2X,'RLOSS=',F8.5)
      WRITE(6,301)T,UPM,CPRMS,TP,UNM,CNRMS,TN,WR,SLIP,TEM,
     2TLM,UA,CA,CB,CC
  301 FORMAT(2X,15F8.5)
      WRITE(6,314)RK4(1),RKR
  314 FORMAT('STATOR TEMP.=',F8.4,3X,'ROTOR TEMP.=',F9.4)
      WRITE(7,303)WR,CA,CB,CC
  303 FORMAT(4(F8.4,2X))
      P=RLOSS+SLOSS
      WRITE(8,304)CB,SLOSS,RLOSS,P
  304 FORMAT(4(F8.4,2X))
      WRITE(9,307)T,RKR,RK4(1)
```

```
  307 FORMAT(3(F8.4,2X))
      WRITE(10,308)PVU,RKR,RK4(1)
  308 FORMAT(3(F8.4,2X))
      WRITE(11,309)T,CA,CB,CC
  309 FORMAT(4(F8.4,2X))
      WRITE(12,310)WR,TN,TP
  310 FORMAT(3(F8,4,2X))
      WRITE(13,311)SLIP,RRP
  311 FORMAT(2(F8.6,2X))
      WRITE(14,312)SLIP,XRP
  312 FORMAT(2(F8.6,2X))
      WRITE(15,313)SLIP,RRN
  313 FORMAT(2(F8.6,2X))
      RKR=RKR/SQ1
      RK4(1)=RK4(1)/SQ2
      RK4(2)=RK4(2)/SQ2
C     IF(SLIP.GE.1.01)STOP
C     IF(TEM.EQ.TLM)STOP
      RETURN
      END

C ***********************************************************************
C *    "PLANT" CONTAINS DIFFERENTIAL EQUATIONS AND                      *
C *    "INTEG" RETURNS NEW INTEGRATED VALUES TO                         *
C *    "MAIN PROGRAM".                                                  *
C ***********************************************************************

            SUBROUTINE PLANT(TDUM,YV,YDOT)
      IMPLICIT COMPLEX(I,V,Z)
      DIMENSION YV(6),YDOT(6)
      COMMON /BL2/IP,IN,VPM,VNM,TP,TN,TEM,TLM,WR,SLIP,ZPM,
     2ZNM,INR,IPR,ZPR,ZNR,VOM
      COMMON/BL3/RL,XL,UP,UN,PHIPN,F,RT,XT,NPHASE,RS,
     2XS,XM,H,TLO,TL2,XCAP,RM
      COMMON/BL4VPM,VNM,Z11,Z12,Z22,IO,ACF
      WR=YV(1)
      SLIP=1.-WR
```

```
      IF(SLIP.GE.0.99999)SLIP=1.0
      IF(SLIP.GE.0.99999)WR=0.0
      CALL CALCZ(SLIP,ZPM,ZPR)
      BSLIP=2.-SLIP
      CALL CALCZ(BSLIP,ZNM,ZNR)
      CALL CALCI(ZPM,ZNM,IP,IN,IO,VPB,VOM)
      CALL CALCT(IP,ZPR,XM,TP,IPR)
      CALL CALCT(IN,ZNR,XM,TN,INR)
      TEM=TP-TN
      TLM=TLO+TL2*WR*WR
      YDOT(1)=ACF*(TEM-TLM)
      RETURN
      END

C *************************************************************************
C *    "CALCZ" CALCULATES POSITIVE AND NEGATIVE SEQUENCE *
C *    MOTOR IMPEDANCE.                                                   *
C *************************************************************************

      SUBROUTINE CALCZ(S,Z,ZR)
      IMPLICIT COMPLEX (I,V,Z)
      DIMENSION R(8)
      COMMON/BL5/ZMAG,ZSTAT,RR(8),XR(8),NCIRC
      DO 10 J=1,NCIRC
   10 R(J)=RR(J)/S
      RM=R(1)
      XM=XR(1)
      DO 11 J=2,NCIRC
      DMI=(RM+R(J))**2+XM*XM
      RM=R(J)*(RM*(RM+R(J))+XM*XM)/DMI
      XM=XM*R(J)*R(J)/DMI+XR(J)
   11 CONTINUE
      ZR=CMPLX(RM,XM)
      Z=ZSTAT+ZMAG*ZR/(ZMAG)ZR)
      RETURN
      END
```

```
C ***********************************************************************
C *     "CALCT" CALCULATES SEQUENCE ELECTROMECHANICAL                   *
C *     TORQUES.                                                        *
C ***********************************************************************

      SUBROUTINE CALCT(IEQ,ZEQ,XM,T,IROTOR)
      IMPLICIT COMPLEX (I,V,Z)
      REQ=REAL(ZEQ)
      B=AIMAG(ZEQ)
      C=SQRT(REQ*REQ+B*B)
      A=REAL(IEQ)
      B=AIMAG(IEQ)
      D=SQRT(A*A+B*B)
      IROTOR=IEQ*XM/C
      CROTOR=D*XM/C
      T=REQ*CROTOR*CROTOR
      RETURN
      END

C ***********************************************************************
C *     "CALCI" CALCULATES SEQUENCE CURRENTS.                           *
C ***********************************************************************

      SUBROUTINE CALCI(ZPM,ZNM,IPM,INM,IO,E,VOM)
      IMPLICIT COMPLEX(I,E,Z)

C ***********************************************************************
C *     MOTOR PERFORMANCE WITH A SOLID PHASE SHORT                      *
C *     CIRCUIT TO GROUND AT THE MOTOR TERMINAL.                        *
C ***********************************************************************

      COMMON/BL6/ZCAP,ZL,ZNL
      ZPS=ZL
      ZNS=ZNL
      ZO=(0.0,0.050)
      ZE=ZO+ZNS*ZNM/(ZNS+ZNM)
      ZT=ZPS+ZPM*ZE/(ZPM+ZE)
```

```
      IPG=E/ZT
      IPM=-IPG*ZE/(ZPM+ZE)
      IA3=IPG*ZPM/(ZPM+ZE)
      ING=IA3*ZNM/(ZNM+ZNS)
      INM=IA3*ZNS/(ZNM+ZNS)
      IO=IA3
      VOM=IO*ZO
      RETURN
      END

C ***************************************************************************
C *    "RTRMAL" CALCULATES THE COEFFICIENTS OF STATE                        *
C *    EQUATIONS FOR ROTOR THERMAL MODEL.                                   *
C ***************************************************************************

      SUBROUTINE RTRMAL(S)
      COMMON/BL1/XY(6),XDOT(6),T,DELT,LINES,L,N,TFINAL,
     2NDIFF
      COMMON/BL7/FDOR,RKR,COEF(1,2),R90,R91,C3,RLOSS
      COEF(1,1)=-1./(R90*C3)
      IF(S.EQ.1.000)  COEF(1,1)=-1./(R91*C3)
      COEF(1,2)=1./C3
      CALL INTRKR(T,DELT)
      RETURN
      END

C ***************************************************************************
C *    "INTRKR" IS NUMERICAL INTEGRATING ROUTINE FOR                        *
C *    ROTOR TEMPERATURE WHICH IN TURN CALLS "COMP".                        *
C ***************************************************************************

      SUBROUTINE INTRKR(TIME,DELT)
      COMMON/BL7/FDOR,RKR,COEF(1,2),R90,R91,C3,RLOSS
      REAL K
      DIMENSION K(4,1)
      TEMR=RKR
      K(1,1)=DELT*FDOR
```

```
      TEMR=RKR+K(1,1)/2.
      CALL COMPR(TEMR)
      K(2,1)=DELT*FDOR
      TEMR=RKR+K(2,1)/2.
      CALL COMPR(TEMR)
      K(3,1)=DELT*FDOR
      TEMR=RKR+K(3,1)
      TIME=TIME+DELT/2.
      CALL COMPR(TEMR)
      K(4,1)=DELT*FDOR
      RKR=RKR+K(1,1)/6.+K(2,1)/3.+K(3,1)/3.+K(4,1)/6.
      RETURN
      END

C ***************************************************************************
C *    "COMPR" COMPUTES ROTOR TEMPERATURE RISE.                             *
C ***************************************************************************

      SUBROUTINE COMPR(TEMR)
      COMMON/BL7/FDOR,RKR,COEF(1,2),R90,R91,C3,RLOSS
      FDOR=0.0
      FDOR=FDOR+COEF(1,1)*TEMR+COEF(1,2)*RLOSS
      RETURN
      END

C ***************************************************************************
C *    "STRMAL" CALCULATES THE COEFFICIENTS OF STATE                        *
C *    EQUATIONS FOR STATOR THERMAL MODEL.                                  *
C ***************************************************************************

      SUBROUTINE STRMAL(S)
      COMMON/BL8/FDOT(2),RK4(2),COEEF(2,4),R7,R80,R81,C1,C2,
     2SLOSS,CLOSS
      COMMON/BL1/XY(6),XDOT(6),T,DELT,LINES,L,N,TFINAL,
     2NDIFF
      DO  2  J=1,2
      DO  2  K=1,4
```

```
2     COEEF(J,K)=0.0
      COEEF(1,1)=-1./(R7*C1)
      COEEF(1,2)=1./(R7*C2)
      COEEF(1,3)=1./C3
      COEEF(2,1)=1./(R7*C2)
      COEEF(2,2)=-(R7+R80)/(R7*R80*C2)
      IF(S.EQ.1.00)COEEF(2,2)=-(R7+R81)/(R7*R81*C2)
      COEFF(2,4)=1./C2
      CALL INTSKR(T,DELT)
      RETURN
      END

C ***********************************************************************
C *    "INTSKR" IS NUMERICAL INTEGRATING ROUTINE FOR                    *
C *    STATOR TEMPERATURE WHICH IN TURN CALLS "COMP".                   *
C ***********************************************************************

      SUBROUTINE INTSKR(TIME,H)
      COMMON/BL8/FDOT(2),RK4(2),COEEF(2,4),R7,R80,R81,C1,C2,
     2SLOSS,CLOSS
      REAL K
      DIMENSION K(4,2),TEMP(2)
      DO  10  I=1,2
10    TEMP(I)=RK4(1)
      DO  20  J=1,2
20    K(1,J)=H*FDOT(J)
      DO  30  J=1,2
30    TEMP(J)=RK4(J)+K(1,J)/2.
      CALL COBP(TEMP)
      DO  40  J=1,2
40    K(2,J)=H*FDOT(J)
      DO  50  J=1,2
50    TEMP(J)=RK4(J)+K(2,J)/2.
      CALL COMP(TEMP)
      DO  60  J=1,2
60    K(3,J)=H*FDOT(J)
      DO  70  J=1,2
```

```
 70   TEMP(J)=RK4(J)+K(3,J)
      TIME=TIME+H/2.
      CALL COMP(TEMP)
      DO  80  J=1,2
 80   K(4,J)=H*FDOT(J)
      DO  90  J=1,2
 90   RK4(J)=RK4(J)+K(1,J)/6.+K(2,J)/3.+K(3,J)/3.+K(4,J)/6.
      RETURN
      END

C ***************************************************************************
C *    "COMP" COMPUTES STATOR AND CORE TEMPERATURE                          *
C *    RISE.                                                                *
C ***************************************************************************

      SUBROUTINE COMP(TEMP)
      COMMON/BL8/FDOT(2),RK4(2),COEEF(2,4),R7,R80,R81,C1,C2,
     2SLOSS,CLOSS
      DIMENSION TEMP(2)
      DO  50  J=1,2
 50   FDOT(J)=0.0
      DO  100  J=1,2
      DO  100  K=1,2
      FDOT(J)=FDOT(J)+COEEF(J,K)*TEMP(K)
100   CONTINUE
      DO  150  J=1,2
150   FDOT(J)=FDOT(J)+COEEF(J,3)*SLOSS+COEEF(J,4)*CLOSS
      RETURN
      END

C ***************************************************************************
C *    "INTEG" IS NUMERICAL INTEGRATING ROUTINE FOR                         *
C *    SPEED WHICH IN TURN CALLS "PLANT".                                   *
C ***************************************************************************

      SUBROUTINE INTEG(T,DELT,N,X,YDOT)
      DIMENSION X(6),YDOT(6),XN(6)
```

Program Listing

```
      DIMENSION FK1(8),FK2(8),FK3(8),FK4(8),FK5(8)
      DELT2=DELT/2.
      DELT3=DELT/3.
      CALL PLANT(T,X,YDOT)
      DO  10  M=1,N
      FK1(M)=DELT3*YDOT(M)
      XN(M)=X(M)+FK1(M)
10    CONTINUE
      T3=T+DELT3
      CALL PLANT(T3,XN,YDOT)
      DO  20  M=1,N
      FK2(M)=DELT3*YDOT(M)
      XN(M)=X(M)+(FK2(M)+FK1(M)/2.
20    CONTINUE
      CALL PLANT(T3,XN,YDOT)
      DO  30  M=1,N
      FK3(M)=DELT3*YDOT(M)
      XN(M)=X(M)+(FK3(M)*9.+3.*FK1(M))/8.
30    CONTINUE
      T2=T+DELT2
      CALL PLANT(T2,XN,YDOT)
      DO  40  M=1,N
      FK4(M)=DELT3*YDOT(M)
      XN(M)=X(M)+(3.*FK1(M)-9.*FK3(M)+12.*FK4(M))/2.
40    CONTINUE
      T=T+DELT
      CALL PLANT(T,XN,YDOT)
      DO  50  M=1,N
      X(M)=DELT3*YDOT(M)
50    CONTINUE
      DO  60  M=1,N
      X(M)=X(M)+(FK1(M)+4.*FK4(M)+FK5(M))/2.
60    CONTINUE
      RETURN
      END
/DATA
0.0001  0.05055      1.00      0.00      0.00      60.00   2.0
```

APPENDIX B

Input Program For SAS/Graph

SAS/GRAPH Program

```
C ************************************************************************
C *   A TYPICAL SAS PROGRAM FOR PLOTTING THE GRAPHS.                     *
C ************************************************************************

      GOPTIONS DEVICE=TEK4107 NOTEXT82 GPROTOCOL=GSAS7171;
      GOPTIONS CBACK=STB COLORS=(YELLOW);
      TITLE1 C=YELLOW H=.1 ' ';
      DATA  POP1;
      INPUT SLIP  RESIS;
      CARDS;
      ;
      RUN;
      DATA LABELS (KEEP=X Y XSYS YSYS TEXT POSITION STYLE);
      SET POP1;
      IF  SLIP=2.000000
      THEN DO;
      XSYS='2'; YSYS='2';
      POSITION='3';
      STYLE='SOLID';X=SLIP;Y=RESIS;TEXT='RR';OUTPUT;
      END;
      RUN;
      FOOTNOTE1 C=YELLOW H=.8'FIGURE 3.2 ROTOR EFFECTIVE    ';
      FOOTNOTE2 C=YELLOW H=.8'              RESISTANCE(P.U.)  ';
      FOOTNOTE3 C=YELLOW H=.8'              VERSUS SLIP.      ';
      PROC GPLOT DATA=POP1;
      PLOT  RESIS*SLIP=1/
      VAXIS=.00720  TO  .02715  BY  .00133
      HAXIS=0.00  TO  2.20  BY  .20
      CTEXT=YELLOW
      CAXIS=YELLOW
      ANNOTATE=LABELS;
      LABEL  SLIP='SLIP';
      LABEL  RESIS='ROTOR RESISTANCE';
      SYMBOL1 C=RED V=D I=JOIN L=2;
      RUN;
```

APPENDIX C

Motor Data

TABLE C.1

Motor Data

General Data

Horsepower	: 18000
Speed	: 1800 RPM Synchronous
Slip	: 0.00722
Voltage	: 13.2 kv, 3 phase, 60 Hz
Current	: 667 A full load

Electrical Model Data

Stator	: R_s=0.00422 p.u.
	X_s=0.0977 p.u.
Mutual	: R_m=237 p.u.
	X_m=4.9 p.u.
Rotor	: R_{rp}=0.00722 p.u. running
	X_{rp}=0.0977 p.u. running
	A=3.3 the ratio of rotor neg. and pos. resistance

Mechanical Model Data

wk^2	: 30015 lb-ft^2 motor
	5540 lb-ft^2 load
H	: 1.74 sec.

Thermal Model Data

Stator	: R_7=20
	R_8=6.67 running
	R_8=20 standstill
	C_s=7.5
	C_c=75
	X=100 c thermal limit
Rotor	: R_9=43.9 running
	R_9=130 standstill
	C_r=4.68
	Z=80 c thermal limit

VITA

Nader S. Moharari was born in Langroud, Iran on May 11, 1957. He attended elementary and part of high school in that city and was graduated from Danesh-O-Honar high school in 1974. The following August he entered Tehran Polytechnic University, and in August 1983 he received a Bachelor of Science degree in Electrical Engineering. During 1984-86 he was an employee of the Iranian state radio and television in the area of installation and launching of the medium wave radio transmitters. In January of 1987 he began study toward a Master's degree in Electrical Engineering at the University of Tennessee, Chattanooga, where he received a teaching assistantship.

The author is a member of Institute of Electrical and Electronics Engineers (IEEE), and plans to pursue a Ph.D. program in Electrical Engineering at the Georgia Institute of Technology after graduation.